DIRECT NUMERICAL SIMULATION OF HOMOGENEOUS ISOTROPIC TURBULENCE – A METHODOLOGY AND APPLICATIONS

by

SARAH MOUSSA HUSSEIN

This dissertation is presented to the Faculty of the Graduate School of

The University of Texas at Arlington in Partial Fulfillment

of the Requirements

of the Degree of

DOCTOR OF PHILOSOPHY

THE UNIVERSITY OF TEXAS AT ARLINGTON

DECEMBER 2018

DIRECT NUMERICAL SIMULATION OF HOMOGENEOUS ISOTROPIC TURBULENCE – A METHODOLOGY AND APPLICATIONS

The following members of the Committee approve this

Doctoral dissertation of **Sarah Moussa Hussein**

Chair

Frank Lu, Ph.D.
Supervising Professor, Research Advisor
Department of Mechanical and Aerospace Engineering
University of Texas at Arlington

Tuncay Aktosun, Ph.D.
Department of Mathematics
University of Texas at Arlington

Zhen Xue Han, Ph.D.
Department of Mechanical and Aerospace Engineering
University of Texas at Arlington

Hyejin Moon, Ph.D.
Department of Mechanical and Aerospace Engineering
University of Texas at Arlington

Donald Wilson, Ph.D.
Department of Mechanical and Aerospace Engineering
University of Texas at Arlington

I hereby declare that this dissertation and the work presented in it are my own and generated by my original research. I confirm that published work of other authors is clearly acknowledged and referenced.

I acknowledge that this material is based upon work supported by the National Science Foundation Graduate Research Fellowship Program under Grant No. 1144240. *Any opinions, findings, and conclusions or recommendations expressed in this material are those of the author(s) and do not necessarily reflect the views of the National Science Foundation.*

To Mama Amira

“At school I learned that an equation

Is when everything on both sides of the equal sign

Balances. After a while I stopped

Crying about the things I couldn’t change.

After a while the fatigue in my heart lifted

So that airplanes didn’t sound like

Bombers anymore.”

- Jay Snodgrass, First Confession in Monster Zero

Acknowledgements

First and foremost I am grateful to Dr. Frank Lu, my outstanding supervising professor and research advisor, for his leadership and guidance. I am thankful for all the time he dedicates to discussing turbulence physics and asking the tough questions. His scholarship and scientific attitude have inspired me throughout this challenging but highly rewarding doctoral journey.

Very many thanks to Dr. Luca Massa for his assistance with the computational research and for sharing his coding methodology. I thank the University of Texas at Austin's Texas Advanced Computing Center staff for their supercomputer allocations and training. I thank the University of Texas at Arlington, the Department of Mechanical and Aerospace Engineering, and the Aerodynamics Research Center for providing supportive environment and resources. I also thank Dr. Tuncay Aktosun, Dr. Bernd Chudoba, and Dr. Yvette Pearson for their assistance throughout my undergraduate and graduate degrees.

Furthermore, I would like to thank my wonderful family and close friends for their support and understanding over the years. Special thanks to Ms. Latifa Said who believed in me from the very beginning.

Lastly, I am grateful for the financial support of the National Science Foundation Graduate Research Fellowship Program without which this work would not have been possible.

Abstract

DIRECT NUMERICAL SIMULATION OF HOMOGENEOUS

ISOTROPIC TURBULENCE – A METHODOLOGY AND APPLICATIONS

Sarah Moussa Hussein, Ph.D.

The University of Texas at Arlington, 2018

Supervising Professor: Frank K Lu, Ph.D.

Turbulence has been a topic of scientific research for years. Characterized by unorganized chaotic motion and irregular fluctuations, it persists as one of the most challenging topics in fluid mechanics despite volumes of documented research and crucial findings. This begs the question: **What is turbulence and why is it so challenging?**

Turbulence research studies cover a wide spectrum of branches from fundamental flow propagation to different turbulence interactions. This research project investigates the simplest class of turbulent flow studies, homogeneous isotropic turbulence. In a quest to advance the fundamental understanding of turbulence physics, a direct numerical simulation tool is developed. The tool generates a turbulent periodic cube with vortical fluctuations and three interaction case studies. The evolution of the velocity

in time is derived from the Navier–Stokes equations. These governing equations are integrated, along with initial and boundary conditions, to formulate turbulence. Fully-developed turbulence is achieved when the Tavoularis (1978) criterion of axial velocity variation is met. Output data sets are collected for numerical analysis.

The turbulence periodic cube geometry is assessed for its applicability in this study. The simplified structure is found to be efficient and facilitated. The interaction case studies of shock–turbulence and detonation–turbulence are compared to an unforced flow interaction. The case studies are statistically analyzed and visualized yielding important conclusions on the effects of the fluctuations, heat release, detonation inherent length scale, and detonation intrinsic instability on the flow behavior. A mutual interaction is found between the turbulence structures and the strong detonation wave. An extension of the long-standing Tavoularis velocity skewness factor is suggested. The proposed velocity skewness vector quantifies the variation of the three velocity components in the three Cartesian coordinates. This comprehensive expression highlights the contribution of the three–dimensional velocity fluctuations to the turbulence state.

Table of Content

List of Figures

List of Tables

Nomenclature

Alphabet	Description
a	speed of sound
BCE	before common era
c_p	specific heat at constant pressure
C	Sutherland's constant
CFD	computational fluid dynamics
CJ	Chapman–Jouguet
d	differential
DES	detached eddy simulation
DNS	direct numerical simulation
E	activation energy
$\mathrm{E_t}$	total energy
H	height
i, j, k	indices corresponding to the three Cartesian coordinates in tensor notation
I	identity matrix

k_0	Arrhenius law pre-exponential term
K	thermal conductivity
Kn	Knudsen number
l	length
l_0	large scale eddy
L	geometric length scale
$L_{1/2}$	half length
Le	Lewis number
LES	large eddy simulation
M	Mach number
Mm	molar mass
N	number of units
P	pressure
Pr	Prandtl number
q	heat flux
Q	heat release parameter
r	unit axial distance

$r(T)$	Arrhenius law reaction rate
R	universal gas constant
R_{gas}	specific gas constant
$RANS$	Reynolds-averaged Navier–Stokes
Re	Reynolds number
R_{ij}	single-point correlation
RMS	root mean square average
RS	Reynolds stress
$sdev$	standard deviation
S	skewness factor
STP	standard temperature and pressure
t	time
T	temperature
$TACC$	Texas Advanced Computing Center
TKE	turbulent kinetic energy
u, v, w	velocity components in the three Cartesian coordinates
var	variance

x, y, z	three Cartesian coordinate components
ZND	Zel'dovich-von Neumann-Döring
α	thermal diffusivity
γ	ratio of specific heats
δ	Kronecker's delta
ε	kinetic energy density
η	Kolmogorov length scale
κ	frequency
λ	reaction progress variable
λ_0	mean free path
μ	viscosity
ν	kinematic viscosity
ρ	density
σ	stress tensor
τ	Taylor microscale
ω	vorticity
Ω	enstrophy

Subscripts	Description
0	initial condition
33	3 × 3; three-by-three
d	detonation
DI	dissipation
EI	universal equilibrium
p	post
ref	reference
s	shock
t	turbulent

Superscripts	Description
T	transpose

Symbols	Description
∂	partial differential
∇	del operator

Accents	Description
$\lvert\ \rvert$	absolute value
$(\bar{})$	average
$\langle\ \rangle$	ensemble average
$(\ )'$	fluctuation
$(\tilde{})$	non-dimensional term
$(\vec{})$	vector

1. Introduction

Turbulence is the most important unsolved problem of classical physics.

- Richard P. Feyman

Along the coast of the Mediterranean Sea, the ancient Phoenician civilization emerged in c. 3200 BCE in land that corresponds to present-day Lebanon and coastal parts of neighboring countries (Khalaf, 2018). The birthplace of the alphabet saw the rise of glass-making, dye production, trade, and ship-building (Mark, 2009). The Phoenicians' location encouraged exploring the sea, as they employed their ships in trade, Figure 1.1, and military pursuits.

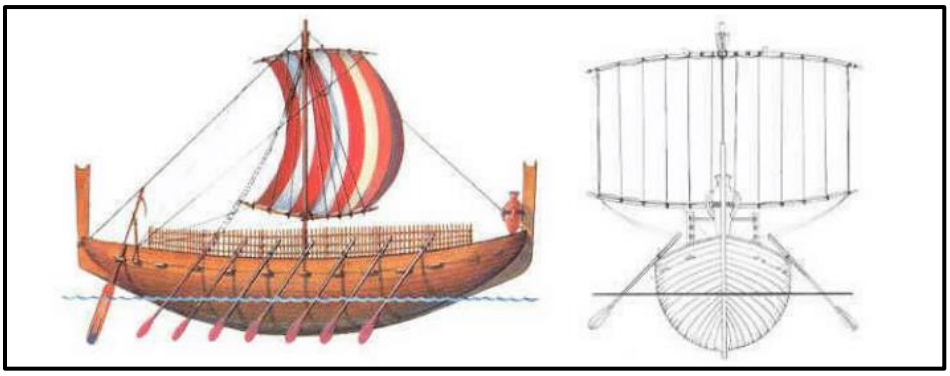

Figure 1.1 Side and front view sketches of a Phoenician wind and human-powered trading ship (Bašić, 2016)

The building and sailing of these ships required knowledge of fluid mechanics, among other skills. Fluid mechanics is the field of study of fluids: liquids and gases, at rest under the subset of fluid statics, and in motion under the subset of fluid dynamics. Fluid mechanics, thus, has been a topic of research since the ancient days of exploring sailing ships as well as development of irrigation systems. It persists today in applications ranging from biological operations of breathing and blood flow, to

engineering applications such as windmills, heating and air-conditioning systems, as well as engines.

Most fluid concepts have theories to describe their phenomena and whenever possible having experiments to support the theories. However, the theories may represent idealized flow properties and geometries. It can be difficult to reproduce theoretical results in realistic experimental setups accurately. One dominant research topic in fluid mechanics is turbulent flow. Despite years of documented work and important findings, it remains a subject that has challenged the greatest minds in science and engineering for years. **What is turbulence and why is it so challenging?**

A fluid can flow in a continuous motion in a laminar or turbulent manner. In a laminar flow, the fluid moves in layers or "laminae," smoothly, in an orderly manner, with no disturbances. The planes of the fluid slide past each other without mixing. In a turbulent flow, described by Leonardo da Vinci early in the 16^{th} century as "turbulenza" (Lesieur, 1987), the fluid shows unorganized, chaotic, complex patterns in its motion. Pope (2000) defines turbulence as a fluid field with irregular, chaotic, unsteady, seemingly random, and certainly unpredictable small-scale behavior. The difference between laminar and turbulent flow fields is shown in a simplified sketch in Figure 1.2. Turbulence is also defined as a three–dimensional chaotic process (Davidson, 2004). The small-scale unorganized regions of the turbulent flow carrying energy are commonly referred to as eddies, although the definition is subjective. The challenge, thus, lies in the fact that no theory, until today, has been able to outline and explain the behavior of turbulent flows. So, experiments and numerical methods are heavily relied on to introduce new knowledge.

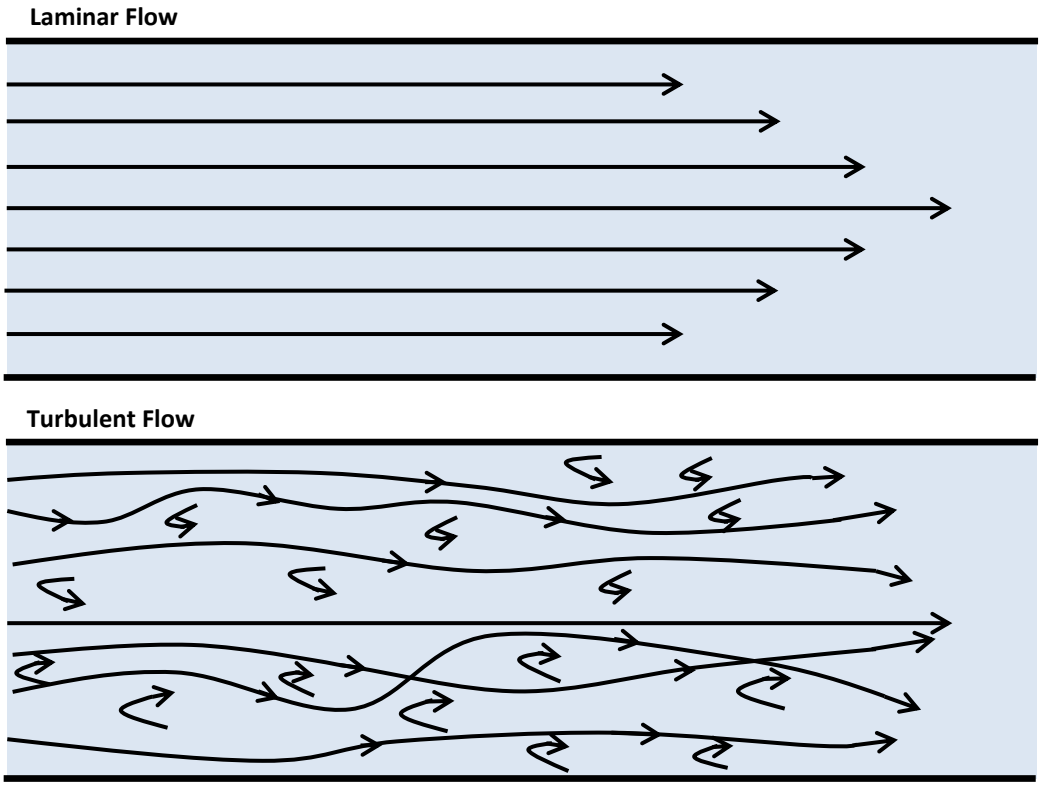

Figure 1.2 A simple sketch of the difference between internal laminar and turbulent fluid field flows in a pipe as adopted from CFDSupport (2013)

Laminar flows are not very common. In fact, most naturally occurring flows are turbulent. Laminar flow can occur internally in pipes and channels or externally such as past a sphere or a flat plate. The flow remains laminar as long as the velocity is low or the viscosity is high. At higher velocities, and lower viscosities, the flow transitions to turbulence. For example, the air flowing through breathing lungs, like the water coming out of a faucet, starts in a laminar manner and then becomes turbulent. Turbulence in the external air flow around an aircraft frame is a source of concern and discomfort to the passengers at different speeds and altitudes. The passengers can sense the translation of the turbulent velocities onto the airframe, which may affect the acceleration at the center of gravity, Figure 1.3. When an aircraft is crossing through a

patch of atmospheric turbulence, the airframe must be strong enough to withstand the gusts preventing overstressing and stalling (Zbrozek, 1958).

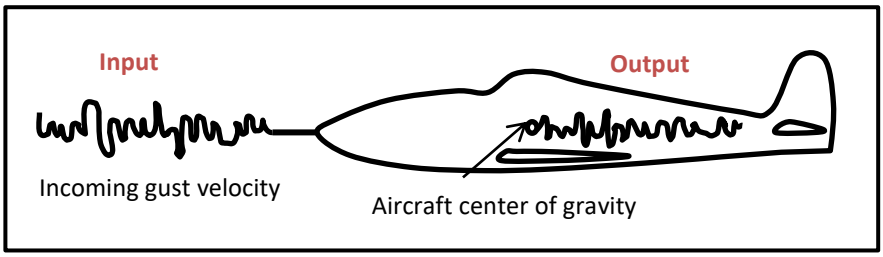

Figure 1.3 Aircraft flying through atmospheric turbulence as adopted from Bendat (2010)

The smoke emerging from a fire is turbulent, and so is the wake produced by a moving ship. Turbulence in large-scale atmospheric and oceanic flows partly dictates the weather. Turbulence maintains the terrestrial magnetic field against natural decay (Davidson, 2004). While turbulence persists as one of the most difficult problems in fluid mechanics today (Liepmann, 1979), better understanding of the structure and mechanics of turbulent flow will allow engineers to enhance the design of systems and improve the quality of life for many. Such improvements include: better flight performance, quieter airplanes, fuel-efficient combustion engines, less expensive wind farms, better weather prediction, amongst other technological applications.

One of the earliest flow visualizations is that of water flow patterns moving from a channel to a lower body of water by da Vinci, shown in Figure 1.4. The water leaves a square hole in a wall and strikes the bottom surface with chaotic, unstructured, swirling behavior. It depicts laminar flow and its transition to turbulence. It is documented that da Vinci described the motion of the water as that of a hair: *"Being pulled down by the weight of the hair and turned by the direction of the curl"* (Gad-el-Hak, 2000). The water,

thus, is being directed by the current and deviated by the random reverse motion in eddy behavior.

Figure 1.4 Leonardo da Vinci's visualization of water patterns flowing from a channel and striking a lower body (Monaghan, 2014)

In turbulent flows, eddies are swirls characterized by the energy they carry due to their velocity. Large eddies form reference length scales for flow analysis; while small eddies formulate the lower limit of experimental and computational grid size resolution. The energy cascade can be thought of as a map of energy flux. The large eddies transfer their energy to smaller eddies; which in turn transfer their energy to even smaller eddies, until the smallest size is reached where energy transfer ends and energy dissipation takes place. Energy dissipation occurs due to the small eddies' sensitivity to the flow viscosity. The statement written by Richardson in 1922 paints a clear picture of the energy cascade: "*We thus realize that: big whirls have little whirls that feed on their velocity, and little whirls have lesser whirls and so on on to viscosity – in the molecular sense*." However, the term cascade was coined by Onsager in the 1940s (Sagaut, 2008). A schematic representation of the energy cascade is shown in

Figure 1.5. This hierarchical breakup of turbulence structures is a simplified outline of the energy flux due to velocity and viscosity. It is important to note that in physical turbulence, the energy cascade is not that structured, involving additional stretching, folding/rolling up, and blob reconnection (Sagaut, 2008).

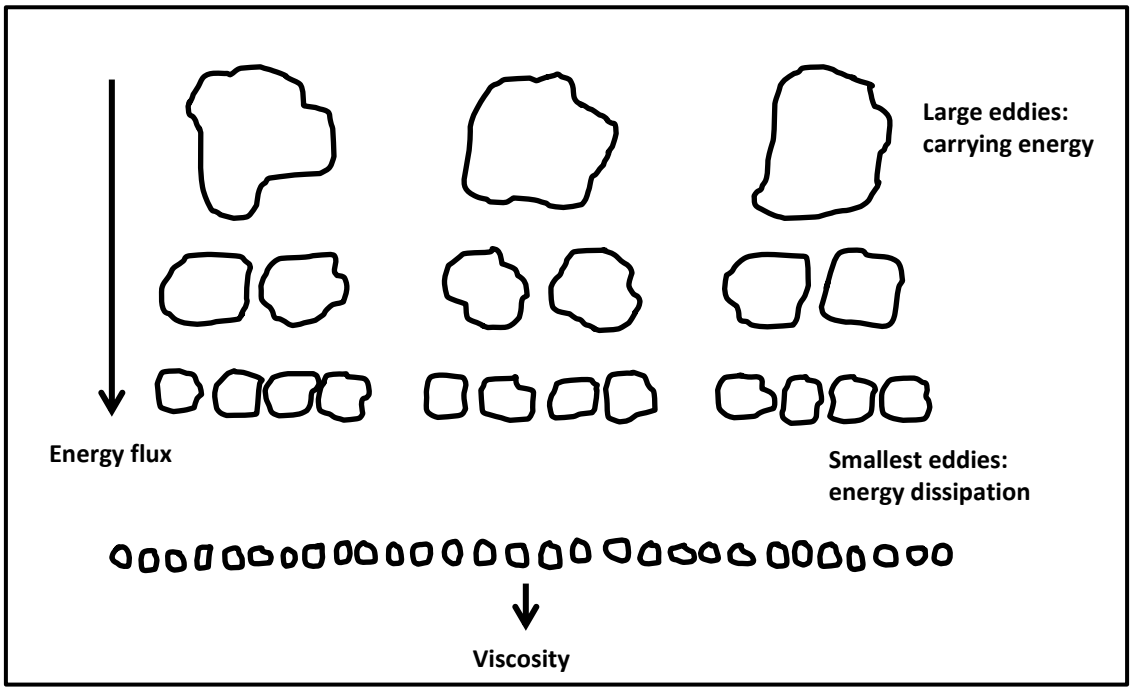

Figure 1.5 Simplified schematic representation of the energy cascade as adopted from Frisch (1995) and Davidson (2004)

The factors governing whether a flow is laminar or turbulent are primarily the velocity and viscosity, combined in the non-dimensional Reynolds number. The Reynolds number is an expression of the ratio of inertial forces to viscous forces (White, 2011). At low Reynolds number, the fluid flow is laminar, while at high Reynolds number, the flow is turbulent. There exists a transitional phase between the two states, a laminar–turbulent transition region, whose parameters depend on the flow type. It is found that at high Reynolds number, decelerating a flow produces vortices that are sensitive to initial

conditions and result in stochastic flow patterns (Liepmann, 1979). The stochastic flow patterns have random probability distributions that call for statistical analysis of turbulence instead of accurate predictability. A turbulent field with varying velocities has vortical fluctuations. A turbulent field with varying temperatures has entropic fluctuations and one with varying pressures has acoustic fluctuations. These fluctuations are often coupled within the same fluid field (Massa, 2011a).

The simplest class of turbulent flows to study is homogeneous turbulence (Pope, 2000). A fluid field is homogeneous when it is invariant spatially (Batchelor, 1953); when the mean quantities of a fluid property are invariant under translation in time and space (Lesieur, 1987). Generally, a homogeneous turbulent field is also isotropic. A fluid field is isotropic when it is invariant with rotation and reflection (Pope, 2000); when the mean quantities of a fluid property are invariant under simultaneous arbitrary rotation of the set of points and of the coordinate axes (Lesieur, 1987). Some may argue that real turbulent flow is neither homogeneous nor isotropic at large scales; but these assumptions facilitate the statistical analysis of turbulent flows with slight Gaussian deviation (Lesieur, 1987). A Gaussian distribution is a theoretical normal distribution with random variables following a perfectly symmetrical bell-shape within set intervals, as shown in Figure 1.6. The random variables are distributed where: 68% occur within one standard deviation of the mean, 95% occur within two standard deviations of the mean, and 99.7% occur within three standard deviations of the mean (Lane, 2013). A flow with slight deviation from the Gaussian distribution can have variations in the velocity, temperature, or pressure properties of the flow. The flow distribution shown in

Figure 1.6 alongside the Gaussian distribution has velocity variations. It can be seen that the flow distribution no longer follows the symmetry of the bell curve.

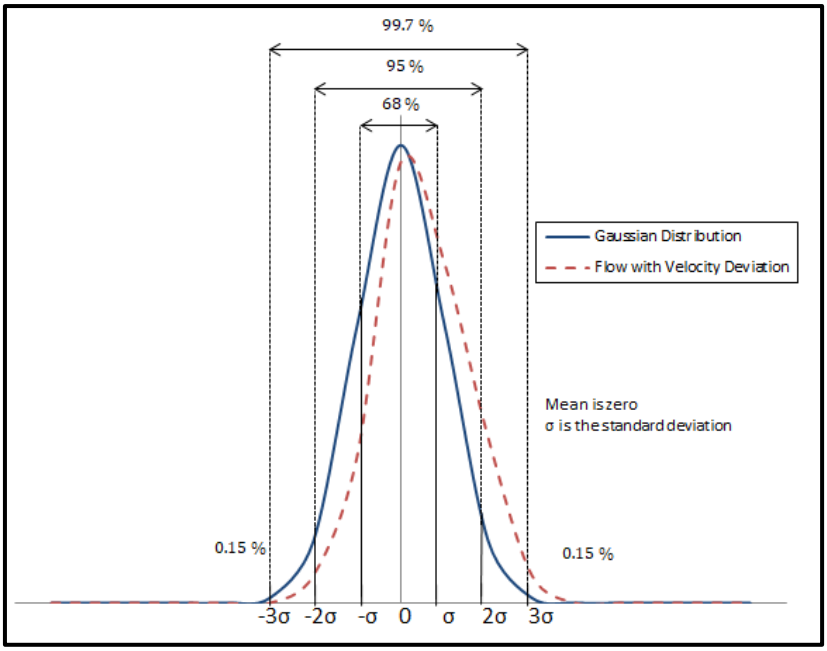

Figure 1.6 Normal Gaussian distribution function compared to the distribution function of flow with velocity deviation

There is not much debate any longer that turbulence can be described by the non-linear Navier–Stokes equations (Lesieur, 1987). Classically, the Navier–Stokes equations referred to the momentum equations of Newtonian fluid behavior; where the viscosity remains constant under applied shear stress. Nowadays, the Navier–Stokes equations refer to the conservation equations of mass, momentum, and energy in fluid fields. They are considered the core of fluid flow modelling describing the complex fluid flow properties from the largest to the smallest length and time scales (Pope, 2000). For the three–dimensional system of non-linear equations under set initial conditions, mathematicians have not been able to prove that smooth solutions always exist. They have not been able to verify that if they do exist, they have bounded energy per unit

mass (Bašić, 2016); that they are unique. This is called the *Navier–Stokes Existence and Smoothness* problem. The Clay Mathematics Institute in May 2000 assigned this problem as one of the seven Millennium problems. The Institute offers a $1,000,000 prize for the first person to provide a solution for the problem. The problem remains unsolved today.

Turbulence theories are based on experiments, thus leading to a mix of semi-empirical laws and deterministic but highly simplified methods (Davidson, 2004). Turbulence mixing and transport properties dominate the fluid mechanics in most large-scale engineering applications (George, 1989). In a turbulent flow, an initial small disturbance amplifies to render a deterministic prediction of evolution properties very difficult (Lesieur, 1987). Turbulence research in the 1970s thus split to two approaches, namely, the statistical approach and the coherence among chaos approach (Lesieur, 1987). The first approach follows Taylor and Kolmogorov and uses average quantities to study cascades without coherence or order in turbulence. The second is associated with experimental work studying the behavior of dynamical systems and flow stability to identify coherent structures in shear flows (Lesieur, 1987). Up until the mid-1970s, key advancements in turbulence studies were achieved experimentally. After that, development involved massive computational power (Davidson, 2011). The level of turbulence research has been increasing at an astounding rate since the 1970s (George, 1989). Large main frame computer hardware allows the numerical setup of turbulence research experiments with a level of detail far more than that which can be achieved in physical experiments (George, 1989). Advancement in analysis tools allows theoreticians to better understand turbulence as well. Turbulence research will continue

to influence drag reduction, noise control, mixing, combustion, and a variety of other engineering applications (George, 1989).

Turbulence research in fluid mechanics and mathematics has been formulated by many great minds over the years. Turbulence research consists of many branches which cannot all be covered in this review. Some of the main scientific contributions in fluid analysis, theory development, wind tunnel testing, computational development, and computational fluid dynamics are summarized in Appendix A, from 1628 until 2017 (Davidson, 2011, Bašić, 2016). This is a summarized, brief list and is not intended as a comprehensive evaluation of all turbulence theoretical, experimental, and numerical works of this time frame; the amount of research work is too grand to fit in this document. Focus is placed on the historical events that led to the current topic of interest: the interactions of homogeneous isotropic turbulence with shock and detonation wave fronts.

The interaction of turbulence with a strong shock has shaped the field of investigation and pioneering research work of many engineers. A shock wave is a thin region, typically of order 10^{-5} cm under standard conditions, across which flow properties change drastically (Anderson, 2011). The changes experienced by the flow pressure, density, temperature, and three velocity terms across a shock wave have been studied and are documented as shock relations in fluid dynamics literature. A visual representation of the fixed wave and the flow properties' variations through the shock are in shown in Figure 1.7.

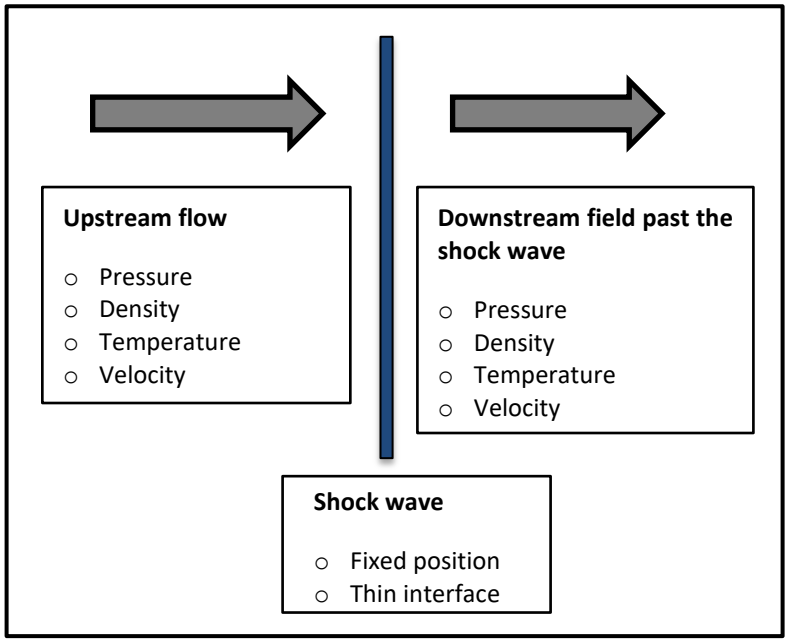

Figure 1.7 Schematic view of the flow properties' variations through a fixed shock wave front as adopted from Sagaut (2008)

Consider next, a detonation which is a continuous combustion that expands and propagates after initiation due to exothermic chemical reactions. In the 20^{th} century, Chapman and Jouguet developed a simple algebraic theory representing the detonation wave as a propagating shock wave accompanied by heat release. The exothermic heat release is confined to an infinitesimally thin shock wave region. Their theory was later developed to a more complex detonation model during World War II by Zel'dovich, von Neumann, and Döring to include a finite reaction rate (Austin, 2003). The advanced theory assumes the shock wave is a thermodynamic process.

Shock–turbulence interaction has been studied as a canonical problem (Lele, 2009). A canonical problem is basic and essential. A basic study contributes to physical understanding while an essential study lays the foundation for more complex cases to follow. Detonation–turbulence interaction extends shock–turbulence interaction studies

to include the effects of rapid chemical energy release via a detonation front (Massa, 2011a). The simplest detonation–turbulence interaction problem is the evolution of a compressible homogenous isotropic turbulent field when subjected to initiation by a strong shock wave. A fluid field is compressible when the density changes significantly with changes in pressure. The strong shock triggers an exothermic chemical reaction to result in the detonation wave. Detonation–turbulence interaction differs from shock–turbulence interaction by three factors:

- The detonation is exothermic, with added heat release complexity.
- The detonation structure has an inherent length scale, while the shock does not.
- The detonation wave has intrinsic fluctuations that cause instability in the detonation front, which are not present in shock waves.

With the scientific advancement we have today, we are still unable to answer the questions that turbulence generates. As a result of such unanswered questions, incidents occur where combustion is unexpected and therefore unaccounted for in safety protocols. This combustion, due to the detonation–turbulence interaction, can occur in highly aerodynamic bodies and rocket engines. It can also occur in handling of combustible gaseous fuels such as hydrogen and biogas. The nuclear power plant explosion in Fukushima, Japan in March of 2011 drew attention to the detonation–turbulence interaction problem. Some of the questions that arise are:

- How does the detonation propagate through the disaster zone?
- Can the detonation, once initiated from the dissociation of the water molecules, be mitigated?

- Does turbulence play a role in destabilizing the detonation wave to make it difficult to control?

These questions on safety, if properly answered, will help improve the design of nuclear and chemical reactors, as well as develop safety precautions and potentially disaster mitigation techniques. The topic of detonation–turbulence interaction inspired this research work.

2. Literature Review and Research Objectives

The study of turbulence allows the improvement of our understanding of fundamental fluid mechanics and the development of better turbulence models. The topic of interest in this research work is homogeneous isotropic turbulence with initial vortical fluctuations when it is subjected to a strong shock wave, which later evolves into a detonation wave upon heat release. A simple low-order model of idealized homogeneous isotropic turbulence also assumes that the flow is fully-developed. A turbulent flow is said to be fully-developed when the propagating flow is independent of constraints, such as boundary conditions, external forces, and viscosity (Lesieur, 1987). The velocity skewness factor of the fluctuating terms is a statistical expression used to quantitatively determine when turbulence has reached fully-developed state. Studies have documented different skewness factors for different types of turbulent flows (Tavoularis, 1978).

In isotropic turbulence, a factor of the streamwise velocity derivative is defined and used to show when turbulence has reached a fully-developed state. The skewness factor of streamwise velocity derivative is defined by Tavoularis (1978) and utilized in various experimental setups as a statistical quantity.

$$S \equiv -\frac{\overline{\left(\frac{\partial u}{\partial x}\right)^3}}{\left[\overline{\left(\frac{\partial u}{\partial x}\right)^2}\right]^{3/2}} \tag{2.1}$$

In Equation (2.1), the partial derivative of the streamwise velocity u is found with respect to the axial direction. The over bar represents the average quantity of the calculated velocity derivatives. Using the expression in Equation (2.1), it can be shown that a flow

with velocities that are distributed symmetrically about the mean will have zero skewness and cannot be shown to have turbulence properties. A Gaussian distribution has zero skewness. Historically, the streamwise velocity in the axial flow direction has been used in skewness studies because it is the velocity measured by probes. Experimental data from nearly isotropic grid turbulence by Batchelor and Townsend (1949), Stewart and Townsend (1951), Mills (1958), Frenkiel and Klebanoff (1971), Kuo and Corrsin (1971), Betchov and Lorenzen (1974), Bennett and Corrsin (1978), and Tavoularis (1978) show that when the negative value of the velocity skewness reaches a measure between 0.4 and 0.5, within a 0.05 margin, then the flow is said to have reached a fully-developed turbulent state. This is shown in Figure 2.1 and corresponding Table 2.1. This range became the reference value for turbulence velocity skewness factor calculations.

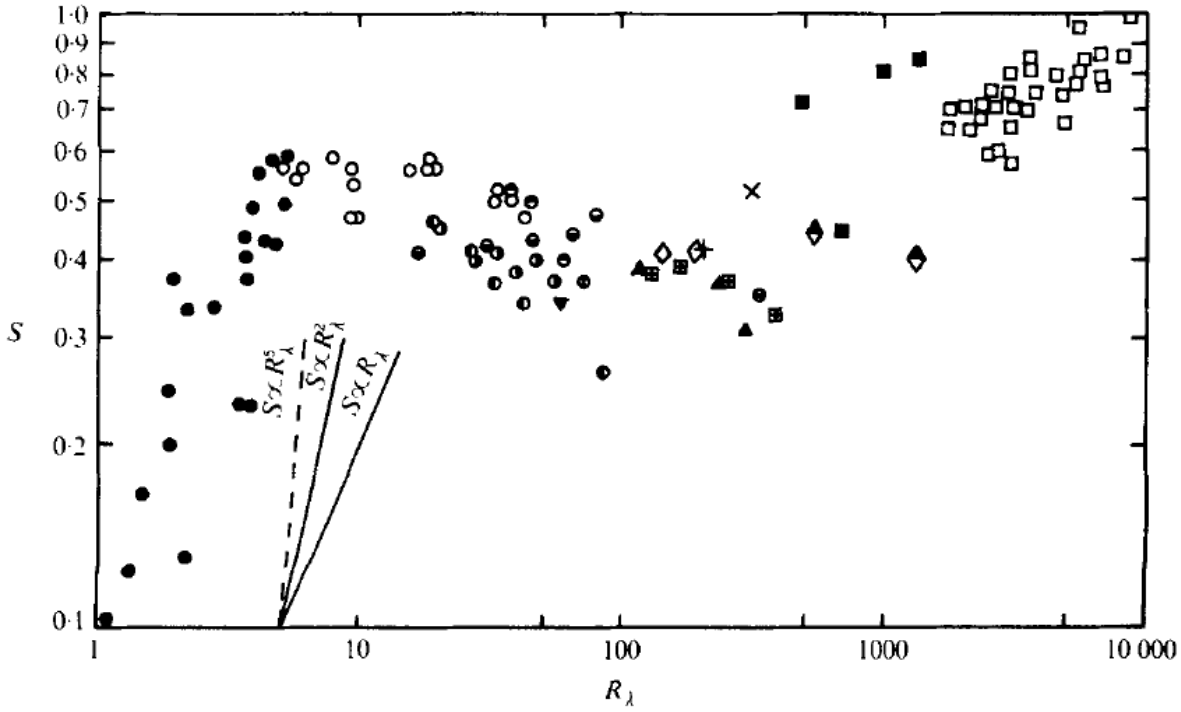

Figure 2.1 Measurements of the velocity-derivative skewness in various turbulent flows plotted vs. the turbulent Reynolds number (symbols are documented in Table 2.1) (Tavoularis, 1978)

Table 2.1 Velocity-derivative skewness diagram symbols (Tavoularis, 1978)

Type of flow	Author(s)	Symbol
Nearly isotropic grid turbulence	Batchelor & Townsend (1949)	◑
	Stewart & Townsend (1951)	◐
	Mills *et al.* (1958)	◒
	Frenkiel & Klebanoff (1971)	◓
	Kuo & Corrsin (1971)	◕
	Betchov & Lorenzen (1974)	◔
	Bennett & Corrsin (1978)	○
	Present data	●
Homogeneous shear flow	Tavoularis (1978)	◇
Duct flow	Comte-Bellot (1965)	▲
	Elena, Chauve & Dumas (1977)	▼
Mixing layers	Wyngaard & Tennekes (1970)	+
	Champagne, Pao & Wygnanski (1976)	×
Axisymmetric jet	Friehe, Van Atta & Gibson (1972)	◈
	New measurements	◆
Boundary layer	Ueda & Hinze (1975)	⊞
Atmosphere	Gibson, Stegen & Williams (1970)	■
	Wyngaard & Tennekes (1970)	□

With the advancement of computational power and resources, the numerical simulation of turbulence emerged. Gotoh (1993), Mahesh (1997), Pope (2000), and Massa (2011) numerically simulated homogeneous isotropic turbulence and used the reference value of $S = -0.5$ to decide when their turbulence has reached a fully-developed state. Note that Tavoularis (1978) dropped the negative skewness sign in his plot, Figure 2.1.

Calculation of the velocity derivative to find the turbulence skewness factor requires defining the turbulence field geometry. Computationally, simple and periodic shapes are preferred for computational efficiency and accuracy. The periodic cube has been a geometry used by researchers investigating the fundamental structure of turbulence (Davidson, 2004), and is shown in Figure 2.2. It is a cube divided into an infinite number of smaller cubes in which the fluid behavior is identical, within a certain prescribed confidence level.

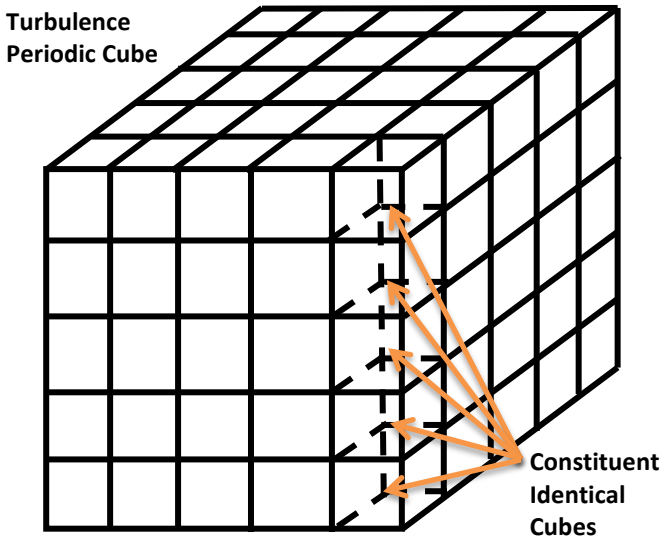

Figure 2.2 Sketch of a turbulence periodic cube composed of smaller identical cubes

Periodicity governs that the properties on one face of the cube are also on the opposite face in a statistical sense. The cube periodicity is a simplified representation of the turbulence and may be criticized as unrepresentative of realistic physical turbulence. However, it allows facilitated and rapid computational simulations. The over-simplification and periodicity are kept in mind in this low-order study and are accepted for the fundamental understanding of turbulence. Higher accuracy models are suggested for following works that represent more realistic turbulence in industrial applications.

2.1 Turbulence Interactions

With the specified topic of interest, all the possible combinations of turbulence and wave front case studies are evaluated to direct the research. The combinations are those with and without turbulence fluctuations, a shock wave, and a detonation wave; which total eight case studies are displayed in Table 2.2.

Table 2.2 List of all possible flow interaction case study combinations between turbulence, a shock wave, and a detonation wave

<table>
<tr><th>Case</th><th>Flow Type</th><th>Wave Front</th><th>Interaction Output</th></tr>
<tr><td>1</td><td>Non-turbulent</td><td>No shock wave</td><td rowspan="2">Flow travels with no fluctuations, continues downstream with no change</td></tr>
<tr><td>2</td><td>Non-turbulent</td><td>No detonation wave</td></tr>
<tr><td>3</td><td>Non-turbulent</td><td>Shock wave</td><td>Flow travels with no fluctuations, experiences normal shock relations</td></tr>
<tr><td rowspan="2">4</td><td>Non-turbulent</td><td>Detonation wave</td><td rowspan="2">Flow travels with no fluctuations, experiences normal shock relations, effects of the heat release, and instability of the detonation wave front</td></tr>
<tr><td colspan="2">Unforced–detonation interaction</td></tr>
<tr><td>5</td><td>Turbulent</td><td>No shock wave</td><td rowspan="2">Flow with initial fluctuations continues downstream with no change; fluctuations may die off</td></tr>
<tr><td>6</td><td>Turbulent</td><td>No detonation wave</td></tr>
<tr><td rowspan="2">7</td><td>Turbulent</td><td>Shock wave</td><td rowspan="2">Flow with initial fluctuations experiences normal shock reactions, amplifications and dampening due to the shock–turbulence interaction</td></tr>
<tr><td colspan="2">Shock–turbulence interaction</td></tr>
<tr><td rowspan="2">8</td><td>Turbulent</td><td>Detonation wave</td><td rowspan="2">Flow with initial fluctuations experiences normal shock reactions, effects of the heat release, instability of the detonation front, amplifications and dampening due to the detonation–turbulence interaction</td></tr>
<tr><td colspan="2">Detonation–turbulence interaction</td></tr>
</table>

The first two cases show the base studies where the initial flow has no turbulent fluctuations and there is no interaction with a wave front. The flow travels with no change. In the third case of non-turbulent interaction with a shock wave, the normal shock relations are applied to the flow, as previously shown in Figure 1.7. The shock relations are well-known; this case does not require additional study. However, the fourth case of non-turbulent flow interacting with a detonation wave is a case study worth looking into. The normal shock relations are experienced by the flow, with additional effects of the heat release and the intrinsic instability of the detonation wave. The case study is called the unforced–detonation interaction; it is investigated as a control for the detonation–turbulence interaction. The term “unforced” refers to the flow having no vortical fluctuation forcing.

The fifth and sixth cases have incoming turbulent flows with set fluctuations and no wave interaction. The turbulence continues to travel with no change due to a wave interaction. The only change that may occur is reduction of the fluctuations or turbulence decay. The seventh case is that of shock–turbulence interaction in which the flow experiences the normal shock relations (as in the third case) in addition to effects due to the imposed turbulent forcing. The flow experiences amplifications and dampening. The case will be investigated and the downstream behavior will be studied in more detail. The eighth and final case is that of detonation–turbulence interaction in which the flow experiences the shock relations as in the third and fourth cases. In addition, as in the fourth case, the flow experiences the effects of the heat release and the instability of the detonation wave front. The flow in the detonation–turbulence interaction experiences amplification, dampening, and other behavior that will be further

investigated. It is expected that there will be a mutual interaction between the detonation wave and the turbulence (Massa, 2011a)

Thus, from the list in Table 2.2, the three case studies that will be the center of this work's research are the unforced–detonation, shock–turbulence, and detonation–turbulence interactions. The unforced–detonation case is studied to compare against the detonation–turbulence interaction as a control eliminating the turbulent fluctuations' effects.

2.2 Shock–Turbulence Interactions

Shock waves and turbulence are completely disparate gas dynamics phenomena. Understanding the interaction of turbulence with shock waves is essential for applications (Lee, 1992) in high–speed flows around aerodynamic bodies and through propulsion systems (Lele, 2009). Much research has been conducted in the study of shock–turbulence interactions, shown in Figure 2.3, where the incoming turbulence with imposed fluctuations interacts with a moving or stationary shock wave and continues to propagate downstream past the wave front.

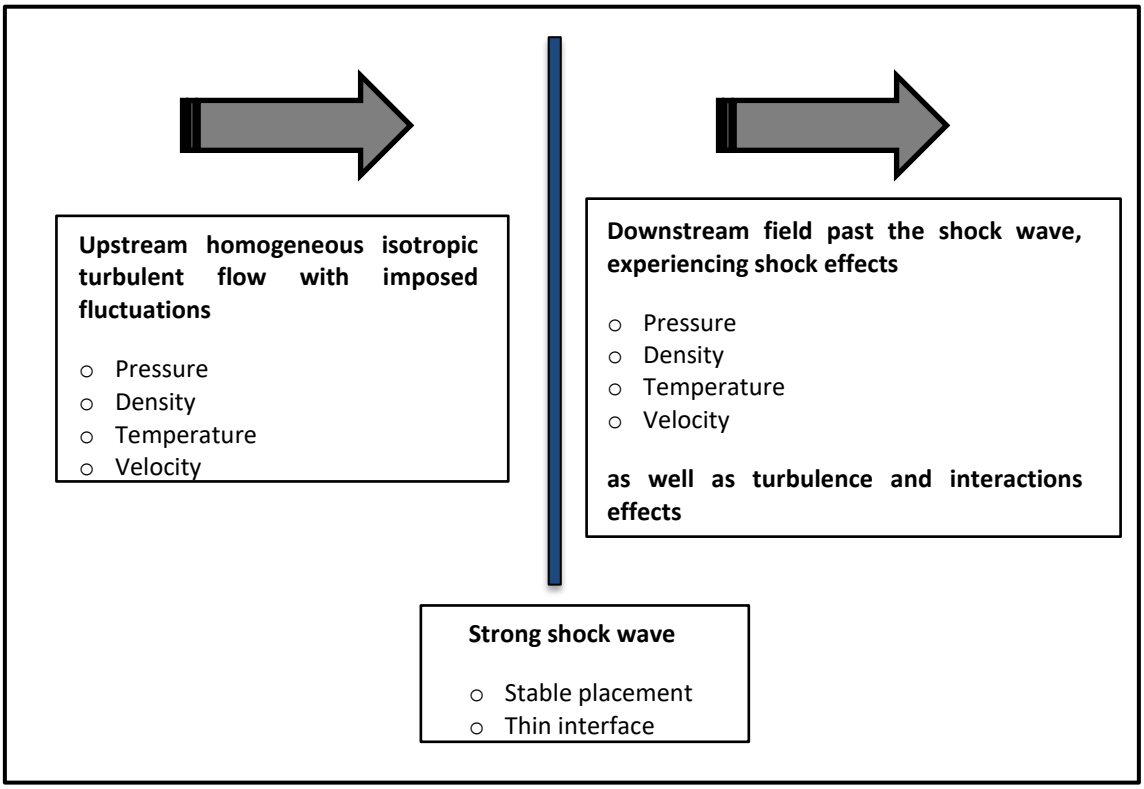

Figure 2.3 Schematic view of a shock–turbulence interaction as adopted from Sagaut (2008)

Shock–turbulence interactions have been studied theoretically (Ribner, 1987, Gavrilyuk, 2006), numerically (Zang, 1984, Lee, 1992a, Lee, 1997, Mahesh, 1997, Bermejo-Moreno, 2010, Grube, 2011, Larsson, 2013), and experimentally (Barre, 1996, Andreopoulos, 2000, Agui, 2005). The idealized homogeneous isotropic turbulence interaction with a shock wave was studied by Andreopoulos (2000) who found that the interaction effects were mutual with the shock exhibiting unsteadiness and deformation following the turbulence interaction. Computational simulation studies of shock–turbulence interactions show amplification of the turbulent kinetic energy, change in turbulent length scales across the shock, and distortion of the shock (Lele, 2009). Shock–turbulence interaction visualizations by Lele (2009), Figure 2.4, depict the turbulent eddies through the interaction and the shock front wrinkling.

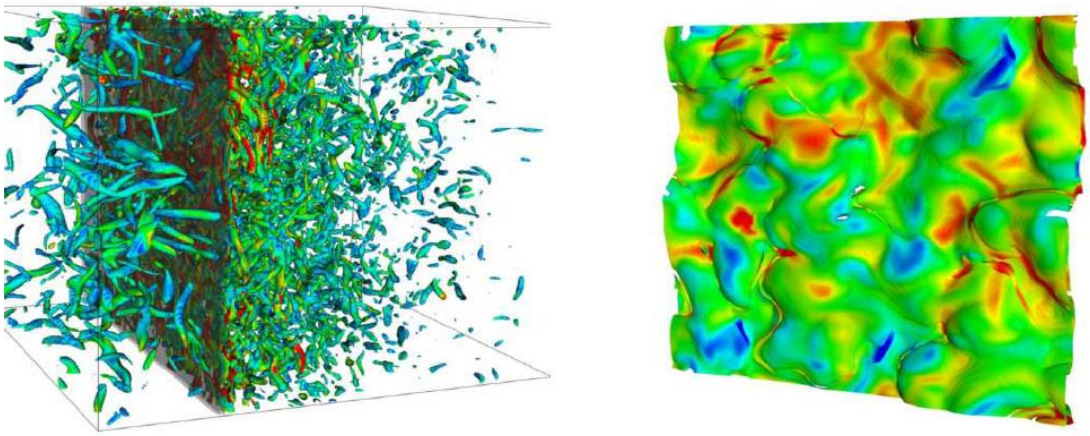

(a) (b)

Figure 2.4 Shock–turbulence interaction: (a) turbulent eddies (green structures, flowing from left to right) are compressed and amplified upon passing through a stationary shock (thin blue sheet) (b) strongly wrinkled shock in the nonlinear regime with strong incoming turbulence, with colors indicating regions of high (red) and low (blue) streamwise velocity (Lele, 2009)

While the interaction of homogenous isotropic turbulence is referred to as a canonical problem in the study of shock–turbulence interactions (Lele, 2009), the interest shifts to the role of the detonation structure on the amplification of the turbulence emanating from a detonation wave (Massa, 2011c) when considering reactions with heat release.

When shock–turbulence interaction models were previously used to analyze disasters such as explosions in coal mines, grain silos, oil and gas industries, and power plants, the causes of the explosions remained mysterious. That is because the models do not take the chemical reaction into consideration. The detonation–turbulence interaction studies add the complexity of the heat release making such models more accurate for disaster mitigation techniques. The detonation–turbulence interaction studies are employed to establish an understanding of turbulence effects on detonation wave stability and the effects of the heat release. The properties these interactions embody reveal important turbulent flow characteristics such as the mutual effects between the turbulence and the intrinsic detonation wave instability.

2.3 Detonation–Turbulence Interactions

With the added complexity of heat release through combustion (Massa, 2009), shock–turbulence interactions evolve into detonation–turbulence interactions. Detonation–turbulence interactions are employed to establish an understanding of the effect of heat release on the propagation of the turbulent flow, the effects of the detonation inherent length scale, and the turbulence effects on wrinkling of the inherently unstable detonation front. Shown in Figure 2.5, a detonation–turbulence interaction occurs when incoming flow with set fluctuations interacts with a traveling or stationary detonation wave and continues downstream of the wave front.

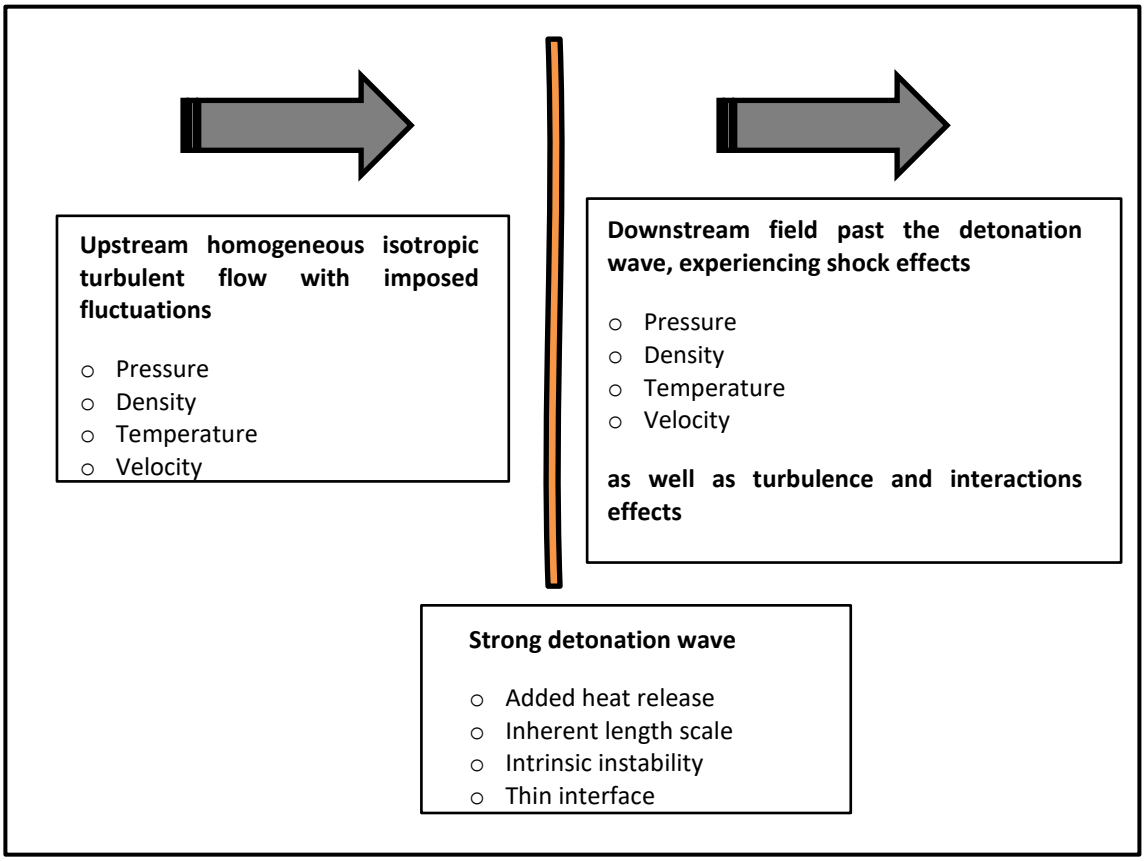

Figure 2.5 Schematic view of a detonation–turbulence interaction as adopted from Sagaut (2008)

While much research has been conducted in the topic of shock–turbulence interactions, there are very limited studies in the field on detonation–turbulence interactions (Massa, 2011a). Detonation–turbulence interactions add the complexity of the presence of an exothermic reaction, the inherent length scale associated with the detonation structure, and the intrinsic instability of the detonation front (Massa, 2011a). The detonation–turbulence interaction of weak homogeneous isotropic turbulence has been studied by Jackson (1993). The single-step Arrhenius law was adapted in detonation–turbulence studies by Short (1998), Jaberi (2000), and Massa (2009, 2011a) to simulate the effects of chemistry on turbulence. Massa extended Jackson's studies (2011c) by considering the effects of the heat release length scale. Conceptual findings of detonation–turbulence interaction studies, such as the instability of the detonation wave (Massa, 2011a), can be utilized to better understand the phenomena occurring during explosions, in the development of detonation engines, and in the safe handling of gaseous fuels such as hydrogen. Detonation–turbulence interaction visualization by Chauhan (2011) shows vortex stretching in detonation–turbulence interaction with high heat release. The visualization, Figure 2.6, depicts small-scale flow motion and detonation wave instability.

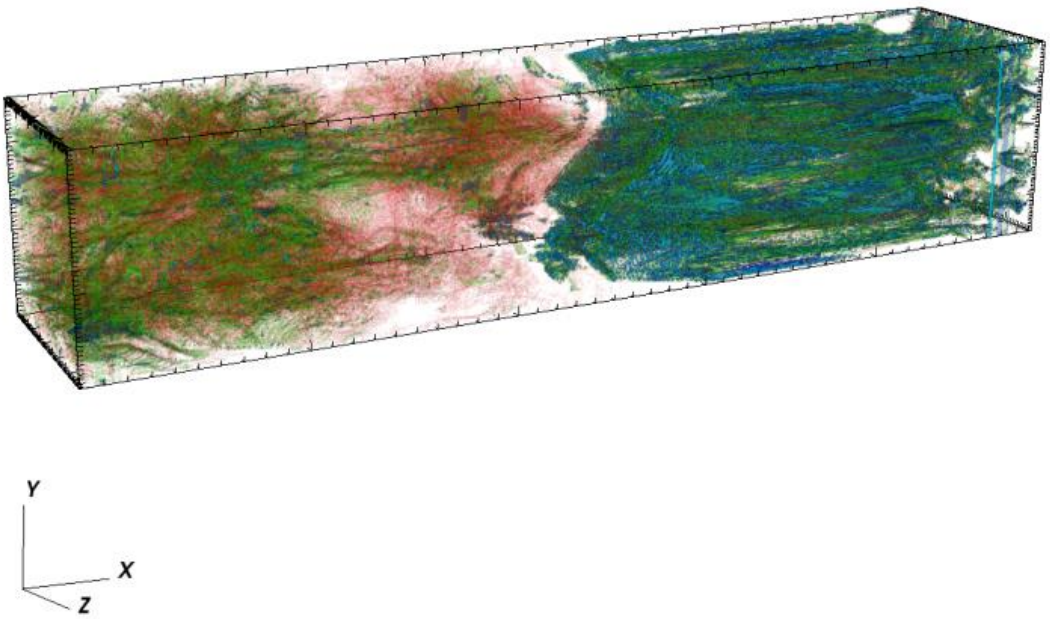

Figure 2.6 Detonation–turbulence interaction: small-scale flow motion showing intense straining and rotation (red) and energy dissipation (green) where the flow travels from left to right, visualization utilizes VisIT through the Texas Advanced Computing Center resources (Chauhan, 2011)

2.4 Framework of turbulence interaction research

The theoretical framework of this study begins with the evaluation of the turbulence field governing equations. The homogeneous isotropic turbulence field behavior is governed by the Navier–Stokes equations. The five coupled non-linear partial differential equations in space and time are the laws of conservation of mass (continuity), conservation of momentum (in x, y, z), and conservation of energy. Additional assumptions of isotropy and imposed fluctuations are specified. The problem lacks closure with five governing equations and six dependent variables: velocity in three spatial coordinates (u, v, w), pressure, temperature, and fluid density. The solution requires an additional equation of state and constitutive relations for viscosity and thermal conductivity for non-reactive systems. The specific heats at constant pressure and at constant volume are defined as well as their ratio γ. All the dependent variables are expressed in terms of the independent variables of space and time (x, y, z, t). Solving the conservation of mass and momentum equations for particular boundary conditions allows the prediction of velocity and pressure information in the given geometry. Solving the energy equation leads to the prediction of the flow field temperature. With increased complexity of the geometry, the equations need to be solved numerically (Pope, 2000).

2.5 Turbulence Modelling and Simulation Techniques

Turbulence models are essential to close forms of time-dependent Navier–Stokes governing equations for compressible or incompressible flows in two or three–dimensional form (Cebeci, 2004). The equations for turbulent motion are well known. Thus, a sufficiently large computer should be able to produce sets of possible solutions (Liepmann, 1979). Several methods of modelling and simulation have been developed over the years to enhance our grasp of turbulence and facilitate flow measurement, analysis, and prediction. It is an interpolation procedure to connect information from experimental setups (Liepmann, 1979). Turbulence simulations are not meant to capture physical phenomena but to perform controlled studies that allow better insight, scaling laws, and turbulence models. The geometry of the studied turbulence is generally not complex as in real configurations. Industrial applications of the turbulence problem require complex geometries that render the idealized simplified solutions of the governing flow equations insufficient. In turbulence simulations, the equations are solved for velocity in time and position for a single occurrence of the turbulence; while in turbulence models, the equations are solved for average velocity, among other flow properties (Pope, 2000). The difficulty in applying turbulence modelling techniques lies in the non-linearity of the governing equations (Liepmann, 1979). Turbulence models and simulation techniques are divided into four main types: Reynolds-averaged Navier–Stokes (RANS) based equations, large eddy simulation, detached eddy simulation, and direct numerical simulation; they are summarized in Figure 2.7.

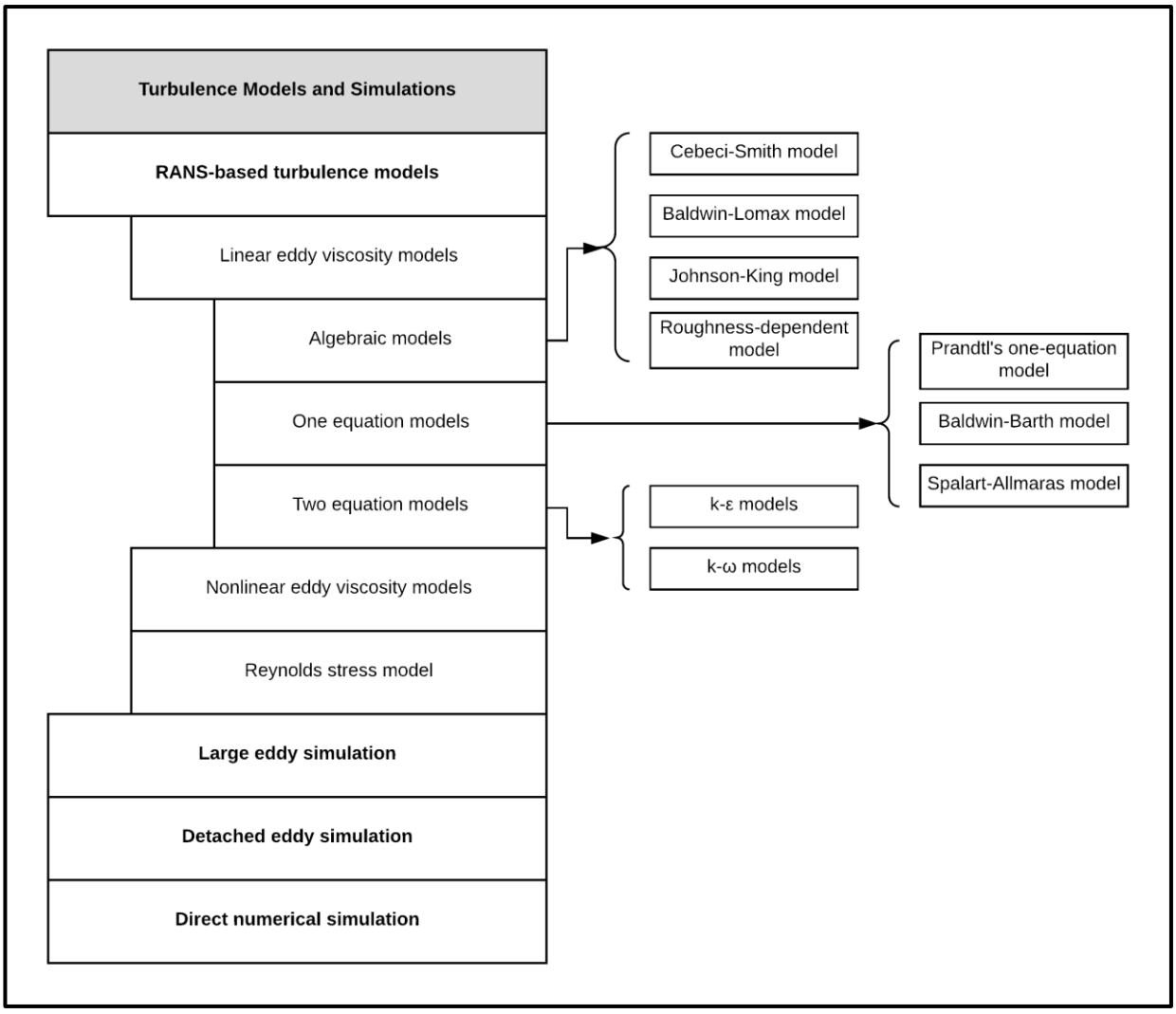

Figure 2.7 Turbulence models and simulation tools as adopted from CFD online (2009)

RANS-based turbulence models are used to compute the Reynolds stresses through eddy viscosity and Reynolds stress models (CFD online, 2009) by averaging the Navier–Stokes parameters. Linear eddy viscosity models are algebraic, one and two equation models. Large eddy simulation is a technique for generating turbulent flows following the Kolmogorov (1941) theory of self–similarity (Muller, 2014). In large eddy simulation, the large scales are considered to be flow dependent while the small scales are universal. Thus, the large scales are resolved while the small scales are modeled. Large eddy simulation faces difficulties in the near-wall regions leading to the development of the detached eddy simulation method that is a hybrid between RANS-based turbulence models and large eddy simulation (Spalart, 1997). Finally, in direct numerical simulation, the Navier–Stokes equations are solved numerically and all spatial and temporal scales are resolved with no need for turbulence modelling (Nagarajan, 2009a, Coleman, 2010).

2.6 Research Approach

Turbulence simulations give approximate solutions in space and time for the non-linear Navier–Stokes equations, while turbulence models are used to give solutions for mean quantities of the dependent variables. For this case study of homogeneous isotropic turbulence aiming to improve our understanding of turbulent structures, the accuracy of the simulations is favored over the average modelling outcomes. Direct numerical simulation and also large eddy simulation can be applied to study the physics of simple turbulent flows at moderate Reynolds numbers. However, it is found that direct numerical simulation provides a direct approach to solving the Navier–Stokes equations (Pope, 2000), acquiring the flow data for turbulence analysis, and resolving all the length and time scales. It is a turbulence simulation technique that allows the numerical solution of the flow governing equations without resorting to turbulence modelling while capturing the whole range of spatial and temporal scales (Pope, 2000, Nagarajan, 2009a, Massa, 2011a). Direct numerical simulation is utilized as an idealized simulation in this study. Large eddy simulation is recommended as a following research step for more complex geometry and realistic turbulence applications.

Pope (2000) suggests a list of factors to be considered when evaluating the different simulation and modelling tools. The factors are summarized in Table 2.3 starting with the level of description of the tool.

Table 2.3 Factors for appraising turbulence modelling and simulation tools as adopted from Pope (2000)

Appraising Factors	Details
1. Level of description	High when a complete characterization of the turbulence is present
2. Completeness	Complete when constituent equations are free from flow-dependent specifications
3. Cost	Dependent on time and computational power requirements
4. Ease of use	Difficulty is increased with non-stationarity, reduced with use of boundary layer equations
5. Range of applicability	Complete model does not make implicit assumptions about flow geometry
6. Accuracy	Compared to experimental work, often computational models possess numerical errors dominated by spatial truncation error

A high level of description is achieved when the tool completely characterizes the turbulence phenomenon. The simulation tools have a level of description that is higher than modelling tools since they provide instantaneous velocity information and not average velocity values. The second appraisal factor is the completeness of the tool. A turbulence simulation is considered complete when the constituent equations are independent of the flow specifications. Turbulence models do not give information on

probability density functions of the velocity, single-point correlations, or turbulence structures. Thus, they are incomplete due to flow dependence. The cost of the tool is the third factor taken into account. The cost increases with time and computational power required for running the tool. Computational cost of direct numerical simulation increases with the cube of Reynolds number. Code development with certain boundary conditions depends on the complexity of the geometry and the software/algorithms used. The code execution depends on the computational resources available. The ease of use of the tool is the next factor considered. The difficulty increases with non-stationarity of the flow and can be reduced by employing boundary layer equations. The fifth factor considered is the range of applicability of the tool. A complete model will not make implicit assumptions about the flow geometry and thus becomes more applicable. Direct numerical simulation is applicable in low to moderate Reynolds number flows. Finally, the accuracy of the tool is appraised. Direct numerical simulation gives approximate solutions to the governing equations that, when compared to experimental data, will have idealized values but show numerical and spatial truncation errors.

Direct numerical simulation studies of homogeneous isotropic turbulence have been documented and published over the past 20 years (Moin and Mahesh, 1998, Massa, 2011a). A direct numerical simulation code is written for this research using references from previous research work in the aspects of flow description, setup of the Navier–Stokes equations, initial and boundary conditions, shock wave structure, and chemical reaction. MATLAB is the coding environment selected for its facilitated coding, analysis, and visualization tools. The code is run through personal and high-performance computers which require memory allocations and computational power. However, these

technical challenges are manageable in this age of computational advancement and through allocations from the University of Texas at Austin Texas Advanced Computing Center (TACC). The MATLAB direct numerical simulation code is applied for the turbulence periodic cube, unforced–detonation interaction, shock–turbulence interaction, and detonation–turbulence interaction studies. Direct numerical simulation is performed as a technique to efficiently acquire data sets for analysis. Using this methodology, a model is built. Hence all the acquired data are strictly computer generated. The approach has several advantages as well as disadvantages.

The advantages of direct numerical simulation over other modelling and simulation tools include:

- The absence of approximations, exact inputs give exact outputs
- The simulation captures broadband spatial and temporal scales
- The chemical properties are simplified, where no real reactants are simulated and no real gases are used

Some disadvantages of utilizing direct numerical simulation:

- Heavy computational requirements for large data sets, longer run time
- The simulation does not produce realistic flow due to heavier computational requirements

2.7 Research Objectives

After surveying the literature and evaluating the different turbulence modelling and simulation techniques, the doctoral research project is outlined.

- **Develop a MATLAB direct numerical simulation tool**. The tool is employed to generate a periodic cube of homogeneous isotropic turbulence and the three interaction case studies: unforced–detonation, shock–turbulence, and detonation–turbulence. Output data from the case studies are collected for analysis.
- **Statistically analyze the properties of homogeneous isotropic turbulence**. The direct numerical simulation computational outputs are analyzed for ensemble velocity averages, root mean square averages, turbulent kinetic energy, and Reynolds stresses. In the interaction case studies, the individual and mutual effects of the turbulence, the shock wave, and the unsteady detonation wave are investigated.
- **Extend shock–turbulence and detonation–turbulence interaction studies to show flow behavior downstream of the front.** While previous studies have shown the effects on the flow velocity fluctuations across the shock, they missed the non-linear dynamics of the energized and highly anisotropic flow downstream of the front. The simulated cuboid computational domain allows the turbulence to travel towards the shock or detonation wave front, interact with the wave, and propagate downstream. Enough space is provided downstream for the flow to experience the direct effects of the shock and the heat release in the near zone then return to isotropy in the far field. The interaction case studies' velocities are

visualized throughout the computational domain to depict different flow behavior and wave properties.

- **Investigate the flow physics of numerically generated turbulence**. The velocity fluctuations in the turbulence are generated numerically using a random number generator algorithm, keeping in mind the statistical property of turbulence velocity skewness factor which defines fully-developed turbulence. The long-standing turbulence velocity skewness factor definition is determined, confirmed, and extended to include components acquired computationally, which could not have been obtained experimentally before.

2.8 Research Contribution Summary

The original contributions of this research work are the (1) development of a direct numerical simulation tool producing simple low-order models of a turbulence periodic cube, unforced–detonation interaction, shock–turbulence interaction, and detonation–turbulence interaction case studies, (2) extending the detonation–turbulence interaction studies to cover dynamics downstream of the wave front, (3) challenging the long-standing turbulence velocity skewness factor definition by increasing the degrees of freedom to evaluate the change of the flow velocity in all three Cartesian coordinates.

3. Direct Numerical Simulation Code Desciption

In building the tool for direct numerical simulation of a simple low-order turbulence field, the simplified geometry of the periodic cube, introduced in Figure 2.2, is selected. This simplified geometry has been used by previous researchers for examining the fundamental structures of turbulence. The turbulence periodic cube is, theoretically, divided into an infinite number of smaller identical cubes called unit cubes in this study, and is shown in Figure 3.1.

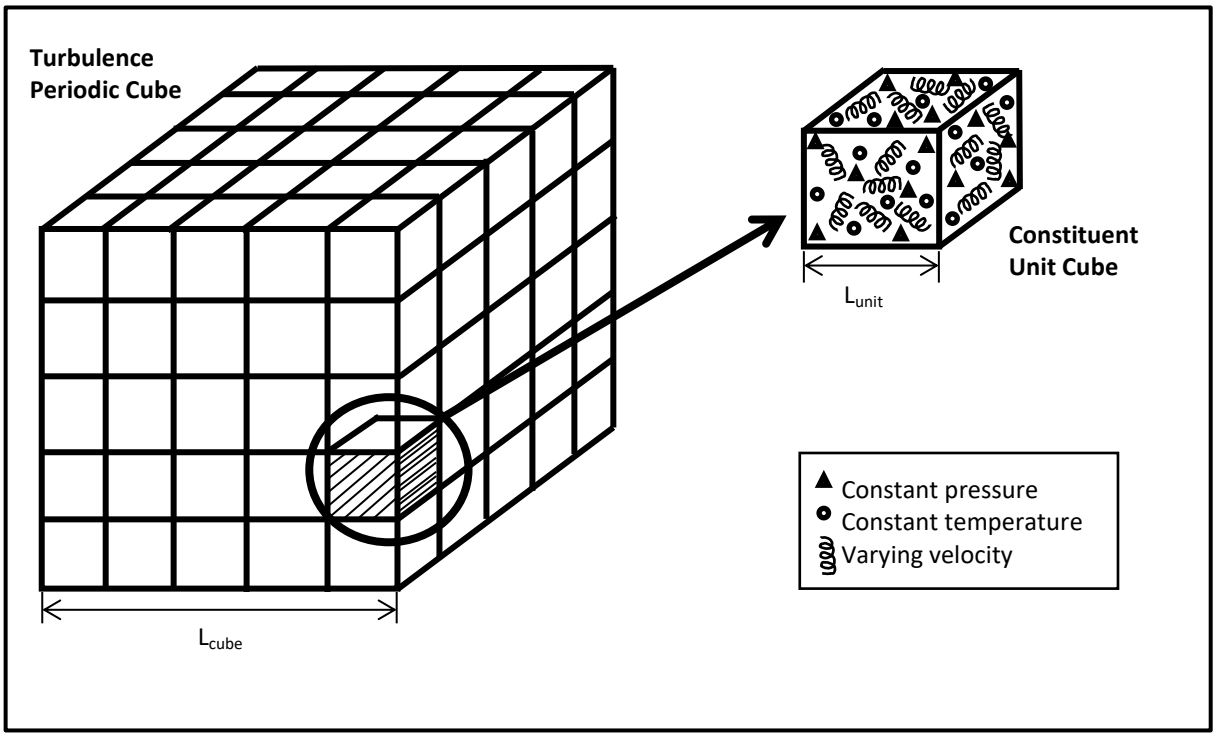

Figure 3.1 Turbulence periodic cube and unit cube visualizations as adopted from Davidson (2004)

The periodicity condition states that whatever happens on one face of the cube happens on the opposite face (Davidson, 2004). The turbulence periodic cube is a simplified, idealized form of turbulence in which the periodicity is numerically imposed and the fluid field is not representative of naturally occurring turbulence. It is a simplification that is accepted for this low-order study of turbulence physics and can be

extended to cover more realistic turbulence properties in following studies. This simplification leads to more efficient and faster numerical algorithms in the computational simulations. Efficient simulations, thus, come at the cost of artificial periodicity.

Cube Size and Resolution

Figure 3.1 presents the periodic cube geometry, as described by Davidson (2004). The cube on the left is the periodic cube of homogeneous isotropic turbulence. It is composed of many smaller cubes, displayed on the right. The size of the smaller cube, referred to as the unit cube, is one unit of measure of distance in the computational setup (since the computational domain does not have a physical length scale). The size of the periodic cube is based on the number of unit cubes in it. The legend shows that each unit cube carries information on the turbulence pressure, temperature, and velocity properties. In this particular study of vortically forced turbulence, the velocity properties vary while the pressure and temperature are held constant in every unit cube and in the periodic larger cube. Each unit cube is a unique turbulence case, but the information carried in the unit cubes are considered to be identical (within a certain confidence level). In this study, limited by computational power and runtime, the turbulence periodic cube consists of 163 units in each coordinate. The turbulence cube, thus, is a $163 \times 163 \times 163$ matrix consisting of $4{,}330{,}747$ unit cubes each carrying a set of properties: temperature, pressure, and velocity fluctuation information. The size of the unit cubes sets the resolution of the code and limits the computations. The grid must be small enough to capture the smallest structure within the turbulence. When at least three

points of the structure are captured, the smallest eddy is resolved, as shown in Figure 3.2.

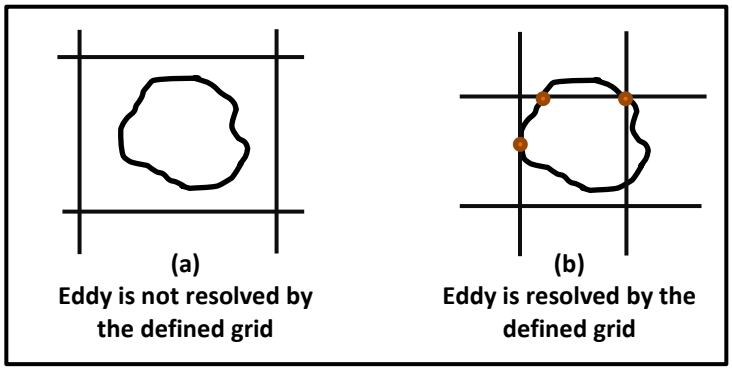

Figure 3.2 Grid sizing diagram showing the (a) smallest eddy not resolved and (b) smallest eddy resolved examples

In this case, from 1 to $1/163$ grid can be resolved in every coordinate of the cube and the grid is spatially regular. The smaller the grid required to capture the eddy structures, the higher the computational requirements. The same applies to the simulation's time resolution where the shortest eddy life-span must be captured to resolve all the data in the time scale.

Length and Time Scales

The fluid in this study is a perfect gas that acts as air in atmospheric conditions of standard temperature and pressure. Unlike air whose ratio of specific heats γ is 1.4, this fluid's γ is set to 1.2 to allow matching with the Chapman–Jouguet detonation speed of stoichiometric methane/air and propane/air at 1800m/s (Massa, 2011a). These conditions are representative of the detonation and the flow speed of interest in this study. The fluid has a mean time between the successive collisions of molecules under atmospheric conditions of 10^{-10}s, average spacing between molecules of $x = 3 \times 10^{-9}$m, and mean free path $\lambda_0 = 6 \times 10^{-8}$ m (Pope, 2000). The generated turbulence is

treated as a continuum with the smallest geometric length scale of $l = 6.135 \times 10^{-3}$m acquired from the grid resolution of 1 to $1/163$. The imposed vortical fluctuations reach up to 51 m/s, corresponding to 1 % of the desired flow speed and up to three standard deviations away from the zero mean. The time scale, thus, is $t = 1.20 \times 10^{-4}$ s which is two orders of magnitude larger than the mean time of constituent molecular collisions. The length scale is four orders of magnitude larger than the intermolecular spacing. The non-dimensional Knudsen number

$$Kn = \frac{\lambda_0}{l} \tag{3.1}$$

for this fluid is calculated as 9.78×10^{-6}. This validates the continuum approach which is applicable when the Knudsen number is much smaller than unity; $Kn \ll 1$ (Pope, 2000).

3.1 Governing Equations

Now that the geometry is clearly defined and the continuum approach is verified, the turbulence governing equations are stated. The turbulence cube is that of a perfect gas with ratio of specific heats $\gamma = 1.2$, a specific heat at constant pressure $c_p = 1005$ J/kg·K, and imposed vortical fluctuations at standard temperature $T_0 = 293.15$ K and pressure $P_0 = 1$ atm. The Navier–Stokes equations are the laws used to describe the turbulence properties through the conservation of mass, momentum, and energy expressions.

The Navier–Stokes Equations

The governing equations are based on the physical laws describing the moving fluid (Currie, 2013) and are the foundation of the numerical simulation of the homogeneous isotropic turbulence in this study.

The conservation of mass leads to the continuity equation, which implies the flow velocity is continuous, namely,

$$\frac{\partial \rho}{\partial t} + \frac{\partial}{\partial x_j}\left(\rho u_j\right) = 0 \tag{3.2}$$

In the conservation of mass equation, ρ is the fluid density calculated using the ideal gas law,

$$\rho = \frac{P}{RT} \tag{3.3}$$

where the universal gas constant is $R = 0.0821$ L·atm /mol·K. The variable t, in Equation (3.2) represents time while x_j and u_j represent the tensor notation of the three Cartesian

coordinates $(\mathrm{x}, \mathrm{y}, \mathrm{z})$ and velocity components $(\mathrm{u}, \mathrm{v}, \mathrm{w})$, respectively. The partial derivatives, with respect to time and space, are evaluated using the central differencing method (here and in all the following equations including partial derivatives). Central differencing is employed to find the variation of a property between adjacent unit cubes: (1) $\mathrm{i}-1$, (2) i,and (3) $\mathrm{i}+1$ as shown visually in Figure 3.3.

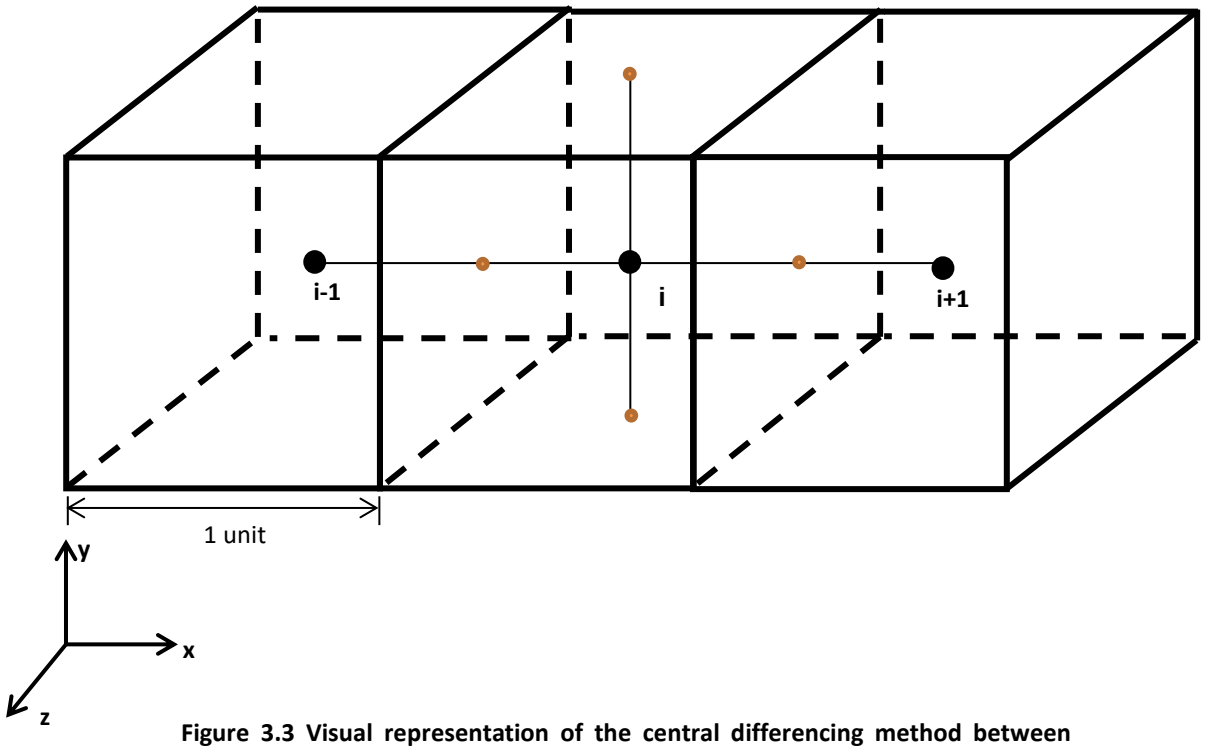

Figure 3.3 Visual representation of the central differencing method between adjacent cells in a cube structure

The variation of any fluid property in a unit cube, say u velocity in cube i, is found by taking the difference of the velocity in the unit cube after, $i+1$, and the unit cube before, $i-1$, then dividing by twice the time or spatial increment in the flow travel direction. The time increment is the difference of the time at $i+1$ and $i-1$ over the total time of travel covering the length of the three unit cubes. The spatial increment is calculated using the length occupied by each unit cube divided by the total length of the cube side in the direction of interest. In Figure 3.3, the spatial increment dx is $\frac{2}{3}$ because

$i-1$ is assigned as zero in the x-direction, i is one, and $i+1$ is two. The total length of the side is three units. The central differencing method for the u velocity gradient in the x-direction is thus,

$$\frac{du}{dx} \approx \frac{u(i+1)-u(i-1)}{2dx} \tag{3.4}$$

The conservation of momentum is a relationship based on the Newton's second law of motion applied to an element of fluid:

$$\frac{\partial}{\partial t}(\rho u_i) + \frac{\partial}{\partial x_j}\left(\rho u_i u_j + P\delta_{ij} - \sigma_{ij}\right) = 0 \tag{3.5}$$

The partial derivatives are evaluated using the central differencing method shown in Equation (3.4). The velocity vectors u_i and u_j both represent the three velocity components in the Cartesian coordinates for $\{i,j\} = 1,2,3$. The fluid pressure P is constant in this study, while Kronecker's delta

$$\delta_{ij} = \begin{cases} 1, i = j \\ 0, i \neq j \end{cases} \tag{3.6}$$

is either zero or unity depending on i and j. The stress tensor is

$$\sigma_{ij} = \frac{\mu}{Re}\left\{\left[\left(\frac{\partial}{\partial x}u\right)i + \left(\frac{\partial}{\partial y}v\right)j + \left(\frac{\partial}{\partial z}w\right)k\right] + \left(u\frac{\partial}{\partial x} + v\frac{\partial}{\partial y} + w\frac{\partial}{\partial z}\right) - \frac{2}{3}I_{33}\left(\frac{\partial u}{\partial x} + \frac{\partial v}{\partial y} + \frac{\partial w}{\partial z}\right)\right\} \tag{3.7}$$

In Equation (3.7), μ is fluid viscosity and is calculated using Sutherland's law for an ideal gas (Sutherland, 1893) in terms of temperature.

$$\mu = \mu_0 \frac{T_0 + C}{T + C} \left(\frac{T}{T_0}\right)^{3/2} \tag{3.8}$$

The constant C is set to 120 K based on the fluid properties. The input viscosity μ_0 and temperature T_0 are employed in the Sutherland's viscosity calculation. The non-dimensional Reynolds number is

$$Re = \frac{\rho u l}{\mu} = \frac{u l}{\upsilon} \tag{3.9}$$

defined with l being the length that the turbulent fluid travels, and υ the kinematic viscosity. The 3×3 identity matrix is:

$$I_{33} = \begin{bmatrix} 1 & 0 & 0 \\ 0 & 1 & 0 \\ 0 & 0 & 1 \end{bmatrix} \tag{3.10}$$

The conservation of energy equation is the application of the first law of thermodynamics to a fluid field (Currie, 2013). The thermal relation is expressed as:

$$\frac{\partial E_t}{\partial t} + \frac{\partial}{\partial x_j}\left(E_t u_j + u_j P + q_j - u_i \sigma_{ij}\right) = 0 \tag{3.11}$$

While most of the other terms have been previously defined, the total energy E_t is calculated for the fluid.

$$E_t = \frac{P}{\gamma - 1} + \rho\left(\frac{{u_i}^2}{2} - \tilde{Q}\lambda\right) \tag{3.12}$$

The non-dimensional heat release $\tilde{\mathrm{Q}}$ and reaction progress λ terms vanish due to absence of heat release in shock–turbulence interaction. In the case of detonation–turbulence interaction, however, the heat release Q is calculated and normalized (Massa, 2011a).

$$Q = \frac{\tilde{Q}}{P_0/\rho_0} = \frac{\gamma(M^2 - 1)^2}{2M(\gamma^2 - 1)} \tag{3.13}$$

The reaction progress λ is a variable used to indicate the beginning of the reaction $(\lambda = 0)$ and the end of the chemical reaction $(\lambda = 1)$. In Equation (3.13), the Mach number M is defined as the ratio of the fluid flow velocity in the direction of interest to the speed of sound under the same conditions.

$$M_i = \frac{u_i}{a} \tag{3.14}$$

The speed of sound at the given conditions is

$$a = \sqrt{\gamma \mathrm{R}_{gas} T} \tag{3.15}$$

where the universal gas constant $R = 0.0821$ L·atm /mol·K is related to the specific gas constant and the gas molar mass.

$$R_{gas} = \frac{R}{Mm_{gas}} \tag{3.16}$$

From the conservation of energy equation, the heat flux q_j is

$$\mathrm{q_j} = -\frac{\gamma}{\gamma - 1}\frac{\mu}{\mathrm{RePr}}\nabla \mathrm{T} \tag{3.17}$$

where the Prandtl number is defined as

$$Pr = \frac{c_p \mu}{K} \tag{3.18}$$

and the fluid's specific heat at constant pressure c_p is 1005 J/kg·K. The fluid thermal conductivity K is found from a trend study of the variation of air thermal conductivity with change in temperature (Bouteloup, 2018), shown in Figure 3.4.

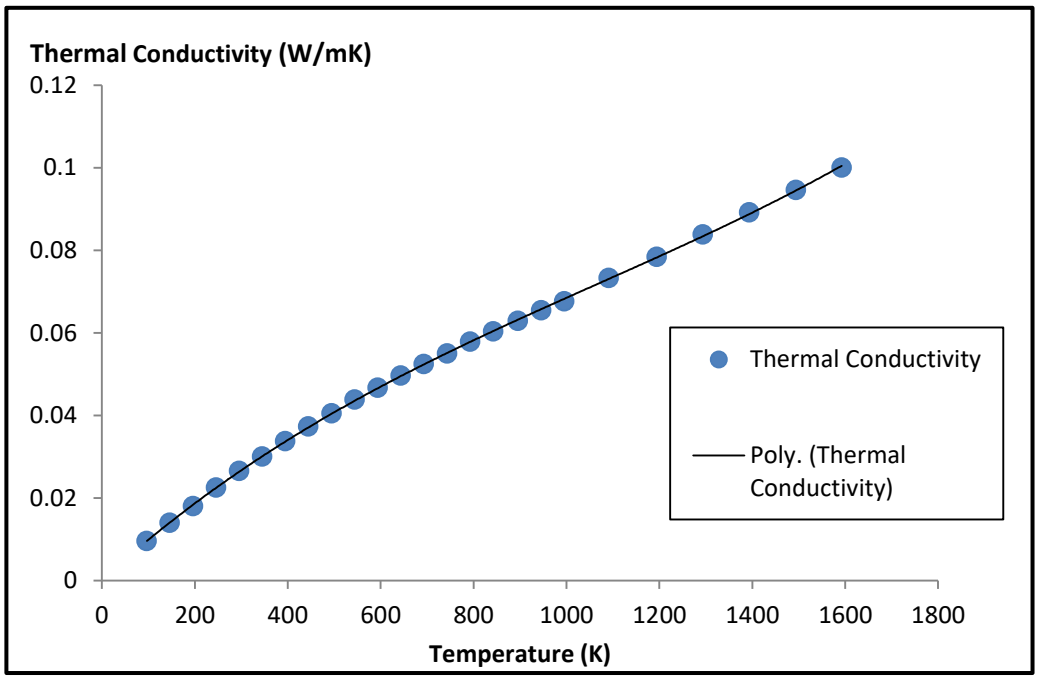

Figure 3.4 Thermal conductivity of air vs. temperature plot using data points from Bouteloup (2018)

The best cubic polynomial fit is used with the temperature at different points of the fluid flow to determine the thermal conductivity. The del operator ∇, used with the fluid temperature in the heat flux equation, is elaborated for scalar and vector quantities in Appendix B.

Normal Shock Relations

In the turbulence cube, the smallest length is set to be the unit of measure in the computational setup. A stationary normal shock wave, even though infinitesimally thin theoretically, in this application is set to occupy unit length in computational coding. The normal shock relations are used to define the post-shock pressure, density, temperature, and Mach number namely

$$\frac{P_{ps}}{P} = \frac{2\gamma M^2 - (\gamma - 1)}{\gamma + 1} \tag{3.19}$$

$$\frac{\rho_{ps}}{\rho} = \frac{(\gamma + 1)M^2}{(\gamma - 1)M^2 + 2} \tag{3.20}$$

$$\frac{T_{ps}}{T} = \frac{[2\gamma M^2 - (\gamma - 1)]\big((\gamma - 1)M^2 + 2\big)}{(\gamma + 1)^2 M^2} \tag{3.21}$$

$$M_{ps} = \left[\frac{(\gamma - 1)M^2 + 2}{2\gamma M^2 - (\gamma - 1)}\right]^{1/2} \tag{3.22}$$

using the properties of the flow ahead of the shock wave (White, 2011). A representation of the shock front, incoming flow, and flow traveling past the shock wave is shown in Figure 1.7. The normal shock relations are applicable to both shock–turbulence and detonation–turbulence interaction case studies. In the detonation–turbulence interaction, an additional heat release relation is defined.

Single-Step Arrhenius Law for Heat Release

The thermodynamic properties of the detonation wave can be calculated by detailed chemical reactions or single-step reaction mechanisms. For this low-order study of homogeneous isotropic turbulence, the chemistry of the detonation–turbulence interaction case study is simplified. The Arrhenius law is used to describe the single-step mechanism of heat release. The Arrhenius law reaction rate

$$r(T) = k_0 e^{-\frac{\tilde{E}}{T}} \tag{3.23}$$

depends on temperature. The pre-exponential factor that sets the temporal scale is $k_0 = 1.2$ for this fluid's properties, as has been previously studied by Massa (2011a). The activation energy E is normalized by the ratio of input pressure to density.

$$E = \frac{\tilde{E}}{P_0/\rho_0} \tag{3.24}$$

The activation energy is found using the reference activation energy vs. heat release diagram, Figure 3.5, from Massa's (2011a) detonation–turbulence interaction study for a perfect gas with $\gamma = 1.2$. The heat release factor is previously calculated in Equation (3.13).

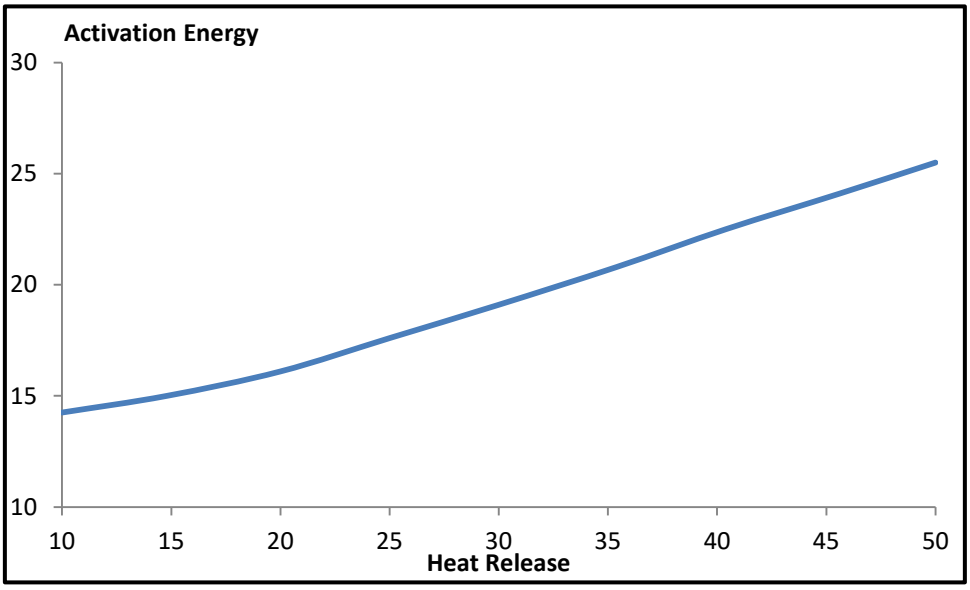

Figure 3.5 Activation energy vs. heat release plot for a detonation–turbulence interaction based on work by Massa (2011a)

This concludes the specification of the numerical simulation governing equations. The direct numerical simulation tool development is discussed next.

3.2 Tool Development

Direct numerical simulation is the turbulence computational method chosen for this study as it provides a direct approach to solve the governing equations and acquire data for analysis. In direct numerical simulation, all the spatial and temporal scales are resolved with no need for a turbulence model. MATLAB is the software selected for the direct numerical simulation coding. Its desktop environment allows design of the fluid geometry and behavior, iteration of the governing equations, data analysis, and visualization. The MATLAB programming language allows coding in matrix and array mathematics directly (Mathworks, 2018a) and is compatible with the University of Texas at Austin's TACC supercomputers. Two direct numerical simulation codes are developed: (1) to generate the turbulence periodic cube, (2) to generate the three interaction case studies of unforced–detonation, shock–turbulence, and detonation–turbulence interactions. The generated turbulence periodic cube is used as turbulent flow input in the interaction case studies. It is important to note that the turbulence flow input velocity of interest in this study corresponds to Mach 5.5. This high speed is selected because in the detonation–turbulence case study, such a speed allows the heat release parameter to sustain an adiabatic flame, without gaining or losing heat, as in small paraffins in stoichiometric air (Massa, 2011a). The output data for analysis is deemed sufficient based on trade studies by Chauhan (2011).

A code outline is presented for each of the two direct numerical simulations in Figure 3.6 and Figure 3.7, where the flowchart shape references are documented in Appendix C. The code components are discussed in detail in the following two sections.

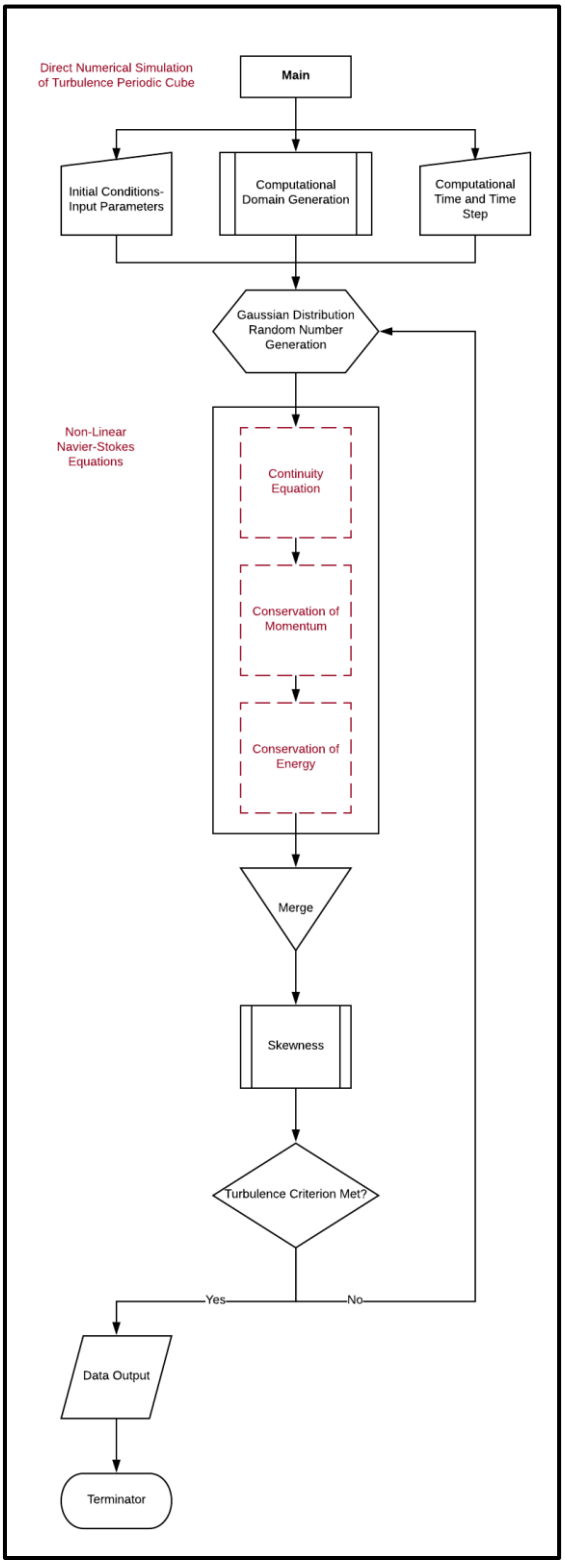

Figure 3.6 Direct numerical simulation code outline for the turbulence periodic cube

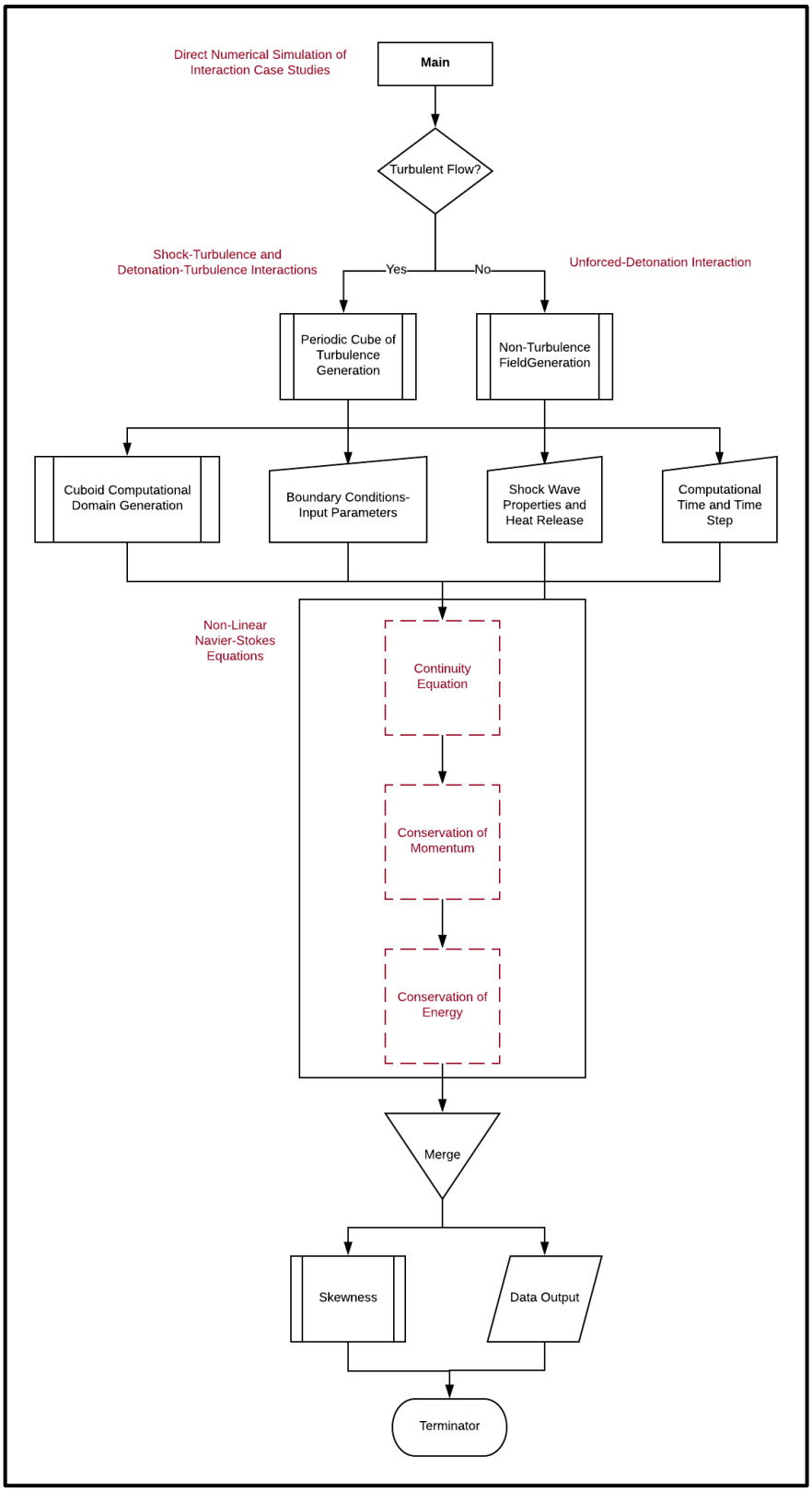

Figure 3.7 Direct numerical simulation code outline for the three interaction case studies: unforced–detonation, shock–turbulence, and detonation–turbulence

Direct Numerical Simulation Code for the Turbulence Periodic Cube

The direct numerical simulation of the turbulence periodic cube, shown in Figure 3.6, begins with the driver program, or main driver. It is the **Main** program that initiates the code whether it is being run on a personal computer or through a high performance supercomputer interface. It is the one program that is accessed directly by the user and edited between different runs. Subsequent subroutines can be included or excluded from the Main driver to change the conditions of the run. Following the Main driver, three programs are defined. In the **Initial Conditions- Input Parameters** program, the initial conditions and input parameters of the fluid are defined. The initial conditions impose the fluid properties of homogeneity and isotropy. In this program, the input parameters are set for velocity, temperature, pressure, and other fluid defining properties (such as the ratio of specific heats). The next program is that of **Computational Domain Generation**, where the periodic cube shape, previously shown in Figure 3.1, is generated. The spatial coordinates and grid resolution are assigned in this program. The temporal scale and time steps are defined in the following program, **Computational Time and Time Step**. The computational time is fixed using the fluid

Table 3.1 Direct numerical simulation of the turbulence periodic cube: code components- Part I

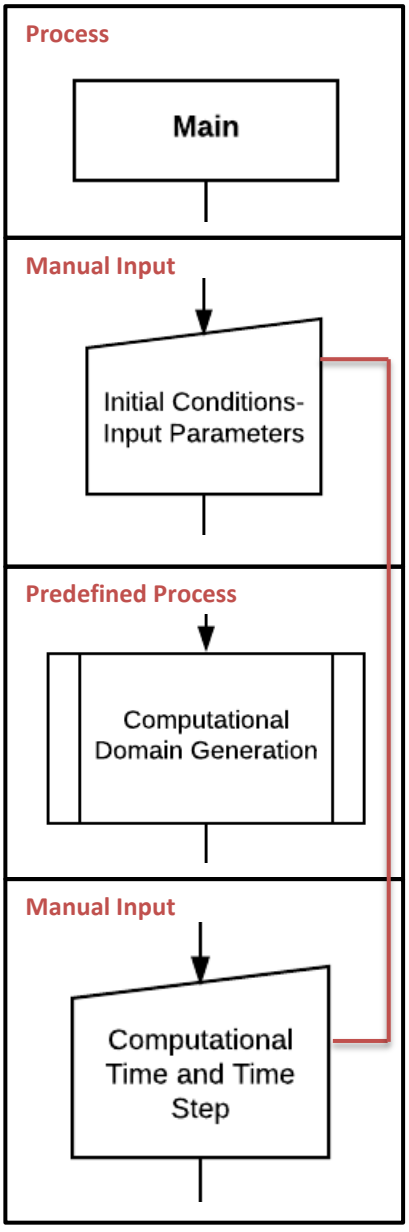

parameters of reaction half length, input density, and input pressure. Initial time is zero, the end time is calculated using

$$t_{end} = 50 \times L_{1/2} \times \left(\frac{\rho_0}{P_0}\right)^{1/2} \tag{3.25}$$

where the reaction half length $L_{1/2}$ is 1 for fully-developed homogeneous isotropic turbulence as defined by Massa (2011a). The time step is the incremental change in time as the computation progresses. It is fixed throughout the computation simulation at 10 steps; small enough to capture the flow physics without drastically increasing the power requirement. The turbulence fluctuations are defined next in the **Gaussian Distribution Random Number Generation** program. In this turbulence study, the fluctuations of interest are vortical. The fluctuations are initiated by an array of normally-distributed random numbers, following the Gaussian distribution shown in Figure 1.6, with mean of zero and standard deviation of 1 % of flow velocity. The mean is zero at this step because the turbulence cube is a still fluid field. In the interaction cases, the turbulence is convected and acquires a mean flow velocity, which is added to the fluctuations. Next, the array of random numbers is run through the governing **Navier–Stokes equations of continuity, momentum and energy**. The non-linearity of the governing equations imparts skew to

Table 3.2 Direct numerical simulation of the turbulence periodic cube: code components-Part II

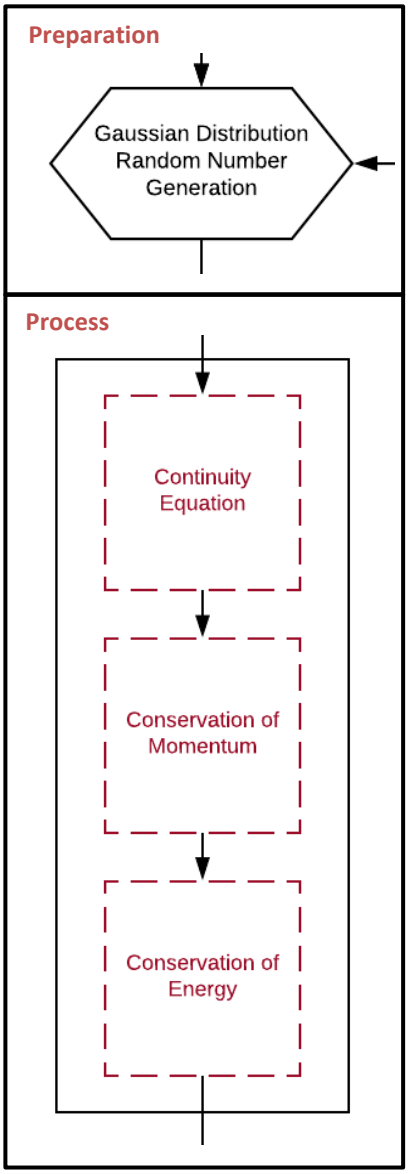

the Gaussian distributed random numbers. The numerical solutions of the Navier–Stokes equations are **merged** together and the turbulence velocity skewness is evaluated. The velocity **skewness** is calculated using Equation (2.1), as defined by Tavoularis (1978). Previous direct numerical simulation studies of turbulence used a skewness value of -0.5 to determine when the fully-developed turbulence has been reached (Gotoh, 1993, Mahesh, 1997, Pope, 2000, and Massa 2011). The numerical simulation, thus, is run and velocity readings are recorded to evaluate the turbulence velocity skewness. Based on the long-standing definition, the skewness needs to reach -0.5 only in the axial direction. This is an important distinction since the current work yields a skewness vector. Thus, the axial velocity skewness in the streamwise direction is calculated and a decision is made whether **turbulence criterion is met**. If the required skewness is met, the temporal evolution of the simulation is concluded and the numerical solutions of the Navier–Stokes equations are collected as **data output** for analysis followed by **termination** of the code. However, if the turbulence skewness criterion is not met in the

Table 3.3 Direct numerical simulation of the turbulence periodic cube: code components-Part III

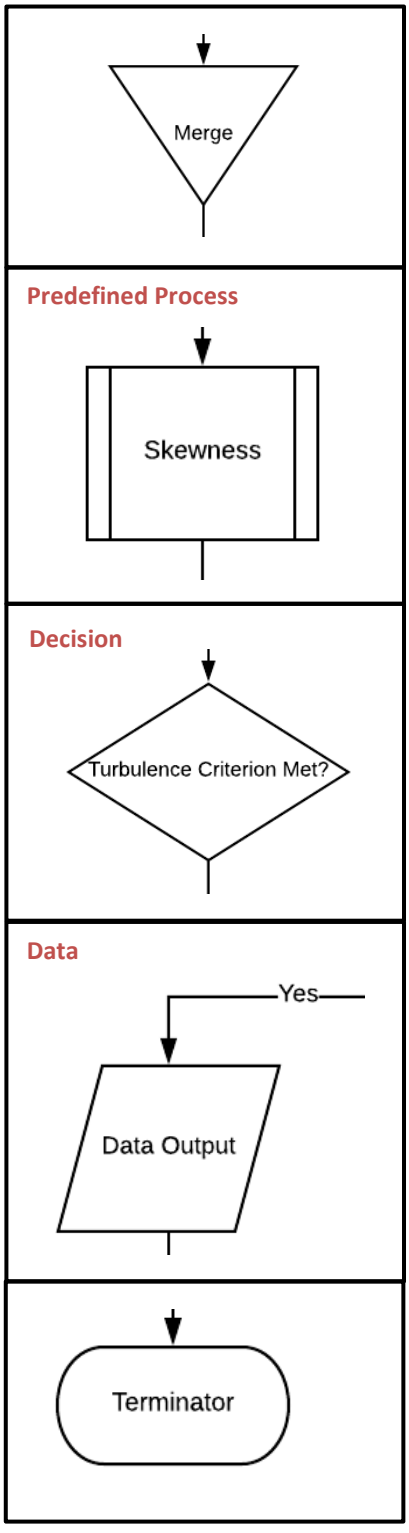

decision process, the program is looped back to the **Gaussian Distribution Random Number Generation** program. A new array of normally-distributed random numbers is generated, run through the Navier–Stokes equations which are solved and the solutions are merged, and finally the streamwise velocity skewness is calculated again. This loop is repeated until the turbulence skewness criterion is met.

This code produces an array of numbers that represents numerical fully-developed homogeneous isotropic turbulence. Based on the shape of the turbulence periodic cube, previously discussed and shown in Figure 3.1, the code output in a single run is used as a unique turbulence unit cube. The direct numerical simulation code is run numerous times to produce the whole turbulence periodic cube composed of $4{,}330{,}747$ turbulent unit cubes. While the definition of the turbulence periodic cube states that the component unit cubes are identical (Davidson, 2004), they are considered to be closely related within a certain confidence level. They all have the same initial conditions and fluid input parameters. They have velocity fluctuations that are produced by the same random number generator from a normal distribution with the same mean and standard deviation parameters. The velocity numerical arrays are then run through the same non-linearity process and evaluated for the same skewness criterion. However, each time the random number generator produces an array of velocities; it is slightly different, while satisfying the overall requirements. Therefore, even when the same skewness criterion is imposed and met by the different runs, the constituent velocity fluctuations will vary slightly making the complete periodic cube a continuous turbulent field with no repetitive patterns or discontinuities.

Direct Numerical Simulation Code for the Interaction Case Studies

The direct numerical simulation code, shown in Figure 3.7, is used to generate the three interaction case studies of unforced–detonation, shock–turbulence, and detonation–turbulence. The direct numerical simulation code is initiated by a **Main** driver program. This program is accessed by the user to define the different conditions in the three interactions. Based on the interaction case study, the type of incoming flow is defined first. A decision is made at this stage about the fluid flow of interest, is it **turbulent flow**? If yes, the direct numerical simulation code for the turbulence periodic cube is used for **periodic cube of turbulence generation**. The code output data are saved and loaded as input to the rest of this current code. This step is utilized for the shock–turbulence and detonation–turbulence interactions. As for the unforced–detonation interaction, the decision is that no turbulent flow is required. Thus, the turbulence periodic cube data are not loaded from the previous simulation. Instead, a **Non-Turbulence Field Generation** program is run. In this program, a simple numerical fluid field is generated with an array of constant velocity and no fluctuations. Next, a series of four programs are run to define each specific interaction case study. First, the computational geometry in which the

Table 3.4 Direct numerical simulation of the interaction case studies: code components- Part I

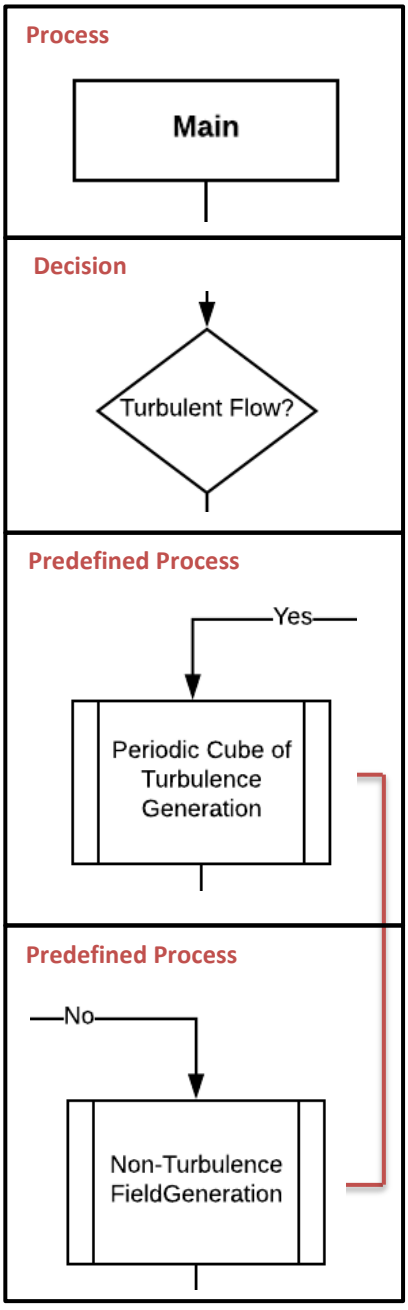

interaction will take place is specified. A cuboid is selected with a cross-sectional area equivalent to the size of the periodic cube, and a length that stretches four times the length of a single side of the cube, as shown in Figure 3.8. The **Cuboid Computational Domain Generation** program creates the domain where the flow begins to travel at the inlet, interacts with the wave front about halfway through the geometry, and progresses downstream past the wave front.

Table 3.5 Direct numerical simulation of the interaction case studies: code components- Part II

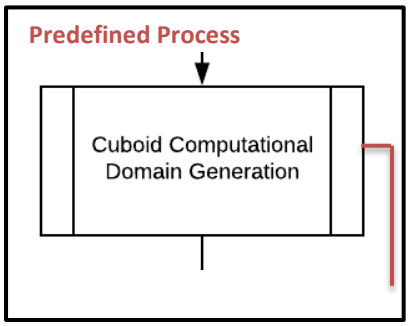

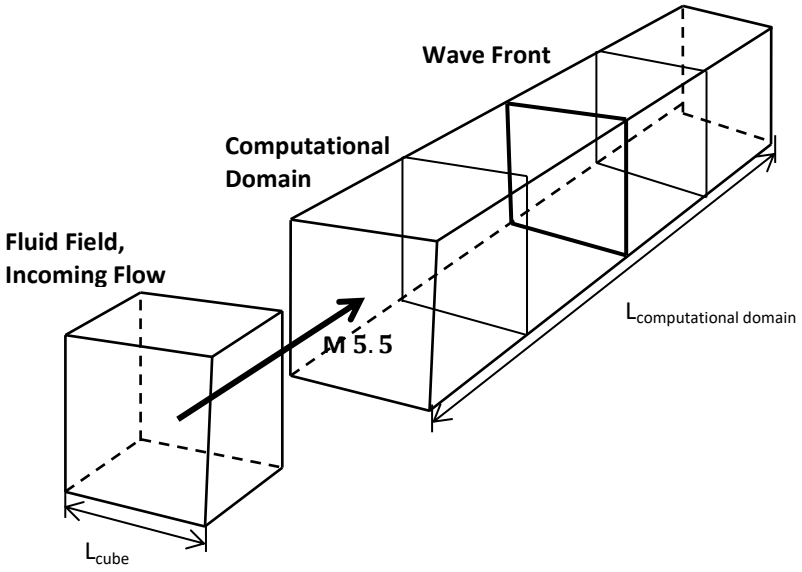

Figure 3.8 Computational domain geometry of the three interaction case studies

In Figure 3.8, the incoming fluid flow cube can be turbulent or non-turbulent and the wave front can be a shock or a detonation wave. Next, the **boundary conditions and input parameters** are specified. The computational domain has non-reflective and subsonic exit conditions (Massa, 2011a). The input parameters are the fluid flow velocity, temperature, pressure, and additional defining properties.

Table 3.6 Direct numerical simulation of the interaction case studies: code components- Part III

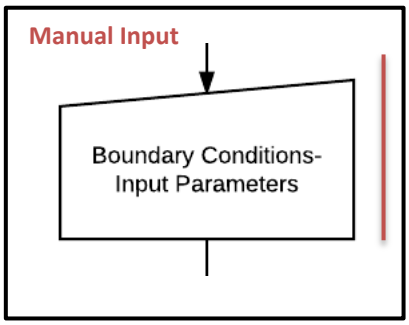

Once the flow properties and the computational domain are outlined, the **shock wave properties and heat release** are set in the following program. The normal shock relations, previously shown in Equations (3.19), (3.20), (3.21), and (3.22), are applied to both the shock and detonation interaction cases. The detonation cases, however, have the additional heat release parameters defined in Equations (3.23) and (3.24). Finally, the simulation **computational time and time step** follow the same guidelines as in the simulation code of the turbulence periodic cube, employing Equation (3.25).

The defined fluid flow properties are run through the governing Navier–Stokes equations of **continuity, momentum, and energy**. These balance equations are utilized to describe the behavior of the fluid flow as it travels through the computational domain. The equations are solved numerically, iteratively, and the results are **merged**. This concludes the interaction case studies' description of the flow physics. However, an additional step is taken, at this time, to calculate the turbulence velocity skewness using in Equation (2.1), as defined by Tavoularis (1978). This is not utilized to evaluate whether the criterion for fully-developed

Table 3.7 Direct numerical simulation of the interaction case studies: code components- Part IV

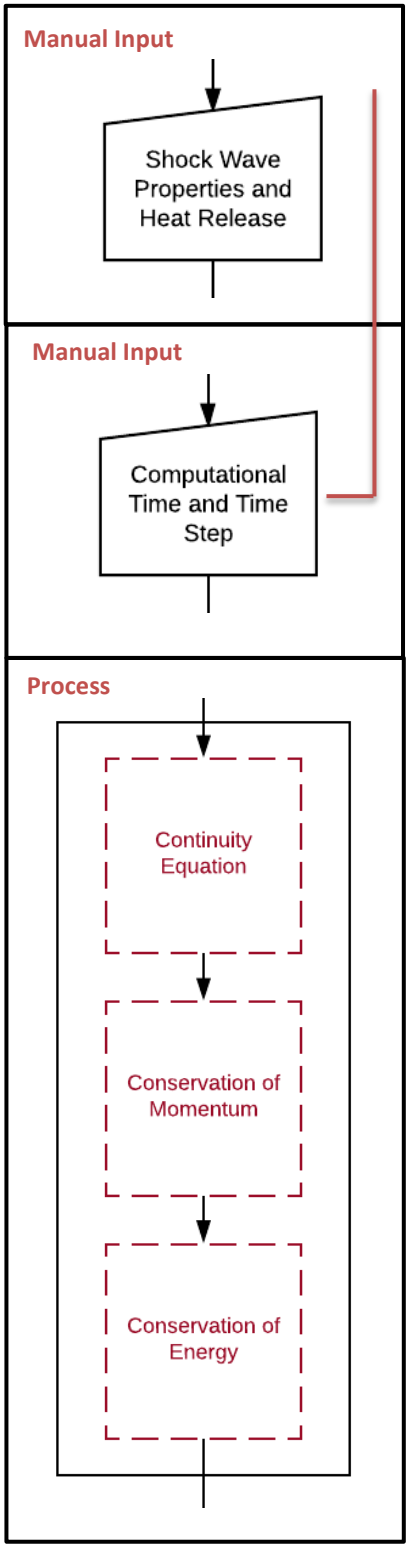

turbulence has been reached, as in the periodic cube simulation code. In this code, the **Skewness** program is employed to extend the skewness analysis and evaluate how the velocity variations are affected by the interactions with the wave fronts throughout the computational domain, past the wave itself. The results of the numerical simulation are saved as **data output** for further analysis and visualization. The code is **terminated**.

Table 3.8 Direct numerical simulation of the interaction case studies: code components- Part V

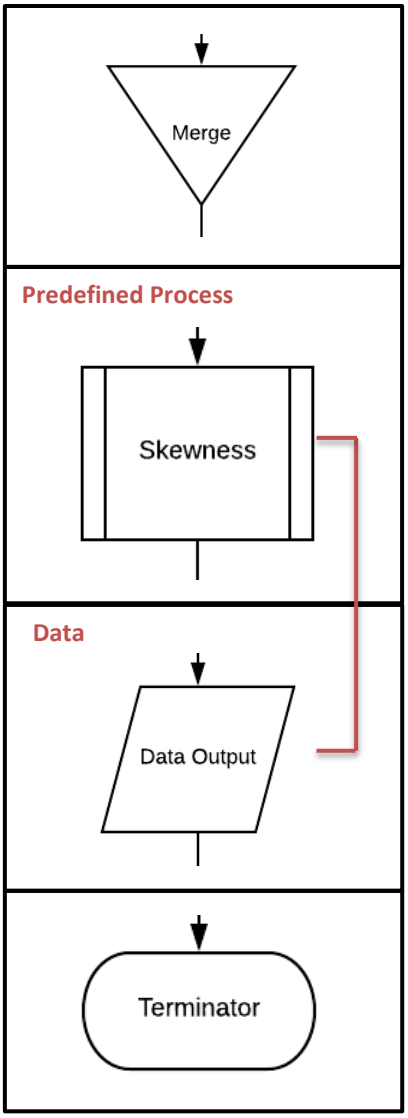

3.3 Convergence Logic

In summary, the direct numerical simulation code is structured primarily around the flow governing Navier–Stokes equations. The essential input parameters are assigned, while other flow parameters are calculated. The fluid flow properties and initial conditions are set. The geometry is outlined based on the application of the code, with its corresponding necessary boundary conditions. The non-linear partial differential equations are numerically solved iteratively with the spatial and temporal scales completely defined. It is ensured that sufficient time is allocated for the simulation to thoroughly process all the information and progress towards arriving at the final output file. The question becomes: **How it is confirmed that the direct numerical simulation logic is correctly converging at the required turbulence or interaction output files?** Two checks are imposed to validate the accuracy of simulation (1) turbulence velocity skewness factor calculation (2) code output data analysis and visualization.

1. The turbulence velocity skewness factor calculation, previously documented in Equation (2.1), is utilized as the checkpoint for assessing the progression of the code past the Navier–Stokes equations. If the skewness values, at the end of the simulation code, are repeated with no change between runs, if the skewness is not reaching the required value (satisfying the Tavoularis (1978) criterion), and if the skewness variations between runs are not within a reasonable range, the code constituent equations are reevaluated. The turbulence skewness factor ensures that the simulation logic has converged to a turbulent field when its value reaches $S = -0.5$ (Gotoh, 1993, Mahesh, 1997, Pope, 2000, and Massa 2011). As for the interaction case studies, the skewness factor calculation allows the

depiction of the velocity variations throughout the computational domain. It is expected that the skewness evolves past the wave front. Once the stretching is observed, it is validated that the velocity output data from the interaction case studies are accurate.

2. The output data file, produced by a program at the end of the direct numerical simulation code, is analyzed for numerical errors, computational noise, and repeated patterns. The accuracy of the output velocities is assessed by ensuring the numerical values are within the expected range (with the previously defined mean, standard deviation, and flow velocity of interest). The turbulent fluctuations are small, when compared to the high speed mean flow velocity. However, as long as the fluctuations' numerical values are consistent with the defined standard deviation, the observed chaotic behavior is attributed to the defined turbulence and not to machine noise. The velocities' data are analyzed to ensure no bounded error occurs producing a bias solution at the inlet or outlet. Such an error would require windowing, as the Blackmanharris, Hanning, Hamming, Gaussian, and Taylor windows (Hussein, 2012). Windowing is used to surpass the leakage problem at the edges of the plots, taper the time history data, and eliminate discontinuities. It is essential in fixing the numerical truncation error. The velocity patterns are closely observed to ensure that the flow is homogeneous and without discontinuities. The velocity results are statistically analyzed and visualized for the turbulence periodic cube and the three interaction case studies; documented in the next chapters. The findings are compared to similar studies published in the scientific literature to validate accuracy.

4. Turbulence Periodic Cube

In the introduction, a question was posed: **What is turbulence and why is it so challenging?** It is challenging to pinpoint where turbulence initiates from or what its origin is. We can, however, characterize the turbulence by its irregularities, diffusivity, Reynolds number, three–dimensional vortical fluctuations, dissipation, and continuum properties. The characteristics of the turbulence depend on the surrounding environment and the turbulence, thus, depends heavily on initial conditions.

This chapter aims to contribute to the fundamental understanding of turbulence using a simple low-order model of idealized homogeneous isotropic turbulence with vortical fluctuations, as shown in the visualization by Donati (2011), Figure 4.1.

Direct numerical simulation of a periodic cube outputs data for statistical analysis of turbulence properties. Afterwards, the turbulence periodic cube is utilized as incoming flow in the interaction case studies of shock–turbulence and detonation–turbulence.

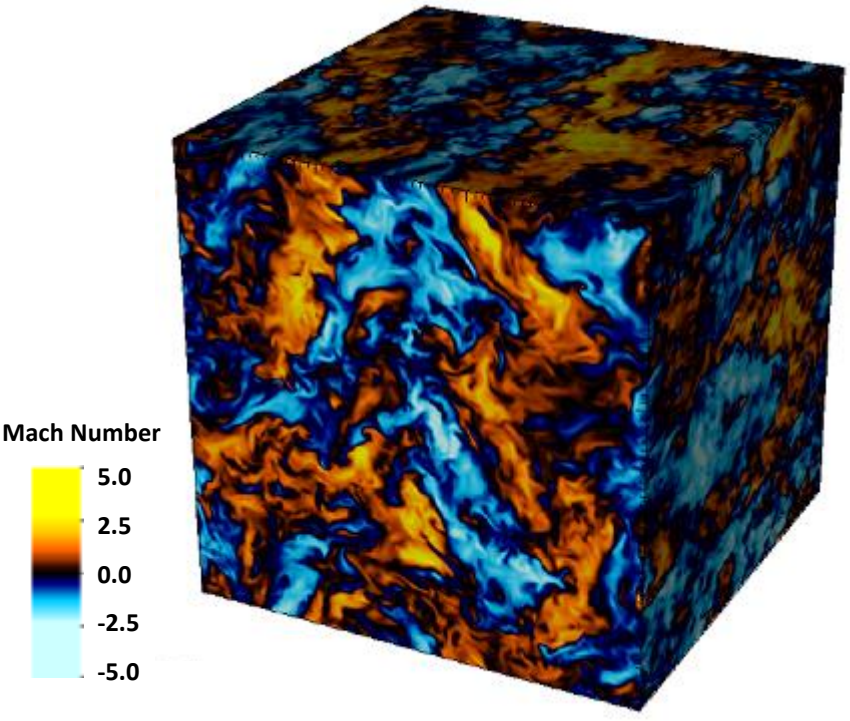

Figure 4.1 Homogeneous isotropic turbulence: pseudocolor plot for dimensionless velocity component u, 256 x 256 x 256 grid (Donati, 2011)

4.1 Turbulence Periodic Cube Properties

The periodic cube, previously shown in Figure 3.1, is the geometry selected to examine the fundamental structure of turbulence. The direct numerical simulation code, Figure 3.6, produces a unique turbulence occurrence with each run in the shape of a unit cube. The unit cubes of turbulence are combined to formulate the larger periodic cube. In this study, the turbulence periodic cube has a size of $163 \times 163 \times 163$ units and is composed of $4{,}330{,}747$ unit cubes, all carrying information on the properties of the fluid velocity, temperature, and pressure. The output data of the simulation code are statistically analyzed to investigate the turbulence properties.

Davidson (2004) states that in a periodic cube, the smaller unit cubes have plane properties that are independent of orientation. Additionally, he outlines three assumptions associated with the use of the periodic cube geometry in the direct numerical simulation of turbulence:

1. The constituent unit cubes, forming the periodic cube shape, are identical at any instant.
2. The pressure which one unit cube imposes on the adjacent cube is negligible since the size of the unit is much larger than the smallest eddy size for the defined fluid.
3. The unit cubes are aligned and stacked where the discontinuities between the edges of the unit cubes do not affect the homogeneity of the turbulence.

After statistical analysis of the turbulence properties, the three assumptions are assessed in this application to evaluate the validity of using the periodic cube shape in a direct numerical simulation of turbulence.

Note that the statistical analysis of the periodic cube focuses on the velocity parameter since the turbulence is characterized by vortical fluctuations. In the direct numerical simulation, the vortical fluctuations emerge as a result of running an array of normally-distributed random numbers, Figure 1.6, through the non-linear Navier–Stokes equations. Based on the velocity skewness criterion, defined by Tavoularis (1978) and others, fully-developed turbulence is achieved when the skewness factor reaches $S = -0.5$. In this study, the turbulence velocity skewness criterion is assessed for this periodic cube application to validate the criterion in direct numerical simulation of a simple homogeneous isotropic turbulence field.

4.2 Turbulence Periodic Cube Statistical Analysis

The periodic cube consists of many unit cubes of turbulence. For statistical analysis of the direct numerical simulation output data, it is important to define the geometry being analyzed: are the statistical properties evaluated over the entire cube, between unit cubes, or over a plane? The periodic cube, of size $163 \times 163 \times 163$ units, consists of $4{,}330{,}747$ unit cubes and is divided into 163 turbulence periodic planes of size $163 \times 163 \times 1$ each, as shown in Figure 4.2.

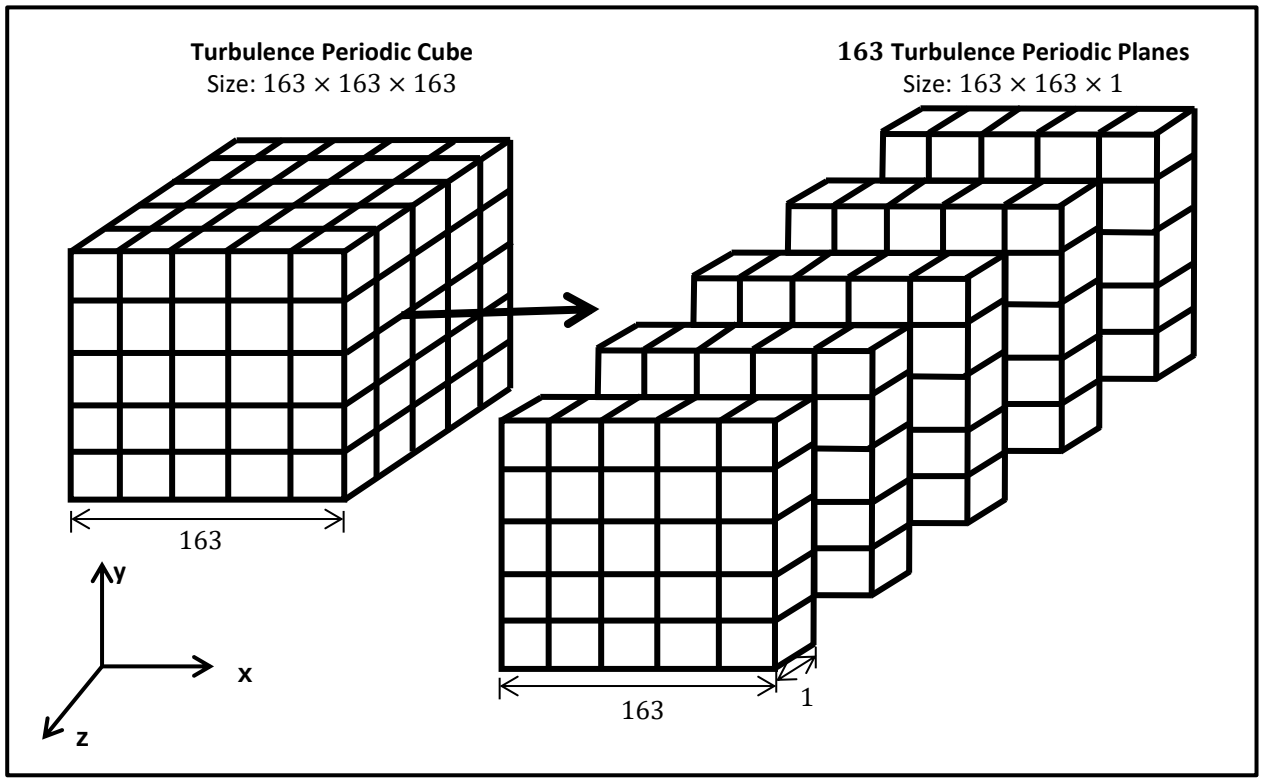

Figure 4.2 Three–dimensional turbulence periodic cube and constituent 163 three–dimensional turbulence periodic planes

Statistical averaging of the data output in the entire periodic cube yields single point values, while statistical averaging of the turbulence periodic planes, shown in Figure 4.2, leads to trend lines of the turbulence behavior throughout the cube. Thus, it is found that the most useful information can be extracted from statistically averaging the planes of turbulence as ensembles. Ensemble averaging over time is similarly used in the direct numerical simulation of forced isotropic turbulence by the Johns Hopkins University turbulence research groups, as shown in Figure 4.3.

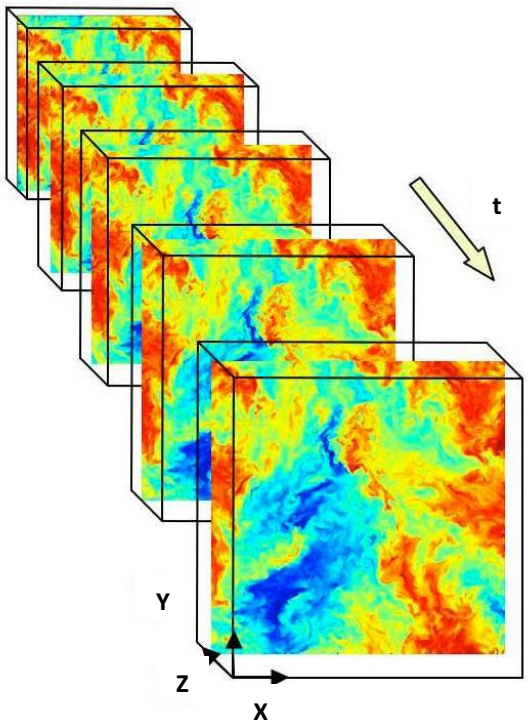

Figure 4.3 Forced isotropic turbulence: direct numerical simulation visualization, evolution over time, 1024 x 1024 x 1024 nodes (Johns Hopkins University, 2018)

Average Velocities

The first step of descriptive statistical analysis in the turbulence periodic cube is averaging the output of the direct numerical simulation code. The average quantities are then utilized in the calculations of other properties and additional statistical measures. Since the turbulence being studied has vortical fluctuations with constant temperature and constant pressure, the velocity is the topic of focus. Note that the fluid field has no mean velocity. Thus, statistical analysis is only of the velocity fluctuations. The fluctuations are initiated from a set of normally-distributed random numbers with a zero mean and a standard deviation that is 1 % of the flow velocity of interest. The turbulence

periodic cube only becomes a moving flow field in interaction case studies that will be discussed later, Figure 3.8.

The velocity fluctuations are averaged over the turbulence periodic planes as ensembles.

$$\langle u \rangle_N \equiv \frac{1}{N} \sum_{n=1}^{N} u^{(n)} \tag{4.1}$$

The side length of the plane is $N = 163$ units. The velocity fluctuations are averaged over the entire periodic cube (Pope, 2000) as

$$\langle u(t) \rangle_L \equiv \frac{1}{L^3} \int_0^L \int_0^L \int_0^L u(x,t) dx_1 dx_2 dx_3 \tag{4.2}$$

where the side length of the periodic cube is $L = 163$ units. The ensemble velocity averages of the three velocity components (u,v,w) are calculated for each of the 163 planes and plotted in sequence in Figure 4.4.

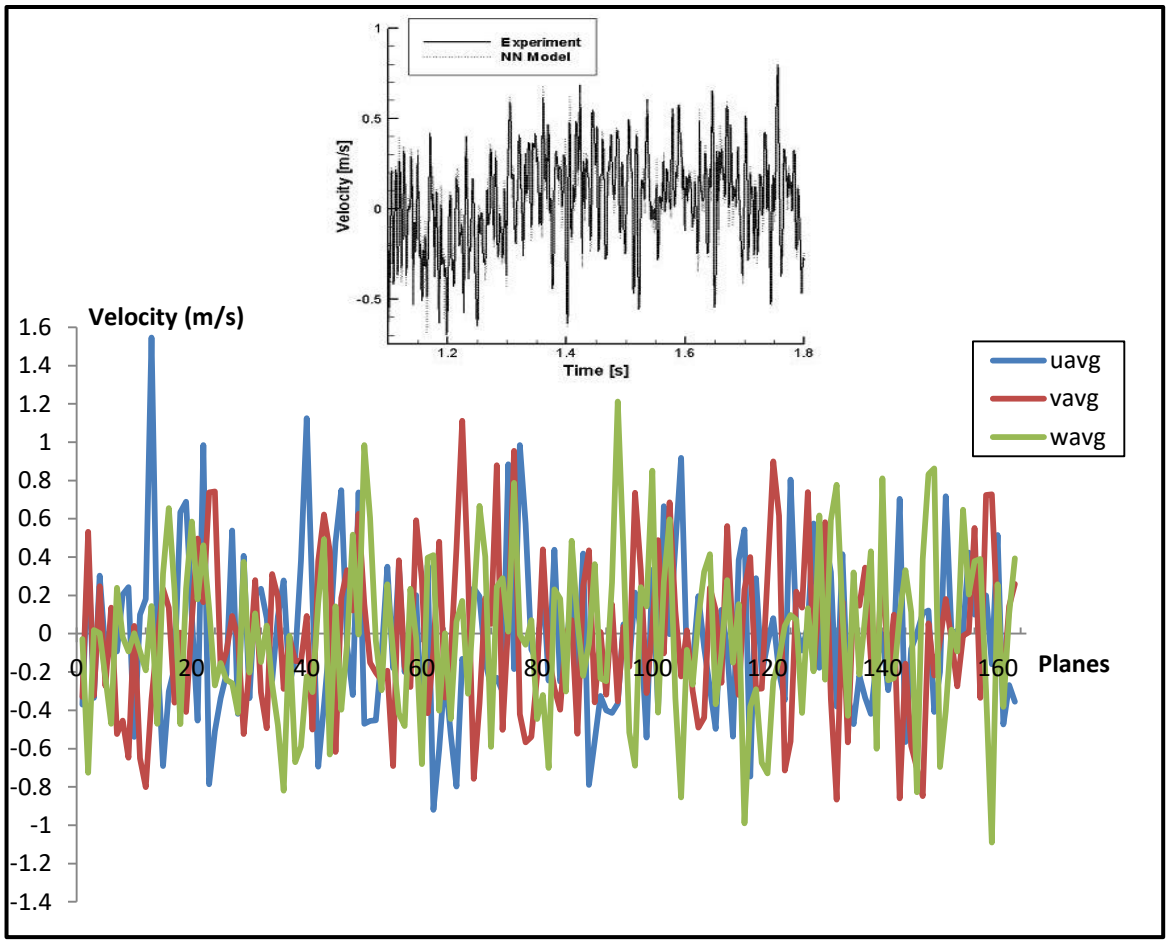

Figure 4.4 Top: Time series of measured (experimental) and modelled (simulated neural network architecture) turbulent velocity fluctuations (Gholamrezaei, 2018) - Bottom: Average velocities in the direct numerical simulation turbulence periodic planes (current study)

The line plots in Figure 4.4 (bottom graph) show the average velocity values, for the turbulence fluctuations in all three coordinates, varying around the mean of zero. This is consistent with the average turbulent velocity fluctuations evolution over time acquired experimentally as well as through other modelling techniques (top graph).

Across the 163 planes in the direct numerical simulation, the three velocity components show different average values but similar trends in the varying close to zero and in an apparently random manner. It is evident that the direct numerical simulation code is producing a homogeneous field without numerically repeating the

exact values of the velocities. This is important because in later analysis, a distinction is made between the different Cartesian planes and their corresponding properties. The velocities, on average, fluctuate between ± 1 m/s (with a few spikes exceeding 1 m/s and reaching 1.5 m/s).

The data in Table 4.1 show that over the entire periodic cube, on average, the three velocity components fluctuate close to zero. The slight deviation from zero is expected due to the nature of the vortical fluctuations and their numerical simulation. As shown previously in Figure 1.6, the slight departure of velocity from a Gaussian distribution yields a shifted distribution away from the original bell-shape with a small non-zero mean.

Table 4.1 Average velocities in the turbulence periodic cube

Turbulence Cube		
u_{avg}	-1.195E-02	m/s
v_{avg}	-1.486E-02	m/s
w_{avg}	-1.458E-02	m/s

Root Mean Square Velocities

The quantitative average is used in the analysis of two properties of interest: the fluctuating term and the standard deviation. In this study of turbulence characterized by vortical fluctuations, the fluctuating term is acquired from the decomposition of velocity, shown in Figure 4.5.

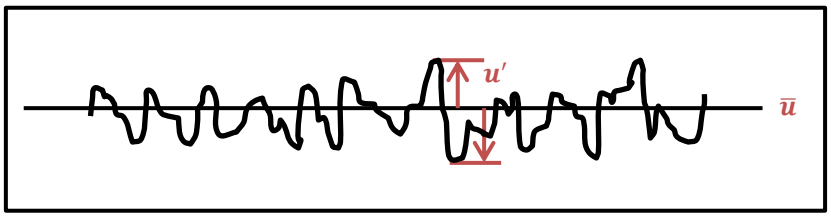

Figure 4.5 Velocity decomposition into mean and fluctuation terms

The velocity is separated into the mean and the fluctuating terms, making the fluctuating velocity definition as follows

$$u' \equiv u - \langle u \rangle \tag{4.3}$$

where the angle brackets denote ensemble averaging. Based on the distribution function, shown in Figure 1.6, the fluctuations vary from one to three standard deviations away from the mean value. The variance is defined as the mean square fluctuation; making the square root of the variance the standard deviation (Pope, 2000).

$$var(u) \equiv \langle u'^2 \rangle \tag{4.4}$$

$$sdev(u) = \sqrt{var(u)} = \langle u'^2 \rangle^{1/2} \tag{4.5}$$

The standard deviation, thus, is calculated by finding the root mean square of the fluctuations. In the direct numerical simulation code, the imposed vortical fluctuations are set to 1 % of the desired flow Mach number of 5.5 making one standard deviation about 17.5 m/s. Once again, due to the nature of the vortical fluctuation generation from the slight Gaussian variation, the standard deviation in the root mean square averages is expected to vary somewhat from the Gaussian value in all three coordinates.

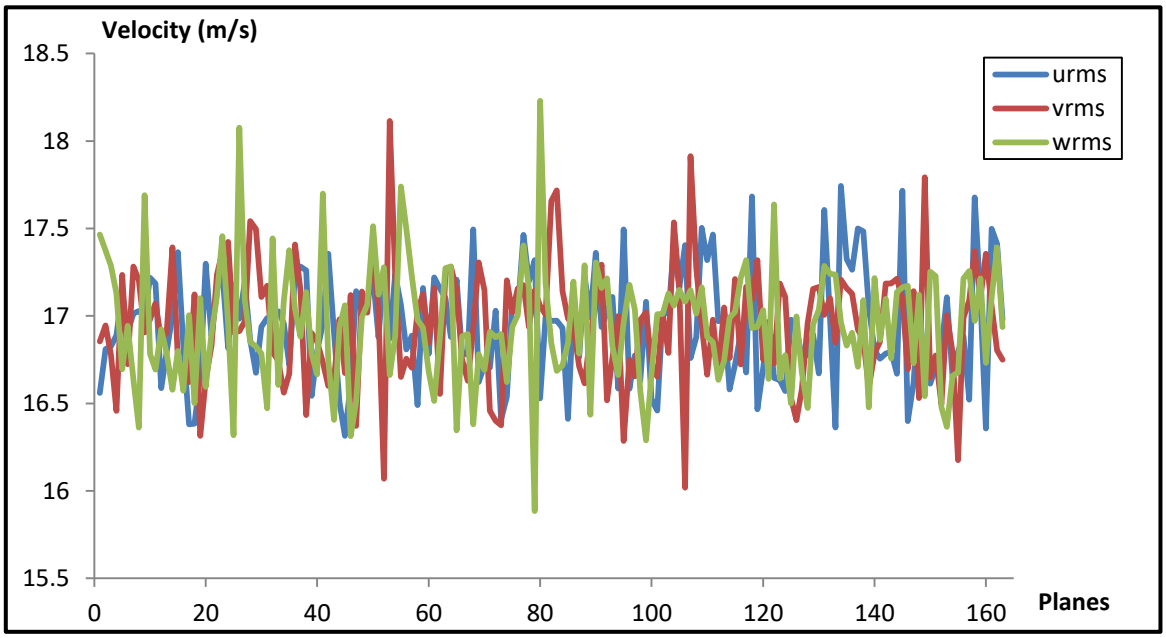

Figure 4.6 Root mean square velocities in the direct numerical simulation turbulence periodic planes

The root mean square velocities are calculated across the 163 periodic planes and plotted in Figure 4.6 for the three coordinate components. It is observed that the root mean square values vary around 17 m/s within ± 1 m/s (with a few spikes and lows exceeding 1 and reaching 1.2 m/s variation). The standard deviation, thus, is close to the expected value on average. The line plots show variation between the individual velocity components (u,v,w) while maintaining the same trend line fluctuations. The fluctuations are expected due the nature of the turbulence.

The root mean square velocity components of the entire periodic cube are documented in Table 4.2. It is found that the root mean square in the periodic cube is close to 17.5 m/s with slight deviation. The slight deviation, as in the

Table 4.2 Root mean square velocities in the turbulence periodic cube

Turbulence Cube		
u_{rms}	16.951	m/s
v_{rms}	16.950	m/s
w_{rms}	16.951	m/s

average velocity, is expected due to the numerical simulation of the fluctuations from the Gaussian distribution, shown in Figure 1.6, followed by the non-linear Navier-Stokes equations.

Turbulent Kinetic Energy

Vortical forcing of the turbulence in the periodic cube creates kinetic energy. Thus, velocity fluctuations must be studied in detail in the energy analysis (Šavli, 2012).The energy is carried within the eddy structures of the turbulence where it is transferred by inviscid processes (first) from the larger eddies to the smaller ones successively through energy flux, as shown in Figure 1.5. At a small enough Reynolds numbers, the viscosity becomes effective, the eddy motion is stabilized. At the level of the smallest eddies, according to the Kolmogorov hypothesis, the energy is dissipated as heat due to viscosity. The turbulent kinetic energy in the periodic cube can be defined as

$$TKE = \frac{1}{2}\langle u_i u_i \rangle \tag{4.6}$$

The density is not taken into consideration in the calculation of the turbulent kinetic energy in this study since the periodic cube of turbulence has constant temperature and pressure. Based on the ideal gas law stated in Equation (3.3), constant temperature and pressure properties yield a constant density throughout the cube.

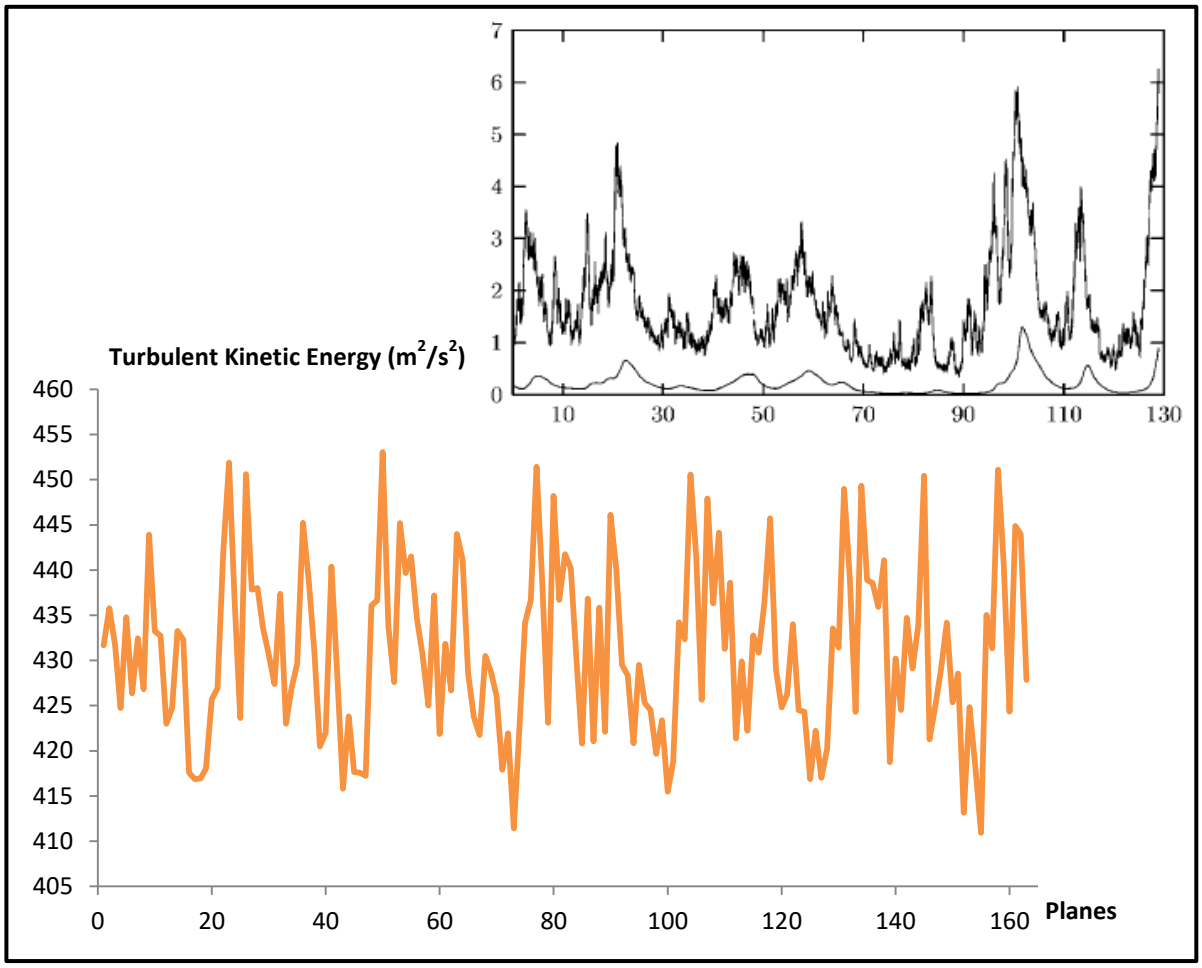

Figure 4.7 Top: Total energy in a homogeneous turbulence with anisotropic forcing, time evolution in direct numerical simulation with spatial resolution of $256x256x256$ (Biferale, 2001) - Bottom: Turbulent kinetic energy in the direct numerical simulation turbulence periodic planes (current study)

The three velocity components are added to calculate the total turbulent kinetic energy, shown in Figure 4.7. The energy across the turbulence periodic planes (bottom graph) varies around a mean of 433.5 m^2/s^2, within one standard deviation value ± 17.5 m^2/s^2. When compared to the normalized total energy profile acquired from the time evolution of computationally simulated homogeneous turbulence with anisotropic forcing (top graph), similar high frequency variations are observed at the large flow scales.

In the turbulence periodic cube, the turbulent kinetic energy is calculated and found to be slightly higher than 430 m^2/s^2, as shown in Table 4.3.

Table 4.3 Turbulent kinetic energy in the turbulence periodic cube

Turbulence Cube		
TKE	430.984	m^2/s^2

While the turbulent kinetic energy in the physical and time domains gives an indication of the strength of the turbulence fluctuations (Šavli, 2012), investigating the energy in the frequency domain gives information on the energy dissipation and its relation to the eddy size. The largest length scale L is determined by the geometry of the periodic cube and is slightly larger than the integral length scale l_0 of the eddy size carrying the most energy. The smaller length scales can be quantified by the Taylor microscale in the inertial subrange, where the energy transfer occurs, and by the Kolmogorov scale in the dissipation range, as shown in Figure 4.8.

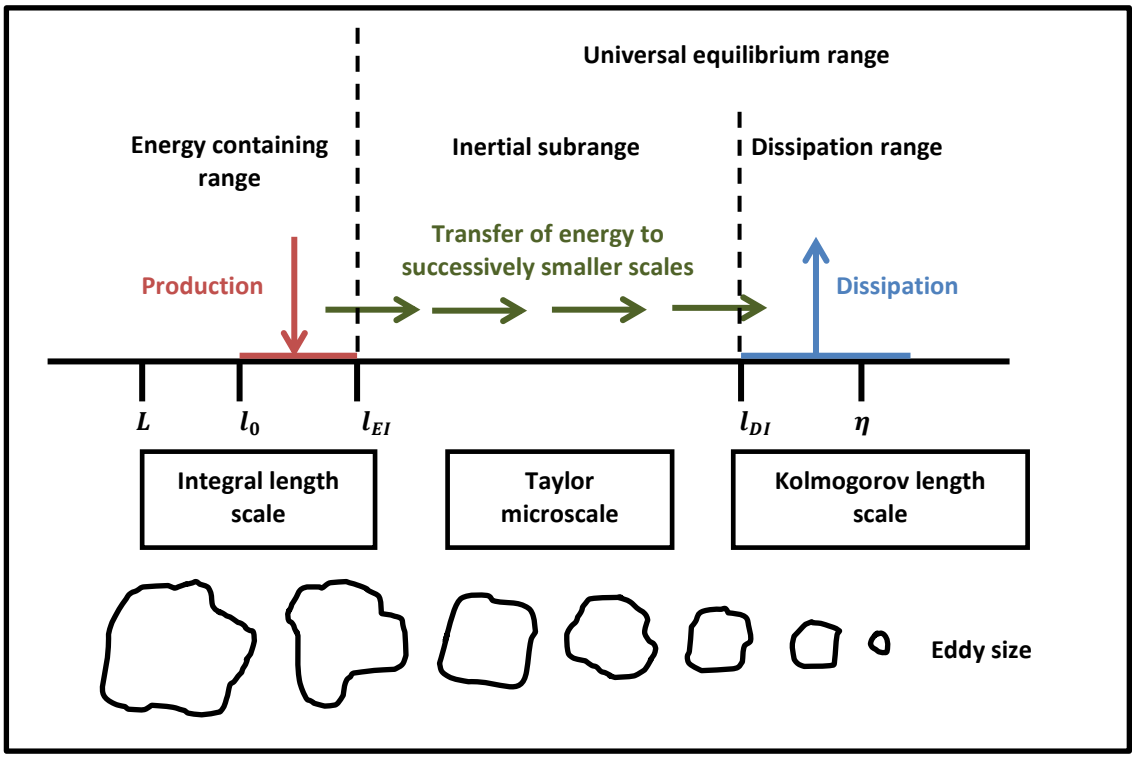

Figure 4.8 Different length scales and ranges in the turbulence energy cascade as adopted from Pope (2000)

For homogeneous isotropic turbulence, however, there is neither production nor transport properties (Pope, 2000). So, the evolution of the turbulent kinetic energy reduces to an energy dissipation expression in the time domain.

$$\varepsilon(t) = -\frac{d(TKE)}{dt} \tag{4.7}$$

Since the dissipation occurs at the smallest eddy size due to viscosity, the smallest length scale is calculated using the energy dissipation expression in Equation (4.7) and the flow viscosity. The Kolmogorov length scale η formed from these quantities is

$$\eta = \left(\frac{\nu^3}{\varepsilon(t)}\right)^{1/4} \tag{4.8}$$

where the fluid kinematic viscosity ν is defined as

$$\nu = \frac{\mu}{\rho} \tag{4.9}$$

and the constituent dynamic viscosity μ and density ρ terms are calculated using Equations (3.8) and (3.3) respectively. The energy dissipation Equation (4.7) is transformed to an expression of frequency using Fourier transform. It is normalized by the turbulence integral length scale. The Fourier transform is a mathematical operation that takes a property in the time domain and expresses it in the spectral domain. The Kolmogorov length scale for this study is calculated using Equation (4.8), inversed to give the frequency κ, and normalized by the integral length scale. The normalized energy dissipation in the frequency domain is plotted in Figure 4.9 against the natural log normalized Kolmogorov scale for the turbulence periodic cube.

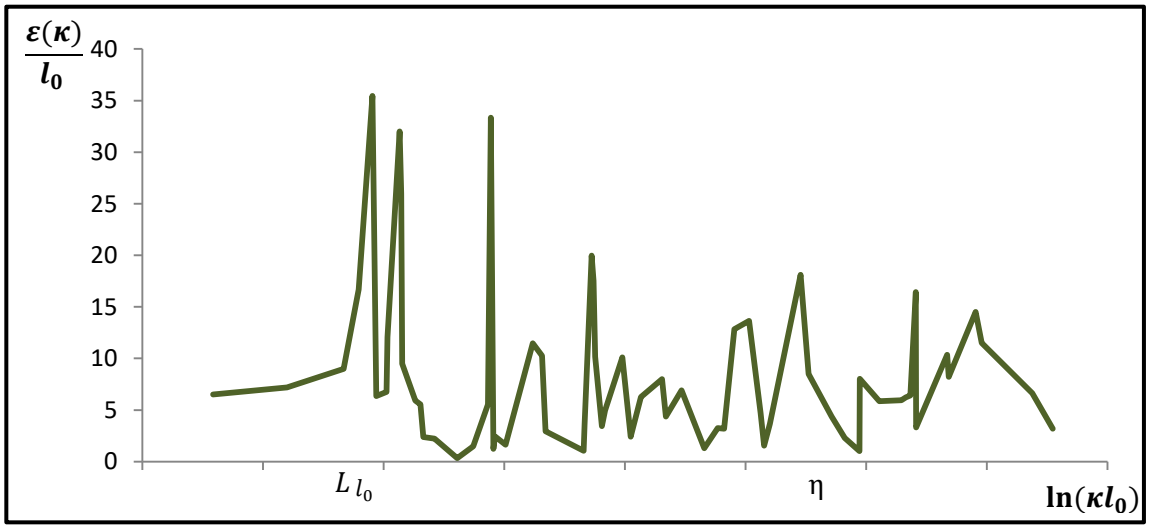

Figure 4.9 Energy dissipation in the turbulence periodic cube

Turbulence in the periodic cube structure needs a continuous supply of energy to make up for the viscosity losses. Otherwise, the turbulence rapidly decays. The energy dissipation vs. Kolmogorov scale plot, shown in Figure 4.9, portrays the energy dissipation from the largest turbulence eddies to the smallest ones. The normalized

energy spectrum, based on Kolmogorov's second similarity hypothesis, is not seen in this periodic cube because homogeneous isotropic turbulence does not have production or transport properties. The energy can only be dissipated. The high frequency variations seen in the large flow scales in Figure 4.7 are absent at the small scales of energy dissipation.

In addition, the plot shows that the turbulence in the periodic cube is not in equilibrium; as seen by the irregularities in the line graph. Once the turbulence cube acquires mean flow axial velocity, then the turbulence will be in equilibrium since the mean travel velocity sustains the turbulence energy. Only then will the energy cascade properties appear clearly.

Reynolds Stress Components

The turbulent kinetic energy relation, shown in Equation (4.6), is a single–point correlation. A single–point correlation is the simplest statistical directionally dependent measure used to determine a relation between two quantities in the turbulence field. This correlation is defined as follows.

$$R_{ij}(r,x,t) \equiv \langle u_i(x,t)u_j(x+r,t)\rangle \tag{4.10}$$

Single–point correlation also leads to information regarding the vortical fluctuations' contribution to the momentum flux frequently referred to as Reynolds stress.

$$RS_{ij} = \langle u_i u_j \rangle \tag{4.11}$$

The density is not considered in the Reynolds stress Equation (4.11), as in the turbulent kinetic energy Equation (4.6), because it is constant throughout this ideal gas in the periodic cube. The Reynolds stress nine component tensor has three diagonal

components: $RS_{uu}, RS_{vv}, RS_{ww}$, which are referred to as normal stress terms, and six off-diagonal components: $RS_{uv}, RS_{uw}, RS_{vu}, RS_{vw}, RS_{wu}, RS_{wv}$, which represent tangential or shear stress terms. The tensor is symmetrical across the diagonal components since $\langle u_i u_j \rangle = \langle u_j u_i \rangle$ and reduces to six terms: three diagonal and three unique off-diagonal components. The three diagonal Reynold stress components $RS_{uu}, RS_{vv}, RS_{ww}$ represent the turbulent kinetic energy constituent terms, are calculated across the periodic planes and plotted in Figure 4.10.

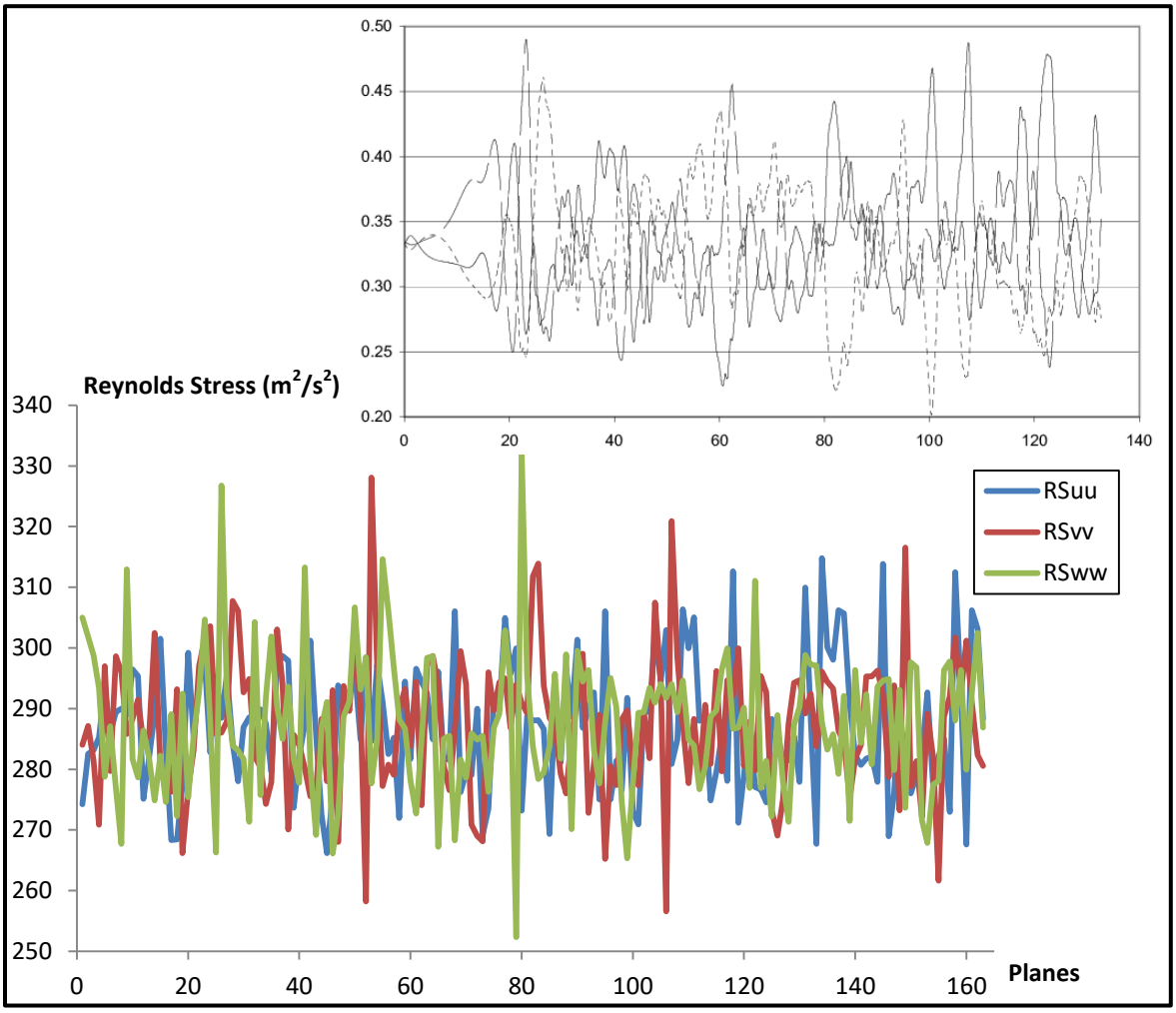

Figure 4.10 Top: Time evolution of the diagonal components of the normalized Reynolds stress in velocity forced turbulence closely following direct numerical simulation (Gravanis, 2011) - Bottom: Diagonal components of the Reynolds stress in the direct numerical simulation turbulence periodic planes (current study)

The normal stress terms (bottom graph) vary around 289 m^2/s^2 within one standard deviation value ± 17.5 m^2/s^2, as in the turbulent kinetic energy line graph shown in Figure 4.7 (with a few spikes and lows reaching up to 43.3 m^2/s^2 variation). When compared to the diagonal components of the normalized Reynolds stress in velocity forced turbulence closely following direct numerical simulation studies (top graph), the

three components are seen to follow the same trend; varying around a mean value between higher and lower disturbances.

The three normal stress diagonal terms are calculated for the entire periodic cube and shown in Table 4.4. All three components at 287.3 m^2/s^2 are close to the mean value of the periodic cube line graphs. Thus, it can be seen that the correlation of the velocity fluctuations in the diagonal Reynolds stress terms is high formulating the momentum in the turbulent kinetic energy.

Table 4.4 Diagonal components of the Reynolds stress in the turbulence periodic cube

Turbulence Cube		
RS_{uu}	287.330	m^2/s^2
RS_{vv}	287.314	m^2/s^2
RS_{ww}	287.323	m^2/s^2

The final step in the statistical analysis of the turbulence periodic cube is the calculation of the three unique off-diagonal Reynolds stress components $RS_{uv}, RS_{uw}, RS_{vw}$ across the periodic planes. These terms are plotted in Figure 4.11.

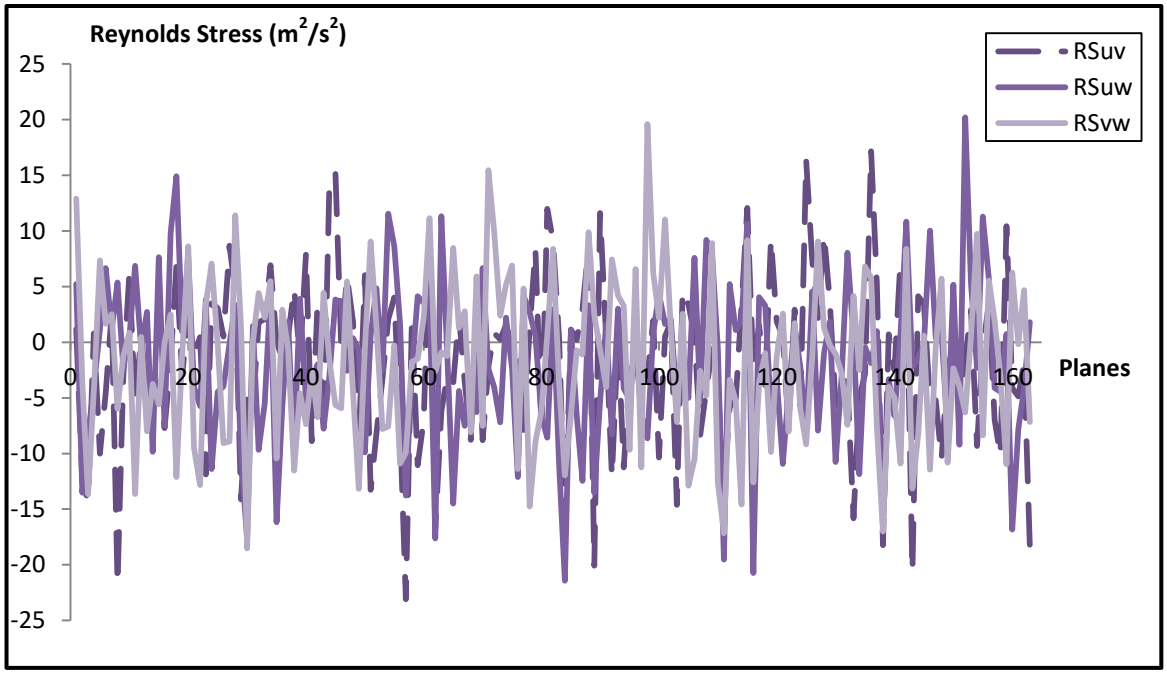

Figure 4.11 Off-diagonal components of the Reynolds stress in the turbulence periodic planes

The shear stress terms are the off-diagonal components of Reynolds stress. In the turbulence periodic cube, they fluctuate around the mean of zero within one standard deviation value ± 17.5 m^2/s^2, similar to the normal stress line graphs' trend shown in Figure 4.10 (with a few spikes and lows reaching up to 23 m^2/s^2). The velocity fluctuations, thus, are weakly contributing to the momentum flux in the cross planes.

The three shear stress terms are calculated for the entire periodic cube and shown in Table 4.5. The three components are between 1.7 m^2/s^2 and 1.8 m^2/s^2. The correlation between the different velocity fluctuation terms in the off-diagonal Reynolds stress components is low compared to that of the diagonal components.

Table 4.5 Off-diagonal components of the Reynolds stress in the turbulence periodic cube

Turbulence Cube		
RS_{uv}	1.761	m^2/s^2
RS_{uw}	1.810	m^2/s^2
RS_{vw}	1.822	m^2/s^2

Numerically, the significant different in the Cartesian coordinate correlations between the diagonal and the off-diagonal Reynolds stress components can be attributed to the nature of the velocity fluctuation distribution, as shown in Figure 1.6. The distribution dictates that each velocity value falls one, two, or three standard deviations away from the mean of zero. When one velocity component is correlated to itself, the variation from the mean is squared and leads to large numerical values of the correlation. When one velocity component is correlated to another Cartesian coordinate component, the variation between the two terms drives the correlation value closer to the mean of zero. It is recommended that future research investigates the single–point correlation in the polar coordinates using coordinate transformation relations outlined by Currie (2013). These correlations could lead to better physical understanding of the Reynolds stress terms and corresponding fluid characteristics.

4.3 Assessment of the Periodic Cube Assumptions

The periodic cube, shown in Figure 3.1, is the shape selected for the direct numerical simulation of homogeneous isotropic turbulence. This simplified geometry facilitates the computational simulation and speeds up the numerical algorithms solving the Navier–Stokes equations. Its use is based on a set of assumptions by Davidson (2004) listed in Section 0. After the statistical analysis of the turbulence periodic cube's vortical fluctuation properties, the three assumptions are assessed in this application.

1. The constituent unit cubes, forming the periodic cube shape, are identical at any instant.

In this study, a $163 \times 163 \times 163$ turbulence periodic cube is simulated. It is composed of $4{,}330{,}747$ unit cubes. The unit cubes are the same size, with the same initial and boundary conditions. They carry the same fluid input properties. Each cube has vortical fluctuations that are numerically simulated by a random number generator from a Gaussian distribution with the same mean and standard deviation. The same random number generator is utilized in the generation of each unit cube. They are run through the same non-linearity process and evaluated for the same skewness criterion. However, each time the random number simulation algorithm is run, a different array of random numbers is generated, still satisfying the turbulence requirements. Thus, the unit cubes are identical in their properties and turbulence criteria but unique in the constituent numerical vortical fluctuation values. The plots of ensemble average velocities, root mean square velocities, velocity correlations, and energy dissipation between the turbulence planes in Section 0 show that the velocities across the periodic planes vary within set intervals without repeated

patterns. This shows that the velocity fluctuations are not identical within the unit cubes. Therefore, while the definition by Davidson (2004) states that the constituent unit cubes are identical at any instant, in this application they are considered to be closely related within a certain confidence level.

2. The pressure which one unit cube imposes on the adjacent cube is negligible since the size of the unit is much larger than the smallest eddy size for the defined fluid.

The pressure in this direct numerical simulation of homogeneous isotropic turbulence is constant. The turbulence is characterized by vortical fluctuations and not acoustic fluctuations. The shape of the periodic cube consists of the grouping of constituent unit cubes. Each unit cube is generated by the simulation outlined in Figure 3.6. Each unit cube has a constant pressure which is the same as that of the entire periodic cube. Based on the numerical algorithm, there is no pressure imposed by one unit cube on the other because the pressure values are not varying based on the unit cube location. The corner cubes, center cubes, and the very bottom ones all have the same pressure. Based on Davidson's (2004) assumption, the lack of pressure transfer between the cubes can be shown by comparing the size of the unit cube to the size of the smallest eddy in the fluid. In the energy dissipation analysis, in Section 0, the different turbulence scales are calculated. The largest eddy scale $l_0$is found to be 9.1961 m while the smallest eddy size, based on the Kolmogorov scale, is found to be 0.0379 m using Equation (4.8). The size of the largest eddy is slightly smaller than the characteristic length of the geometry structure L which is found to be 10.3258 m. When these physical lengths are

matched to the non-physical unit length measurements in the periodic cube, a unit becomes equivalent to 0.06335 m, which is larger than the smallest eddy size of 0.0379 m. Thus, the cubes are not communicating through the pressure field with the size of the unit cube being larger than the smallest eddy in the defined fluid.

3. The unit cubes are aligned and stacked where the discontinuities between the edges of the unit cubes do not affect the homogeneity of the turbulence.

The periodic cube consists of individual unit cubes each acquired from a numerical simulation run. The generated $4{,}330{,}747$ cubes are aligned and stacked to give the periodic cube of size $163 \times 163 \times 163$ units, as shown in Figure 2.2. The statistical analysis of the turbulence periodic cube is performed over the periodic planes, shown in Figure 4.2, and the line graphs are evaluated to assess the unit cube edge effects. First, the line graphs in Section 0 are investigated for possible pattern repeatability that may indicate that the unit cubes are not unique. Any repeatability shows that the field is no longer homogeneous because the mean quantities are no longer spatially invariant. The graphs are assessed for discontinuities indicating that the structural combination of the periodic cube leaves traces of rough edges between the constituent unit cubes. The analysis plots do not show repeated patterns, discontinuities, or sharp edges. The plots consistently show no indication that the edges of the unit cubes affect the data distribution in the periodic cube. Thus, based on the statistical analysis of the turbulence periodic cube with vortical fluctuations, it is verified that the unit cubes are stacked and aligned where their edges are not affecting the homogeneity of the turbulence.

4.4 Assessment of the Turbulence Velocity Skewness Criterion

The velocity skewness factor is used in the direct numerical simulation of the homogeneous isotropic turbulence periodic cube. The skewness factor definition was set by Tavoularis in 1978 as shown in Equation (2.1) and still stands as the reference expression used to determine when turbulence has reached fully-developed state. Previous experimental and computational research have shown that a value of -0.5 is the velocity skewness factor required in the case of isotropic turbulence to reach fully-developed state. Pan (2017) documents the time evolution of the velocity skewness in two simulation studies of homogeneous isotropic turbulence, shown in Figure 4.12. In both cases, the skewness converges to the desired -0.5 value in time.

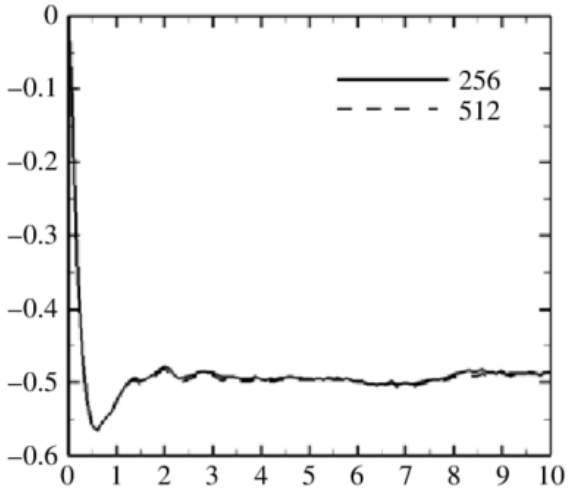

Figure 4.12 Convergence study for simulations of the decay of compressible homogeneous isotropic turbulence: the evolution of the skewness of the velocity derivative in time (Pan, 2017)

This criterion is employed in the direct numerical simulation code of this study to generate the unit cubes of turbulence, as shown in Figure 3.6. The documented skewness value of -0.5 is sought in the streamwise direction. Since the definition shows the variation of the streamwise velocity in the x-direction, it will be referred to as S_{ux} and the velocity skewness expression in Equation (2.1) is updated to

$$S_{ux} \equiv -\frac{\overline{\left(\frac{\partial u}{\partial x}\right)^3}}{\left[\overline{\left(\frac{\partial u}{\partial x}\right)^2}\right]^{3/2}} \tag{4.12}$$

When evaluating the skewness of the velocity fluctuations in the turbulence periodic cube in this application, the shape geometry and fluid properties are considered. The periodic cube is a still fluid field. Thus, there is no significance to the coordinate assignment since there is no direction of travel and subsequent transverse planes. The periodicity of the cube dictates that what occurs on one face of the cube occurs on the opposite side, Figure 2.2. The homogeneity and isotropy of the turbulence ensure that the mean quantities of a fluid property are invariant under translation and rotation/reflection respectively. The lack of directional preference in the cube geometry and fluid properties brings to light the question: **Is the streamwise velocity variation the important skewness factor to consider in the turbulence assessment?**

Proposing Additional Velocity Skewness Components

The velocity skewness components in the y and z-directions are defined following the Tavoularis (1978) expression in Equation (4.12) as follows.

$$S_{vy} \equiv -\frac{\overline{\left(\frac{\partial v}{\partial y}\right)^3}}{\left[\overline{\left(\frac{\partial v}{\partial y}\right)^2}\right]^{3/2}} \tag{4.13}$$

$$S_{wz} \equiv -\frac{\overline{\left(\frac{\partial w}{\partial z}\right)^3}}{\left[\overline{\left(\frac{\partial w}{\partial z}\right)^2}\right]^{3/2}} \tag{4.14}$$

This study evaluates all three velocity skewness components for the periodic turbulence cube. Similarly, Nagarajan (2009a) evaluated the time evolution of the three velocity skewness components for homogeneous isotropic turbulence in two direct numerical simulation studies, Figure 4.13. Starting at zero velocity skewness, the simulations are allowed to progress until all three skewness components converge to the desired value of -0.5.

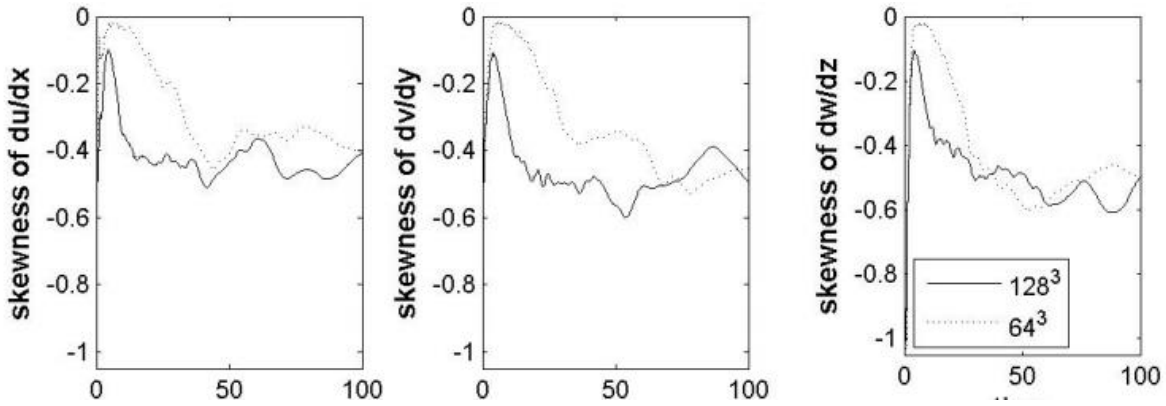

Figure 4.13 Time evolution of the three velocity skewness components in two direct numerical simulations of homogeneous isotropic turbulence (Nagarajan, 2009)

The three skewness components for this study are evaluated for 163 unit cubes, not over time, and shown in Figure 4.14. Note that the central differencing method, shown in Figure 3.3 and Equation (3.4), is used in the differential calculations of the skewness components and yields the same values for dx, dy, dz since the spatial distribution in the cube is the same in all three coordinates.

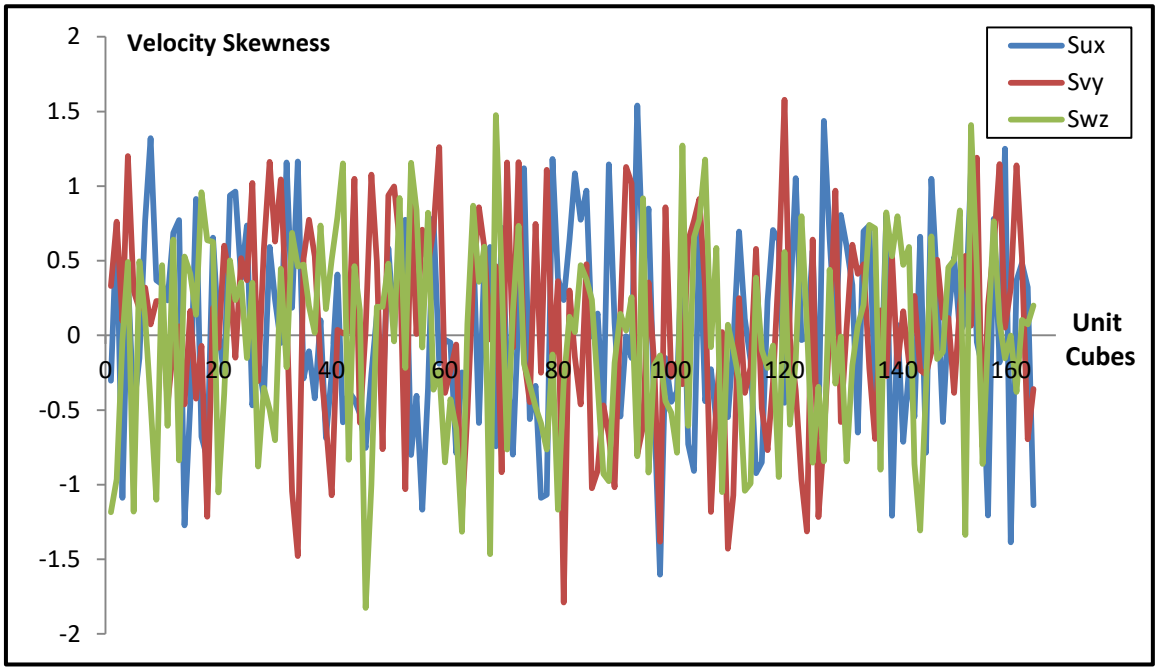

Figure 4.14 Velocity skewness components for a sample of 163 unit cubes

Figure 4.14 shows that within the periodic cube, the skewness components vary in magnitude between -1 and 1 (with a few spikes reaching up to 1.5 and dips reaching up to -1.8 variation) over a set of 163 unit cubes. The periodic cube consists of many unit cubes, however only 163 are selected for this analysis for better visual representation of the skewness values and to match the statistical analysis in the periodic planes' graphs, shown in Section 0.

The three velocity skewness components are averaged over the entire periodic cube and found to be close to zero, as documented in Table 4.6.

Table 4.6 Velocity skewness components in the turbulence periodic cube

Turbulence Cube	
S_{ux}	0.03011
S_{vy}	0.03021
S_{wz}	0.02999

The analysis in Figure 4.14 shows that two additional graphs are required. The first is the velocity skewness components' distribution diagram over the entire periodic cube to document the numerical values of the skewness components in all the unit cubes. The second is the plot of the skewness components' occurrence frequencies in the entire periodic cube.

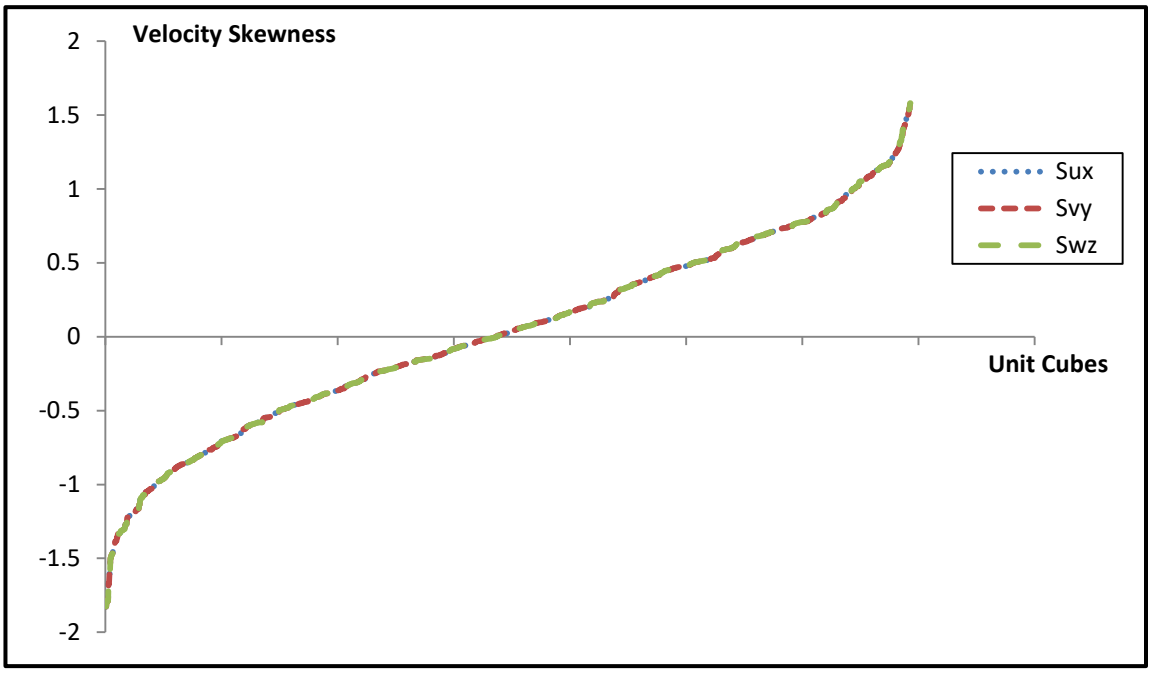

Figure 4.15 Velocity skewness components' distribution in the turbulence periodic cube

Since the plot in Figure 4.14 only shows the velocity skewness components corresponding to 163 unit cubes, the distribution of all the unit cubes' skewness components is plotted in Figure 4.15. The distribution graph shows that the highest skewness reached is 1.5 and the lowest is -1.8. The distribution also highlights the mean velocity skewness in the periodic cube around zero, which agrees with the documented values in Table 4.6.

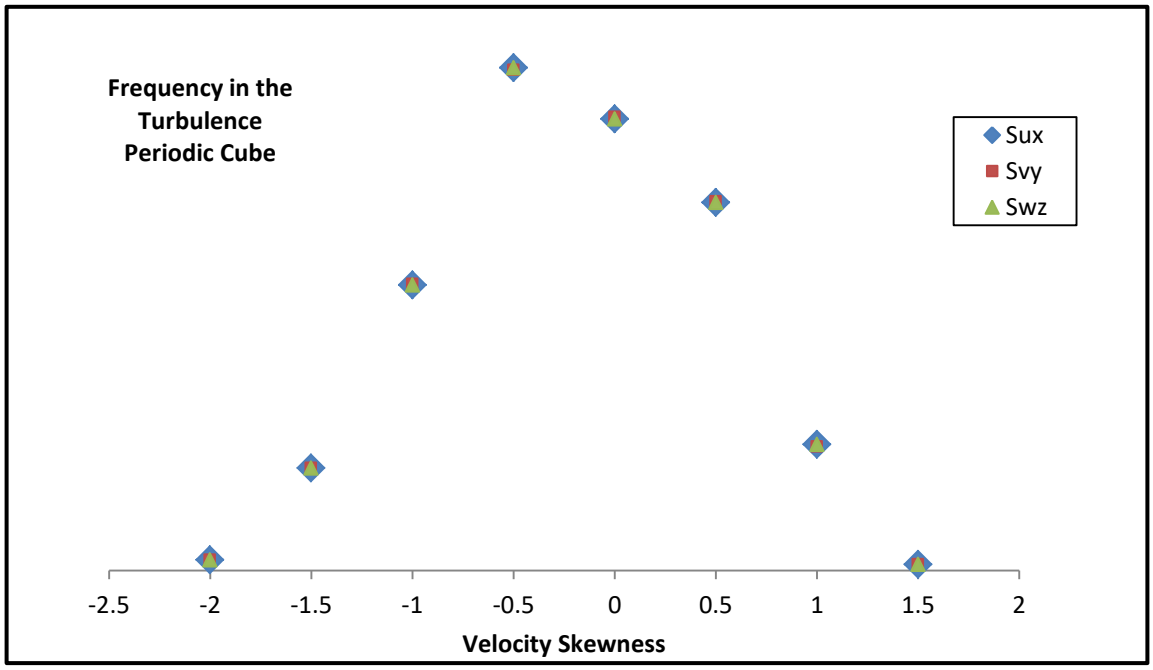

Figure 4.16 Velocity skewness frequencies in the turbulence periodic cube

Figure 4.16 shows the frequencies of occurrence of the different velocity skewness values, shown in the distribution diagram in Figure 4.15. It is found that all three skewness components behave similarly; the frequencies of occurrence are very close within each set interval. It is found that the most occurring velocity skewness measure is the desired value of -0.5. This is expected as it is the requirement for code termination. The vortical fluctuations in this direct numerical simulation study may have a higher or lower skewness value based on the array of random numbers generated within the unit cube during the run; the simulation advances and loops until the desired skewness is reached in at least one direction.

For truly isotropic turbulence, the three velocity skewness components should be the same for a large enough geometry. But with the numerically simulated and non-linearized random numbers, the velocity fluctuations' arrays are not exactly the same. While some may say they are the same within a set confidence interval, in this

application, the differences are studied to evaluate their significance and uniqueness. This is crucial in determining their importance when addressing the question regarding the skewness long-standing definition.

In the unit cubes, the velocity fluctuations are averaged to give a single skewness value for each component. When the velocity skewness is reached in at least one coordinate, the simulation terminates. However, sometimes the required skewness is reached in two and even three coordinates before the end of the simulation. Thus, due to computational advancements, all three skewness factor coordinates are assessed in this study for each unit cube and used to characterize the turbulence state. **So, what happens when the velocity skewness criterion is reached in one, two, or three coordinates? Is one case more turbulent than another or more developed?** Three case studies in which the skewness criterion in a unit cube is reached in: (a) one, (b) two, and (c) three coordinates are documented in Figure 4.17.

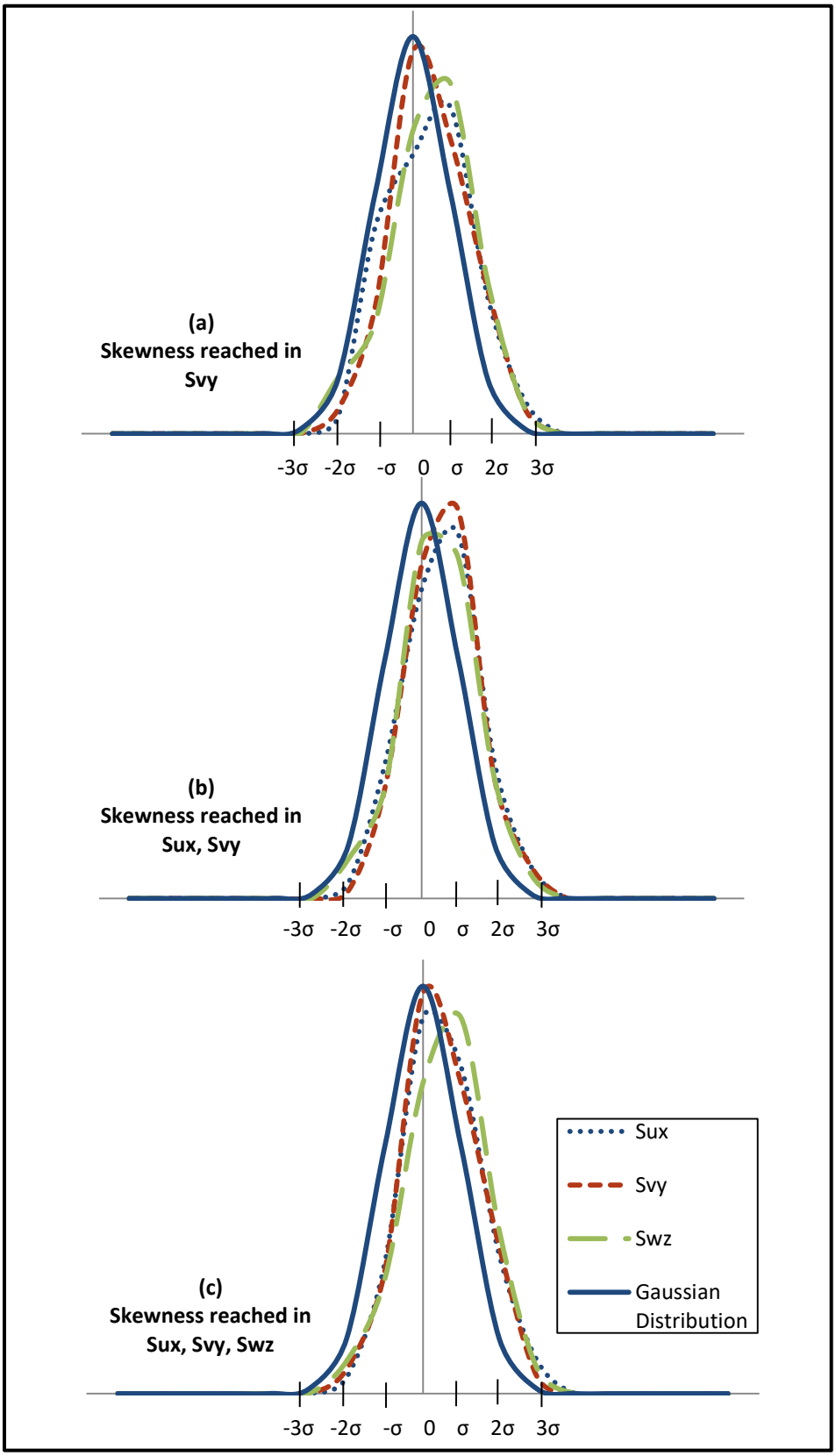

Figure 4.17 Case studies in which the skewness criterion is reached in (a) one (b) two and (c) three coordinates in unit cubes of turbulence

In each unit cube, a single skewness value is obtained for each component by averaging the velocity in a defined coordinate. In Figure 4.17, the velocity skewness measures are not documented, but rather the distribution of the velocity fluctuations leading to the skewness values are plotted against the reference Gaussian distribution. The three case studies show unit cubes in which:

(a) The skewness criterion is reached in one of the three coordinates, S_{vy}

(b) The skewness criterion is reached in two of the three coordinates, S_{ux} and S_{vy}

(c) The skewness criterion is reached in all three coordinates, S_{ux}, S_{vy}, and S_{wz}

The numerical simulation yields millions of such distributions for the unit cubes. The three shown in Figure 4.17 are selected as representative samples to display the observed trends. In this numerical simulation code, it is found that the most occurring case is that of the velocity skewness reaching the Tavoularis criterion in two coordinates. The least occurring case is that of the velocity fluctuations in all three coordinates reaching the desired skewness. This is strictly due to the computational simulation time previously defined in Equation (3.25). For a turbulent field, the velocity skewness is expected to shift from the normal distribution of the Gaussian plot slightly away from the mean, but still maintain the shape and the intervals of standard distribution, as shown Figure 1.6.

This expected trend is in fact observed in (a). In the one coordinate where the skewness criterion is met, the plot shape is the closest to the Gaussian distribution, with a slight deviation. In the other two coordinates, irregular shapes are observed. The velocity fluctuation plots are shifted away from the Gaussian distribution, but do not

maintain the bell-shaped curve. When the desired skewness is reached in two coordinates, drawing such clear distinctions is not as easy. In (b) the two plots corresponding to the velocities reaching the desired skewness maintain the bell-shape and are closer to the Gaussian distribution height than the one case that has not reached skewness yet. However, the third case does not show irregular behavior. Finally, when the skewness criterion is reached in all three coordinates, the trends are even more challenging to depict. In (c) all three plots resemble the Gaussian distribution with slight deviation. However, velocity distributions in different coordinates may shift farther away from the mean and not reach the highest point, as in the reference bell curve.

It is found that when the skewness criterion is reached in one coordinate and the simulation terminates, the other two are underdeveloped and show clear disturbances. The velocity fluctuations in the one coordinate that reaches the desired criterion are locked and cleared of surrounding disturbances. However, as velocity fluctuations reach the desired skewness level in additional coordinates within the simulation time, clear trends are not as easily observed. The velocity fluctuations continue to be affected by the fluctuations in the other coordinates. The fluid field carries more disturbances within the different coordinates. If the data that is skewed in more coordinates is considered more turbulent, then that is in fact observed in these case studies. When the fully-developed criterion is sought in multiple coordinates, as proposed in this discussion, it must be noted that the data become more disturbed and the computational cost increases. Thus, the turbulence becomes more chaotic and inherent instabilities are amplified.

The question thus becomes: **Is the Tavoularis criterion for streamwise velocity variation sufficient to characterize the turbulence state?** In this discussion, three skewness components are introduced and analyzed. For the turbulence interaction case studies, the velocity skewness vector is proposed. The three components evaluated in the turbulence periodic cube study become the diagonal terms of the nine component skewness tensor.

$$S_{u_i x_j} = \begin{bmatrix} S_{ux} & S_{uy} & S_{uz} \\ S_{vx} & S_{vy} & S_{vz} \\ S_{wx} & S_{wy} & S_{wz} \end{bmatrix} \tag{4.15}$$

The proposed velocity skewness vector takes into consideration all three velocity components and their variations in all three Cartesian coordinates. It is a comprehensive assessment of the velocity skewness parameter and is used to evaluate whether the long-standing Tavoularis skewness factor is sufficient for characterizing the turbulence state or if it can be extended to include more components that carry additional information.

5. Turbulence Interaction Case Studies

The turbulence periodic cube, in Figure 3.1, is simulated and statistically analyzed to understand the fundamental turbulence structures. The next step is to introduce the cube of homogeneous isotropic turbulence into the computational domain, shown in Figure 3.8, as incoming flow to the interaction case studies of interest: shock–turbulence and detonation–turbulence interactions. An assessment of all the possible combinations of turbulent flow interactions with wave front types, for this topic of study, is documented in Table 2.2. As a result, a third case study is added: unforced–detonation interaction. A direct numerical simulation code, Figure 3.7, is utilized to generate all three case studies and is run through the computational resources of the Texas Advanced Computing Center at the University of Texas at Austin due to its high computational power requirements. The output data of all three interactions are collected and statistically analyzed.

5.1 Turbulence Interaction Case Studies' Properties

The computational domain of the interaction case studies, shown in Figure 3.8, is the cuboid of size $815 \times 163 \times 163$ units. The periodic cube of turbulence of size $163 \times 163 \times 163$ units and previously defined fluid properties starts at the inlet of the domain and travels through the 815 units axially. The thin wave front is placed halfway through the domain allowing enough space for the turbulence periodic cube to travel, interact with the wave front, and propagate downstream of the wave. In the case of shock–turbulence interaction, the wave is a stationary normal shock. In the cases of unforced–detonation and detonation–turbulence interactions, it is a normal shock with added heat release, creating an inherently unstable detonation wave. Both wave front types are fixed and do not propagate once they interact with the traveling flow. The turbulence case studies have an incoming periodic cube with vortical forcing, while the unforced case has no velocity fluctuations; the velocity is constant in the entire periodic cube. In all three case studies, the same velocity of interest is used corresponding to Mach 5.5. Based on the fluid field properties, the velocity becomes 1747.77 m/s. This velocity is imposed in the axial direction only and is selected as it allows the heat release parameter in the detonation case studies to sustain an adiabatic flame as in small paraffins in stoichiometric air.

Unforced–Detonation Interaction

The first case study is the interaction of an unforced field with a detonation wave. It is introduced as a third case study to the two main cases of turbulence interactions as a control to compare against the detonation–turbulence and eliminate the turbulence effects. A similar unforced–shock interaction is not proposed because it simply

represents a flow interacting with a normal shock wave, which has very well understood and documented equations. The unforced field has no vortical forcing, and thus the velocity is constant, as are the fluid temperature and pressure. All the other fluid properties are the same as those in the turbulence periodic cube. The unforced periodic cube, shown in Figure 5.1, is introduced to the computational domain, travels at the velocity of 1747.77 m/s (Mach 5.5) through the cuboid, interacts with the inherently unstable detonation wave, and propagates downstream of the wave front.

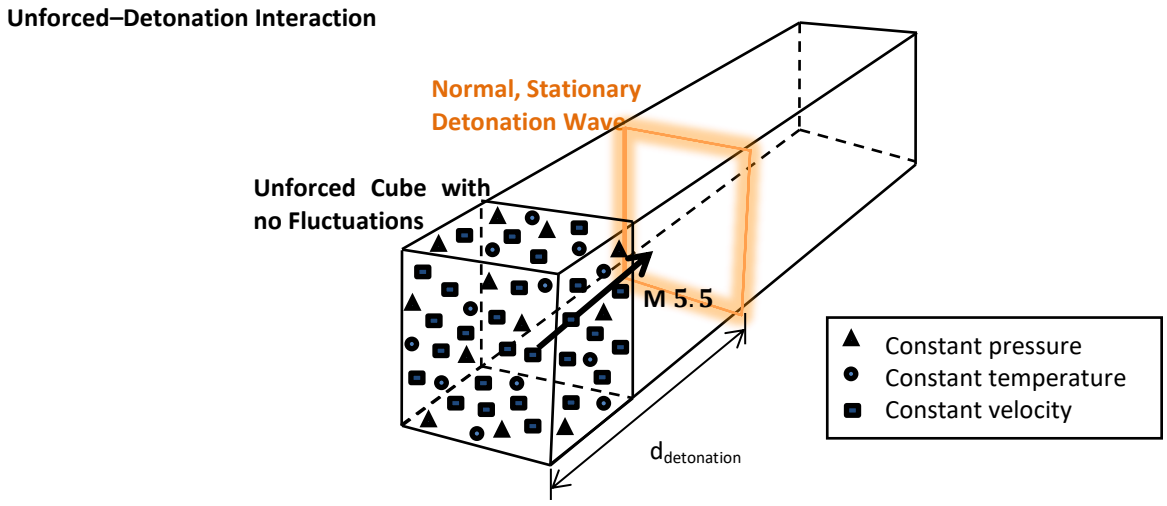

Figure 5.1 Computational domain of the unforced–detonation interaction case study

This case study allows the analysis of the effects of the heat release and the detonation instability without any additional disturbances from the flow itself. The incoming constant flow velocity, temperature, and pressure will experience changes post-shock based on the normal shock relations and heat release, outlined in Section 0. However, no coupling effects are present.

Shock-Turbulence Interaction

The second case study is the interaction of the homogeneous isotropic turbulence periodic cube with a shock wave. Much research has been conducted in this topic for flow with vortical fluctuations and its interaction with a moving or stationary shock. Thus, it is utilized as a reference to ensure the validity of the direct numerical simulation code when the output data is compared to documented literature. In this study, the incoming fluid flow has vortical fluctuations and acquires mean travel velocity of 1747.77 m/s in the axial direction. Similarly to the unforced–detonation case, the periodic cube starts at the computational domain inlet and travels down the cuboid. It interacts with the fixed shock wave and continues to travel downstream while the shock wave remains stationary, as shown in Figure 5.2.

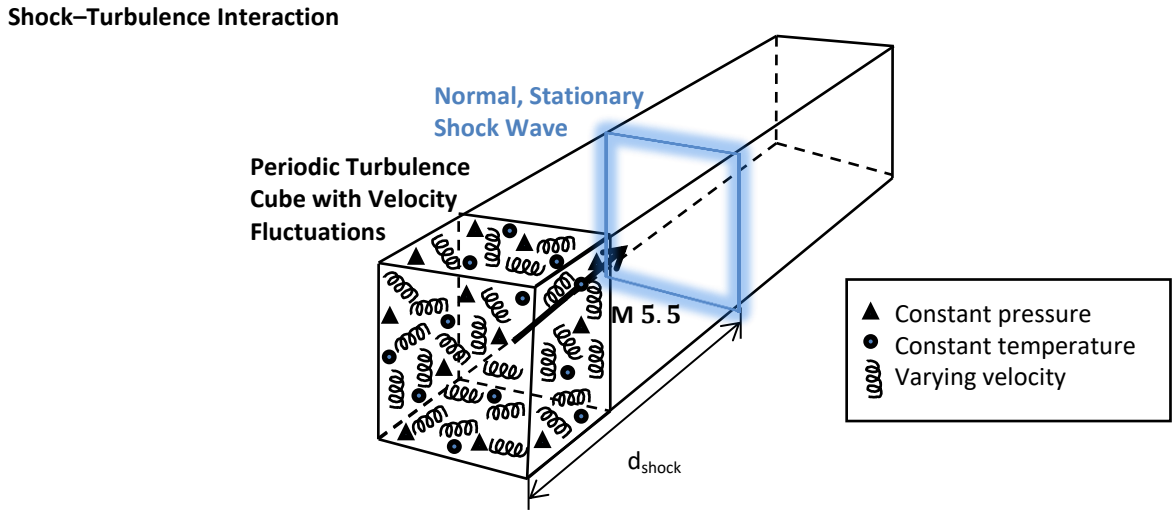

Figure 5.2 Computational domain of the shock–turbulence interaction case study

The flow properties of velocity, temperature, pressure, and density are altered by the normal shock relations, as shown in Figure 2.3. The incoming fluid flow with turbulent instabilities experiences amplifications and dampening due to the interaction with the shock wave.

Detonation-Turbulence Interaction

The third and final case study is the interaction of the homogeneous isotropic turbulence periodic cube with a detonation wave. This study differs from the shock–turbulence interaction in the fact that it has an exothermic reaction with the added heat release complexity. Moreover, the detonation structure has a length scale associated with it and intrinsic fluctuations that cause instabilities, both which are not present in the shock wave. Fewer researchers have investigated the detonation–turbulence interaction case study, when compared to the works in shock–turbulence interaction. This study aims to establish an understanding of the effects of heat release, the detonation length scale, and the intrinsic wave instability on the propagation of the turbulent flow. The incoming turbulent flow has vortical fluctuations and travels with a mean axial velocity of 1747.77 m/s as in the shock–turbulence interaction. The flow starts at the computational domain inlet, travels through the cuboid, interacts with the detonation wave, and continues to travel downstream of the domain, as shown in Figure 5.3. Throughout the interaction, the detonation wave placement remains stationary.

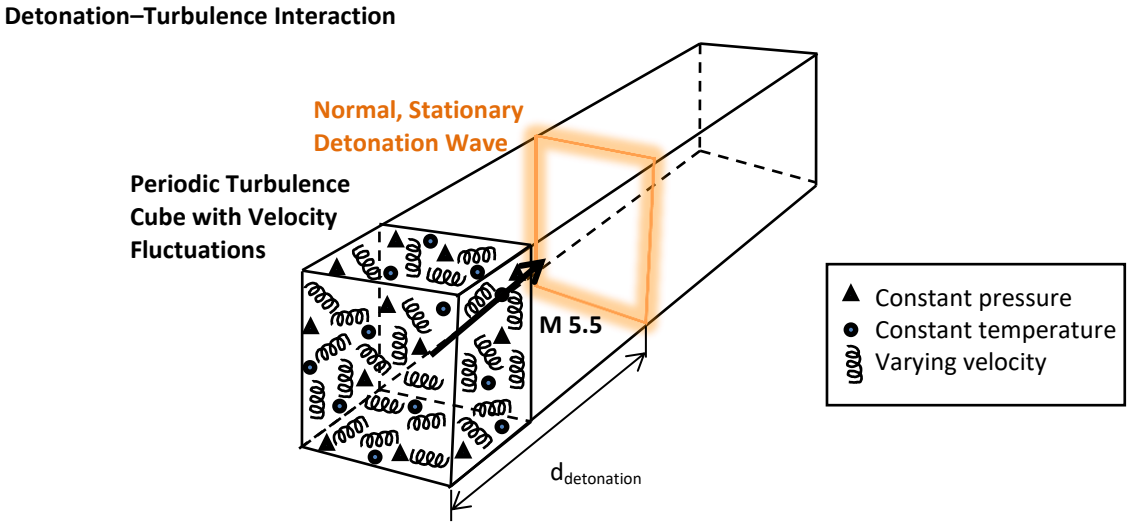

Figure 5.3 Computational domain of the detonation–turbulence interaction case study

The flow properties of velocity, temperature, pressure, and density are changed by the normal shock relations and the single-step Arrhenius law upon the interaction, as shown in Figure 2.5. The incoming turbulent fluid flow experiences amplifications and dampening due to the interaction with the detonation wave. The effects of the turbulence, the detonation structure, and their interaction are assessed in this case study.

5.2 Turbulence Interaction Case Studies' Statistical Analysis

After the computational domain and interaction parameters are defined, the direct numerical simulation data output is analyzed. The equations utilized in the statistical analysis of the fluid flow properties in the three interaction case studies are the same as those used in the turbulence periodic cube statistical analysis. Thus, the equations in Section 0 are not stated again. The data in each square plane is averaged into a single point. The points are then connected over the 815 planes to create a line plot depicting the evolution of the fluid property through the computational domain, as shown in Figure 5.4.

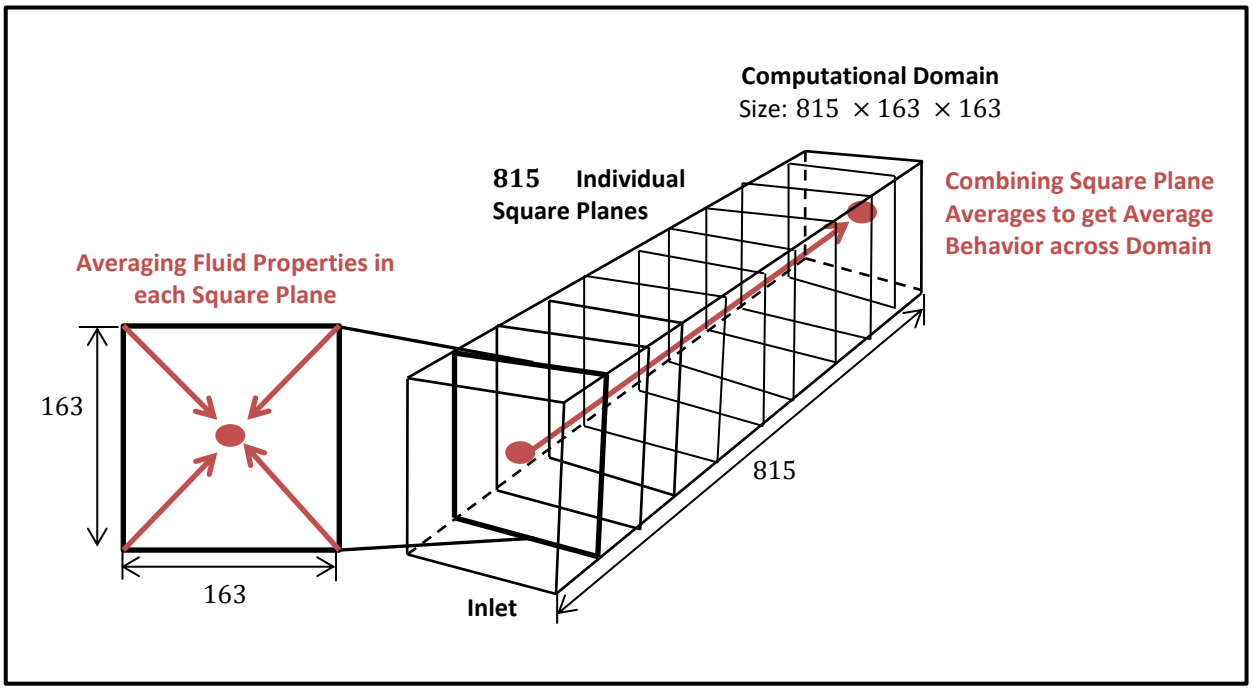

Figure 5.4 Averaging fluid properties in individual square planes and combining the averages over the computational domain

Average Velocities

The axial flow velocity is set in all three case studies as 1747.77 m/s. The transverse velocities in the periodic cubes are different between the turbulent and unforced case studies. In the turbulence periodic cube, the transverse velocities are the velocity fluctuations with mean of zero and a standard deviation set to $1\ \%$ of the incoming travel velocity (with slight deviation). In the unforced case study, however, there are no velocity fluctuations and thus the transverse velocities are zero. The difference in the velocity ranges dictates plotting the average axial and transverse velocities separately.

The axial velocities of all three case studies are averaged, using the technique shown in Figure 5.4, and plotted alongside the normal shock solution and the ideal Zel'dovich, von Neumann, Döring (ZND) detonation model, in Figure 5.5. The normal shock solution is based on the relations documented in Section 0. It shows the velocity drop as a step function. The ideal ZND detonation model is based on the equivalent detonation relations (Glassman, 2008), one–dimensional ZND model developed by Shepherd (1986), and numerical simulation studies by Massa (2011a). The velocity experiences a sharp drop followed by a rise and a return to isotropy farther downstream.

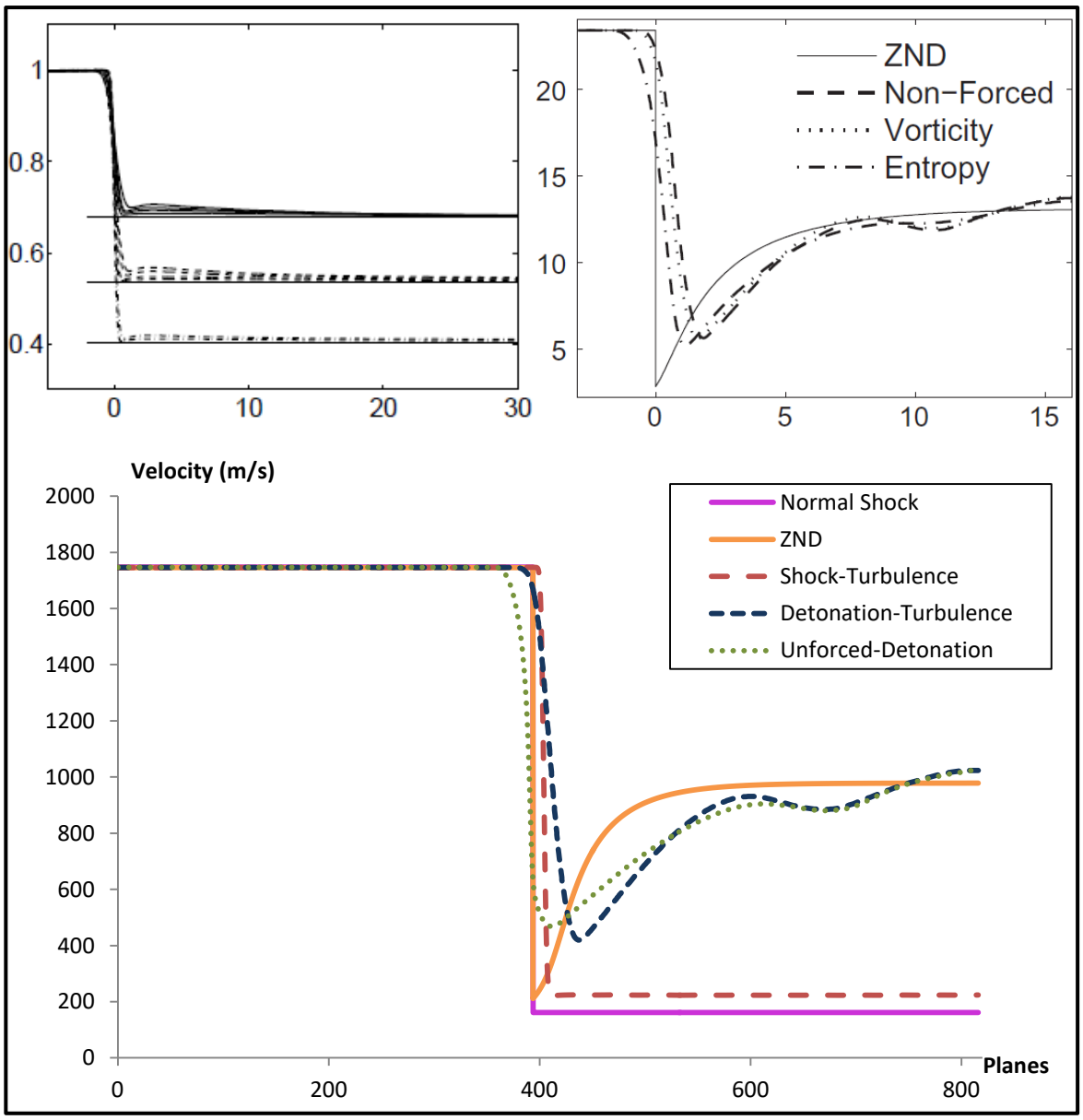

Figure 5.5 Top left: Normalized shock–turbulence interaction average axial velocity profiles at Mach $1.27, 1.5, 1.87$, direct numerical simulation study (Larsson, 2008) - Top right: Normalized unforced–detonation, vortically forced and entropically forced detonation–turbulence interaction average axial velocity profiles at Mach 5.5, direct numerical simulation study (Massa, 2011a)- Bottom: Average axial velocity profiles in unforced–detonation, shock–turbulence, and vortically forced detonation–turbulence case studies at Mach 5.5 compared to the normal shock solution and ideal ZND detonation model, direct numerical simulation (current study)

Larsson (2008) shows that the larger Mach numbers denote larger shock jumps, top left diagram. At Mach 5.5, the shock–turbulence average velocity profile, in the current study's bottom diagram, follows the step function shape with a significant jump. However, the step is shifted to the right, when compared to the normal shock solution, behind the shock wave front and sustains a higher energy level post-shock. These two effects, thus, are attributed to the incoming flow turbulence.

Massa (2011a) compares the detonation–turbulence interaction average axial velocity profiles of two forcing types to the ZND model, top right diagram. The detonation–turbulence velocity profile in this current study, bottom diagram, follows the general shape of the ZND model solution. The shifting of the velocity profile is observed again at the wave front location. However, the downstream behavior is more complex in the presence of fluctuations, as is observed in Massa's (2011a) diagram. The drop in velocity does not reach the lowest point that the ZND model proposes. The velocity profile rises but fluctuates in an attempt to reach the ZND level and return to isotropy.

The unforced–detonation case study follows the general shape of the ZND detonation model, as in Massa's (2011a) diagram. It experiences a velocity drop prior to any of the other case studies. In the absence of turbulence, this is attributed to the unsteadiness of the detonation wave. The velocity profile reaches a minimal in the drop that is higher than that predicted by the ZND model and follows the detonation–turbulence interaction fluctuation pattern downstream. The higher minimum velocity and downstream variations are thus attributed to the detonation wave length scale and intrinsic instability.

Therefore, the average velocity deviation is a stretch in the flow response to the shock wave properties and is attributed to the turbulence instabilities present in the shock and detonation–turbulence interactions. The unsteadiness of the detonation wave causes the unforced–detonation case study to begin to drop ahead of the wave front. The detonation length scale and intrinsic instability cause the fluctuations of the flow downstream when compared to the ideal ZND model. The flow is attempting to return to isotropy but is experiencing dampening due to the detonation effects. Both detonation case studies also show the lowest average velocity higher than that in the ideal ZND model making all three case studies' direct post-shock velocities higher than the theoretical values. This can be attributed to the numerical simulation and the non-linearity of the Navier-Stokes equations used to generate the fluid properties in the three case studies.

After analyzing the average axial velocity profiles, the transverse velocity profiles are plotted for all three case studies and compared in Figure 5.6.

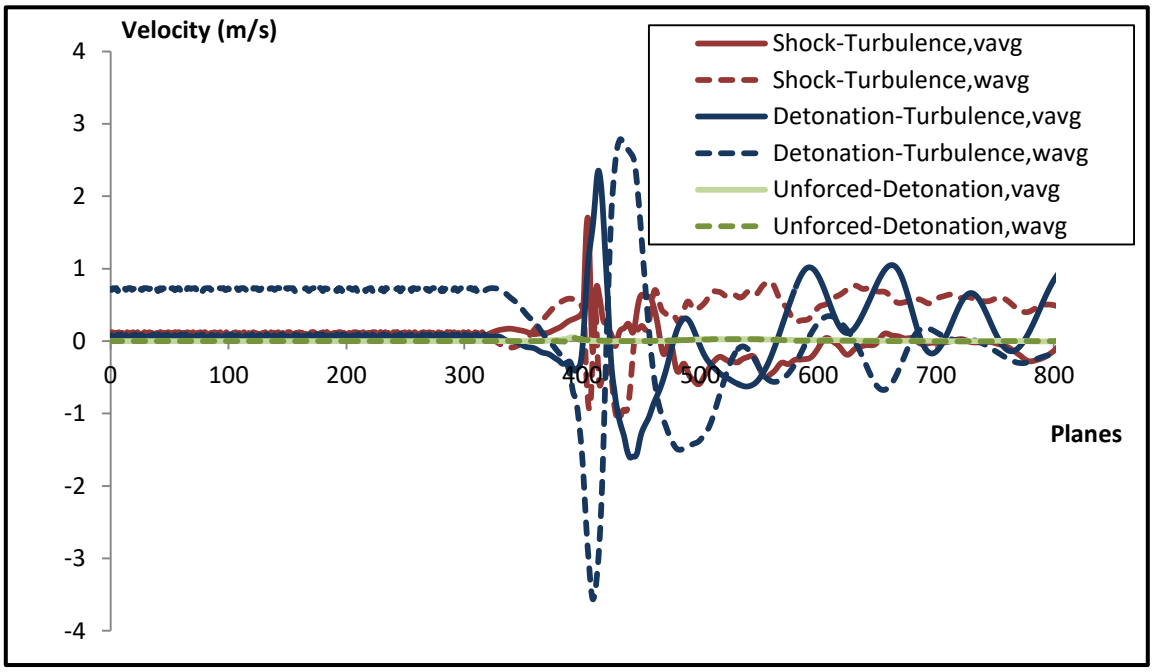

Figure 5.6 Average transverse velocities in the three case studies

Since the velocities in the transverse planes are low, they never reach Mach 1. Thus, the normal shock relations cannot be applied to predict the velocity profile downstream. Instead, the mass flow rate relation is used

$$\rho v = \rho_{PS} v_{PS} \tag{5.1}$$

where the density term is calculated using the ideal gas law, Equation (3.3). The density post shock is calculated using the normal shock relations because it represents the fluid properties in the computational domain. Figure 5.6 shows that in the unforced–detonation case study, the transverse velocities start around zero and continue in the same manner across the entire computational domain. However, in the two turbulence case studies, the transverse velocities experience amplification and dampening. Even

though the velocity values are still on average close to zero, these variations are attributed to the turbulent fluctuations not the shock or detonation waves.

It must be noted that the detonation–turbulence interaction case studies' transverse velocity profiles show more distinct fluctuation patterns post-shock. The detonation case studies in the axial velocity profiles also show fluctuations in the far field of the computational domain. So, the detonation structure is consistently causing varying patterns downstream of the wave front not present in the shock–turbulence interaction case.

Root Mean Square Velocities

As previosuly defined in Equation (4.5), the root mean square averages represent the square root of the variance; the standard deviation of the velocities. In the turbulence case studies, the turbulence vortical fluctuations have a standard deviation set to $1\ \%$ of the incoming velocity of 1747.77 m/s. Thus the standard deviation is about 17.5 m/s in all three coordinates. As for the unforced–detonation case study, the flow has no vortical fluctuations. Thus, the standard deviation is zero is all three coordinates. The root mean square velocities are plotted in all three coordinates for the three case studies in Figure 5.7.

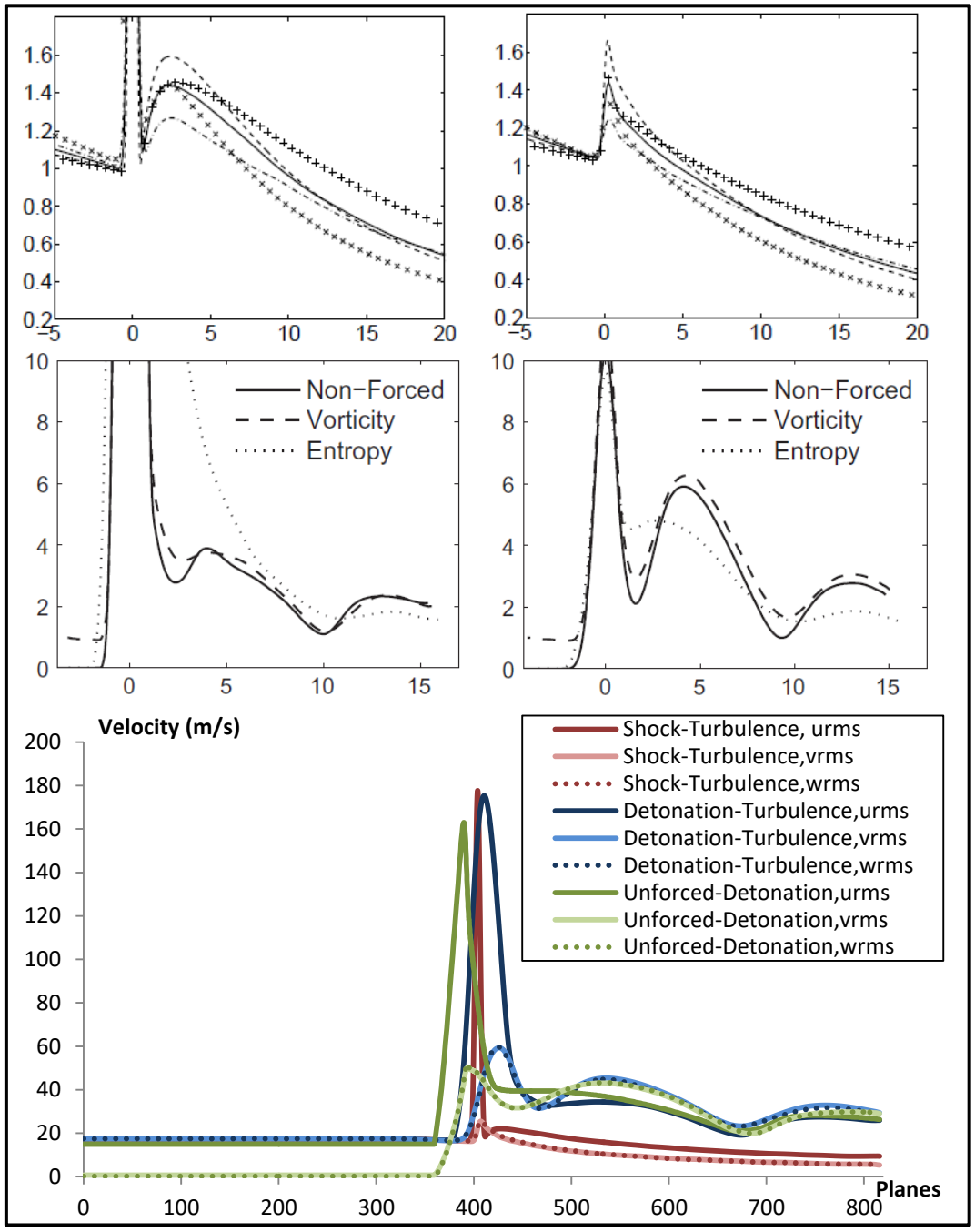

Figure 5.7 Top left to right: Normalized shock–turbulence interaction velocity variance profiles in the streamwise and transverse directions at Mach 1.27 (dash-dot), 1.5 (solid line), and 1.87 (dash), plus and cross denote turbulent Mach number variations, direct numerical simulation study (Larsson, 2008) – Middle left to right: Normalized unforced–detonation, vortically forced and entropically forced detonation–turbulence interaction longitudinal and transversal velocity variance profiles at Mach 5.5, direct numerical simulation study (Massa, 2011a)- Bottom: Root mean square velocity profiles in unforced–detonation, shock–turbulence, and vortically forced detonation–turbulence case studies at Mach 5.5, direct numerical simulation (current study)

Larsson (2008) documents the streamwise and transverse velocity variance profiles for the shock–turbulence interaction, while Massa (2011a) documents them for the unforced–detonation and detonation–turbulence interaction case studies. The profile shapes of the root mean square velocity in the current study diagram can be compared to the four other velocity variance diagrams as it is only scaled differently.

The root mean square velocity profiles, ahead of the wave fronts in the bottom graph of Figure 5.7, show consistent standard deviation values in all three cases. The turbulent cases have a standard deviation close to expected 17.5 m/s value in all three coordinates, while the unforced–detonation case study has a standard deviation close to zero in all three coordinates.

The axial root mean square profiles, in the three case studies, show the patterns of rapid rise followed by rapid decline around the wave front position.The shock–turbulence interaction root mean square velocity profile shows a narrow rise and decline while the detonation cases show wider spread distributions. The shock–turbulence interaction root mean square velocity profile shows a smooth decay downstream to values lower than the initial standard deviation, consistent with Larsson's (2008) observations. However, the detonation case studies show the expected detonation-induced fluctuations downstream, as in Massa's (2011a) graph. The effects of the detonation are experienced ahead of wave front in the unforced–detonation case study due to the instability of the detonation and the absence of the turbulence.

The transverse root mean square profiles also experience rise and decline around the wave front, but the maximum velocities are much lower than those in the axial

directions. That is the reason they are plotted separately by Larsson (2008) and Massa (2011a). Downstream, all three case studies' transverse velocities follow the trends of the axial velocity profiles. In the shock–turbulence interaction, the transverse velocity profiles decay to values lower than the initial standard deviation while the two detonation case studies' transverse velocity profiles experience fluctuations.

Thus, the detonation causes a wider spread distribution of standard deviation values around the wave front, early rise and decline in the absence of turbulence ahead of the wave front, and variations downstream. The shock–turbulence interaction velocity fluctuations are not as strong and cannot sustain the isotopic velocity levels downstream of the wave front.

Turbulent Kinetic Energy

The evolution of the turbulent kinetic energy through the computational domain is evaluated for all three case studies. The flow's turbulent kinetic energy in the physical and time domain is associated with the root mean square velocities and calculated using Equation (4.6). The turbulent kinetic energy profiles of the three case studies are plotted and compared in Figure 5.8.

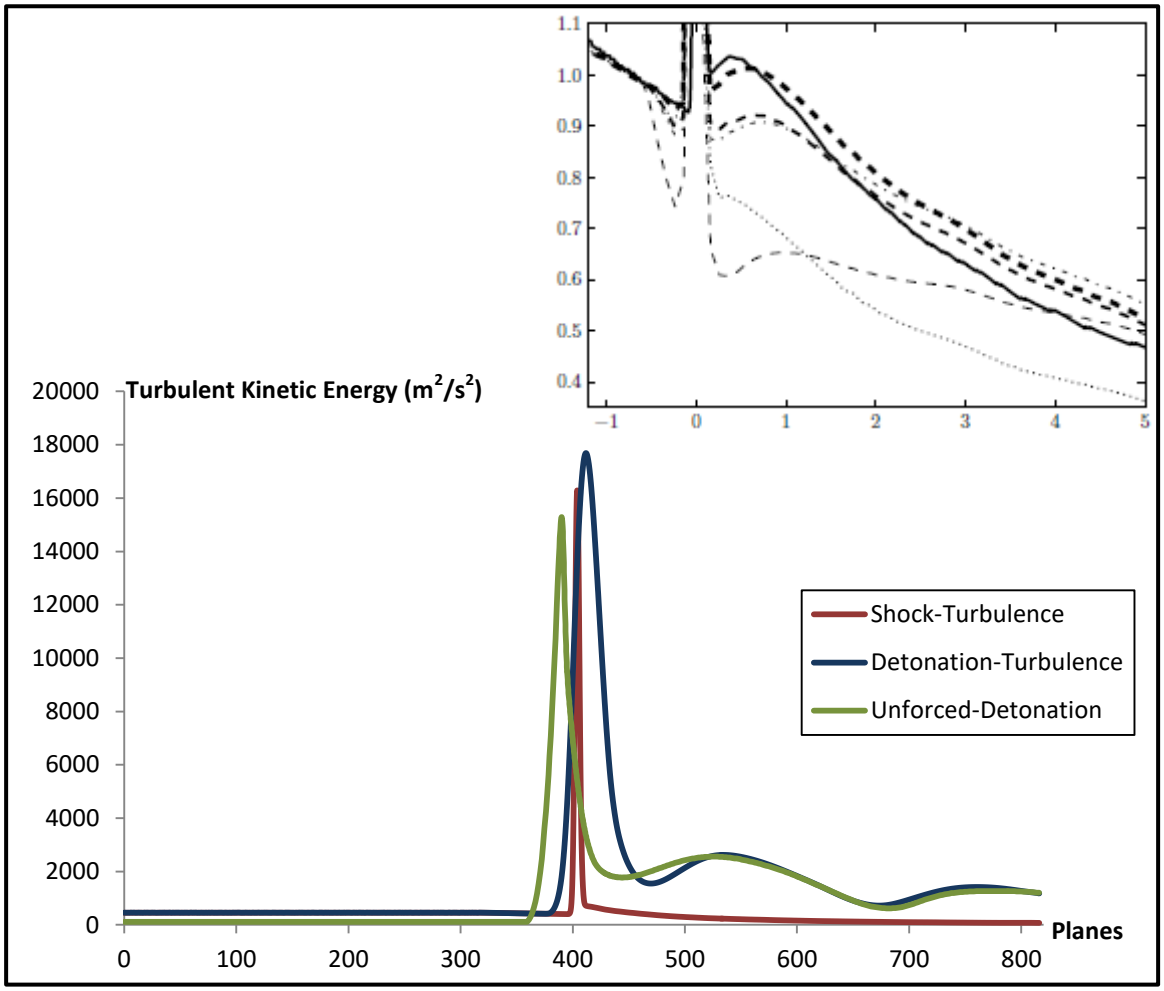

Figure 5.8 Top: Normalized shock–turbulence interaction turbulent kinetic energy at Mach 1.5, direct numerical simulation (solid line), large eddy simulation (dashed line- thickness increasing with increasing numerical solution accuracy) (Bermejo-Moreno, 2010) - Bottom: Turbulent kinetic energy in unforced–detonation, shock–turbulence, and detonation–turbulence case studies at Mach 5.5, direct numerical simulation (current study)

Documented direct numerical and large eddy simulation studies often cutt off the rise in the velocity profiles across the shock front and focus instead on the shock near zone. This is seen in Bermejo-Moreno's (2010) top turbulent kinetic energy of shock–turbulence interaction diagram.

Ahead of the wave front, the fluid flows show low energy levels especially in the unforced–detonation case study where the energy profile is close to zero, as shown in bottom graph of Figure 5.8. Upon the flows' interaction with the shock and detonation wave fronts, the turbulent kinetic energy levels spike. In the shock–turbulence interaction, the turbulent kinetic energy experiences a sharp rise followed by a sharp decline and steady reduction downstream of the shock, consistent with Bermejo-Moreno's (2010) visual. The turbulent kinetic energy, thus experiences a spike across the shock wave.

In the detonation case studies however, unforced and turbulent flows experience a rise and decline around the detonation wave over a wider region. This is attributed to the unsteady detonation wave front. In addition, the detonation causes turbulent kinetic energy fluctuations downstream of the wave front. The two case studies maintain higher energy levels downstream when compared to the shock–turbulence interaction. The detonation is found to energize the flow. The unforced–detonation case study experiences the effects of the unsteady detonation wave front ahead of the other two case studies due to the absence of the turbulence; a trend observed in the average axial velocity and root mean square velocity profiles before. While all three root mean square velocity components are involved in the calculation of the flow turbulent kinetic energy, the axial velocity plays the biggest role since its numerical values are significantly higher than the transverse velocities.

While the turbulent kinetic energy in the physical and time domain indicates the strength of the turbulence fluctuations, it is found that the vortical fluctuations in the shock–turbulence interaction are weaker than those in the detonation–turbulence

interaction. The shock–turbulence interaction has less turbulent kinetic energy overall and the flow is unable to retain higher levels of energy in the computational domain far field.

Reynolds Stress Components

As the root mean square velocities are employed in the turbulent kinetic energy calculations, they are utilized in the correlation relation of the vortical fluctuations to evaluate the Reynolds stress components. The three diagonal ($RS_{uu}, RS_{vv}, RS_{ww},$) and the three unique off-diagonal ($RS_{uv}, RS_{uw}, RS_{vw}$) components are calculated using the Equation (4.11) to show the vortical fluctuations' contribution to the momentum flux. The Reynolds stress tensor's diagonal components forming the normal stresses in the three interaction case studies are shown first in Figure 5.9. These are the turbulent kinetic energy constituent terms.

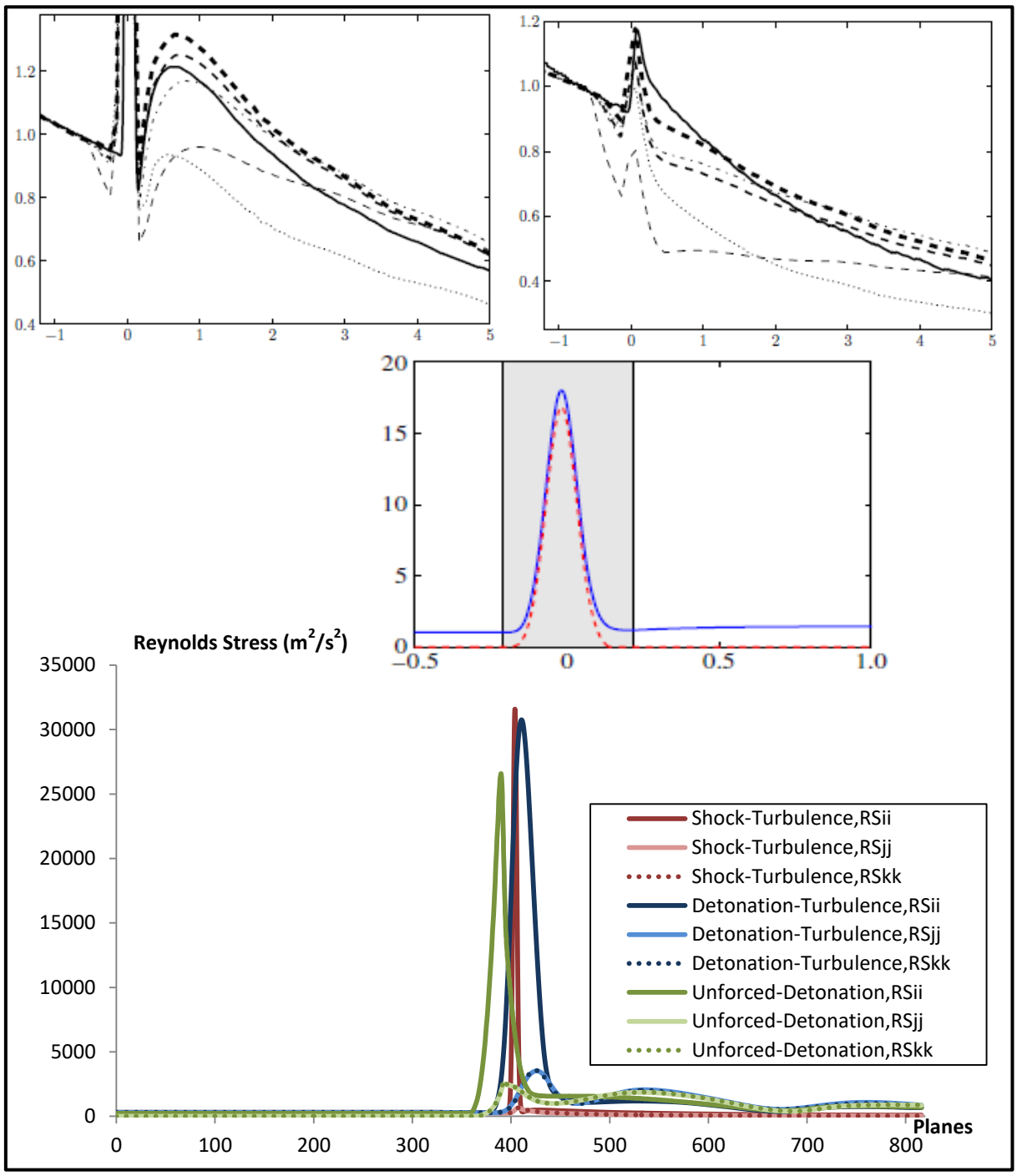

Figure 5.9 Top left to right: Normalized shock–turbulence interaction streamwise and transverse Reynolds stress components at Mach 1.5, direct numerical simulation (solid line), large eddy simulation (dashed line- thickness increasing with increasing numerical solution accuracy) (Bermejo-Moreno, 2010) – Middle: Zoomed out view showing the full peak shock–turbulence interaction streamwise Reynolds stress at Mach 1.5 (solid line) and at Mach 3.5 (dashed line), direct numerical simulation study (Larsson, 2013) - Bottom: Normal stress components in unforced–detonation, shock–turbulence, and detonation–turbulence case studies at Mach 5.5, direct numerical simulation (current study)

Bermejo-Moreno (2010) documents the streamwise RS_{uu} and transverse RS_{vv} Reynolds stress components in shock–turbulence interaction through direct numerical and large eddy simulation studies. Only one transverse component is documented as it shows similar trends to RS_{ww}. Larsson (2013) zooms out of the shock–turbulence interaction streamwise Reynolds stress component to depict the full peak and shows narrow distrubution for higher Mach number. In the current study, the distribution in all three case studies is even narrower at Mach 5.5 and the full peaks are plotted.

The normal stress components are found to have low momentum values ahead of the shock in all three case studies, bottom graph of Figure 5.9. The momentum spikes upon the interaction with the shock and detonation waves then declines. Farther downstream, the velocity fluctuations vary but do not quite return to the levels of pre-shock isotropy. In the unforced–detonation case study, the detonation instability initiates the momentum spike in the axial direction ahead of the wave front. The maximum stress reached in the axial direction is lower than those reached by the other two turbulence case studies.

In the shock–turbulence interaction, RS_{uu} has the highest spike value but the narrowest spike shape when compared to the detonation cases. In the transverse coordinates, the normal stress components of RS_{vv} and RS_{ww} experience a small rise across the shock followed by steady decline downstream to values lower than the initial pre-shock correlations, as is documented by Bermejo-Moreno (2010). The two detonation cases have wider distribution of the RS_{uu} normal stress component. The detonation contributes to extending the momentum flux and retaining it downstream of

the shock through fluctuations. In the transverse coordinates, RS_{vv} and RS_{ww} reach higher correlation values than in the shock–turbulence interaction and retain higher momentum in the computational domain far field.

It is found that the normal stress components carry large momentum flux in the three case studies, with the component RS_{uu} being the most prominent. The shock–turbulence interaction shows narrow rise and decline, with continued decay downstream. The detonation case studies display wider distributed normal stress spikes, and fluctuations downstream. While the shock–turbulence interaction velocity fluctuations seem to fade away, the detonation wave front plays an important role in energizing the flow and sustaining higher velocity fluctuation strength across the computational domain.

The shear stress components; off-diagonal Reynolds stress terms in the interaction case studies are shown in Figure 5.10.

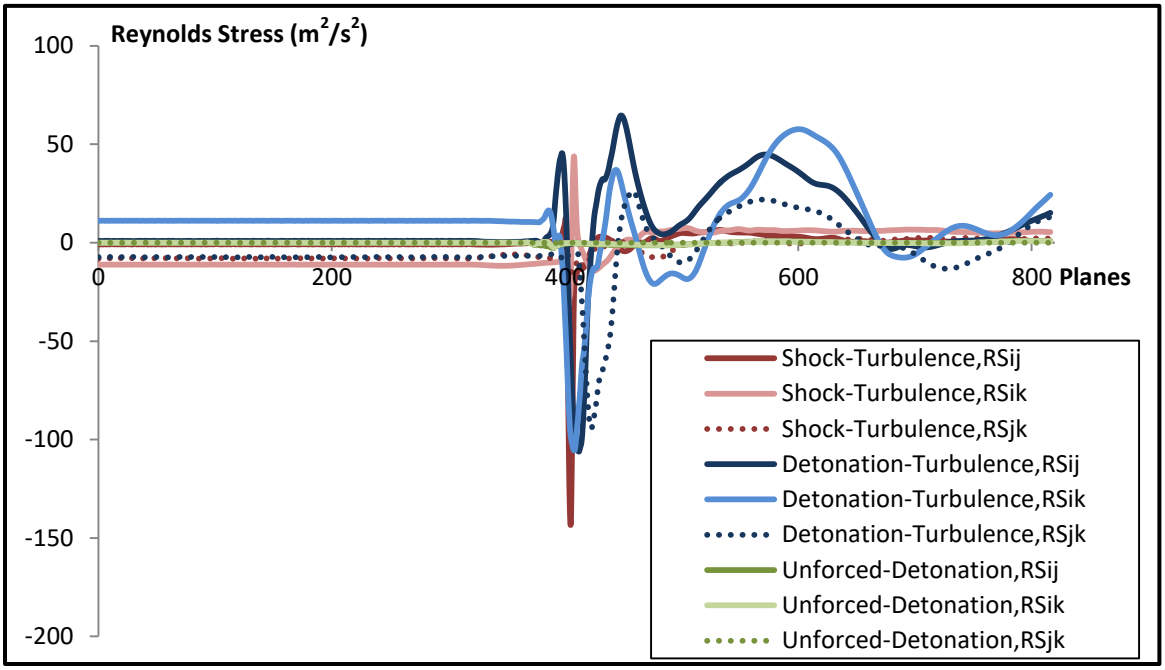

Figure 5.10 Shear stress components in the three case studies

The shear stress components depict the correlation of different velocity terms in the Cartesian coordinates. The three tangential stress components $RS_{uv}, RS_{uw}, RS_{vw}$ are shown in Figure 5.10 for all three case studies. When one velocity component is correlated with another, the shear stress values drop drastically, compared to the normal stresses in Figure 5.9. When the velocity is stretched in the direction of travel, the velocities in the transverse directions are compressed following the law of conservation of momentum. This phenomenon is portrayed in a diagram shown in Figure 5.11.

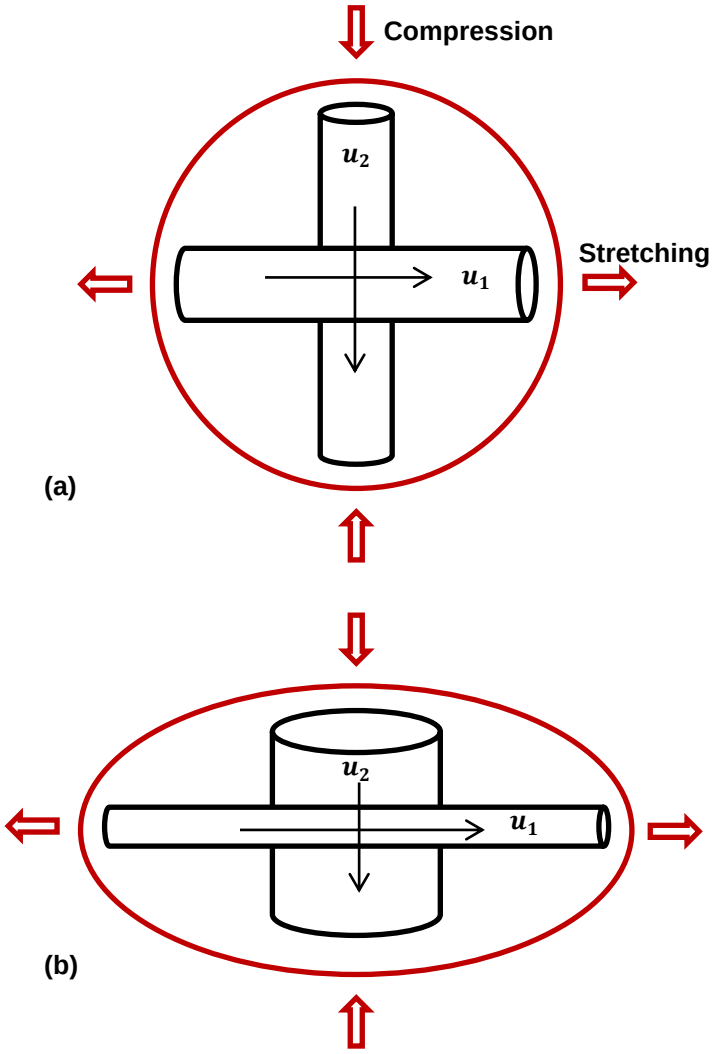

Figure 5.11 Velocity correlations in the flow field: (a) before stretching, (b) after stretching as adopted from Tennekes (1999)

Based on the law of conservation of momentum, when the velocity in the direction of flow travel is amplified, the velocity in the transverse direction is attenuated. Thus, the shear Reynolds stress components are expected to yield negative velocity correlations.

The shear stress components show values close to zero ahead of the shock wave in all three case studies. While the unforced–detonation case study maintains tangential stress levels close to zero throughout the computational domain, the stresses in the

turbulent case studies show some variations. The shock–turbulence interaction shows negative correlations across the shock interface. The detonation–turbulence interaction, however, shows some positive correlation. This is attributed to the heat release parameter.

The detonation–turbulence interaction is the one case study with the most evident fluctuations in the shear stress components. The shear stress components, overall, have much lower correlations than the normal stress ones. Since the correlation plots of turbulent kinetic energy and normal stresses follow the root mean square trends very closely, it is recommended to evaluate the correlations of the velocity fluctuations in the polar coordinates next. The polar coordinate transformation can show more information leading to better physical understanding of the fluid flow properties and interaction evolution.

5.3 Turbulence Interaction Case Studies' Visualizations

The computational simulation of the three interaction case studies produces large amounts of flow defining data in the space and time domains. Statistical analysis designates the data into descriptive and quantitative average properties. Two–dimensional flow visualizations are introduced in the direct numerical simulation case studies to display important flow behavior within the defined geometry. Such flow behavior has been previously explored experimentally by using soot foils, for example, to depict the propagating detonation cellular structures and transverse waves within a channel. The effects of wave confinement are depicted, as well as the instability of the detonation wave in the works of Austin (2003), Figure 5.12.

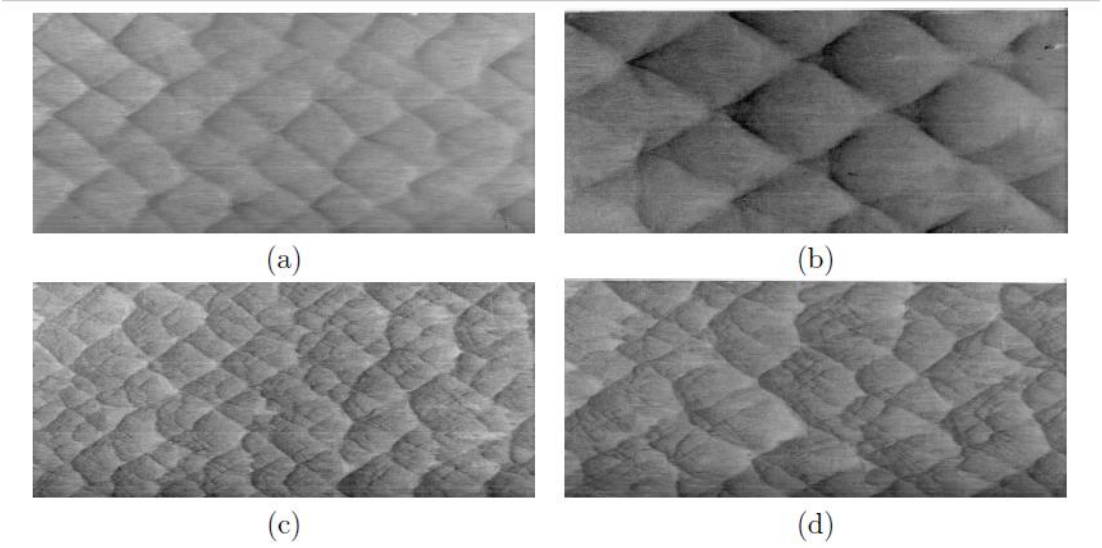

Figure 5.12 Sample experimental soot foils from weakly unstable detonation (a) $2H_2O_212Ar$ and (b) $2H_2O_217Ar$, and from highly unstable detonation (c) $H_2N_2O1.33N_2$ and (d) $C_3H_85O_29N_2$, detonation propagates from left to right, foils mounted downstream of the window section of a narrow channel (Austin, 2003)

The observed detonation cellular structures in Figure 5.12 are also obtained through computational simulation of a detonation wave propagating through a narrow channel. The works of Chinnayya (2013) in Figure 5.13 show transverse and incident shock

waves affixed on triple points whose trajectories through the domain govern the cellular structures. Different channel heights are explored to determine the effects of scale reduction on the dissipative phenomena.

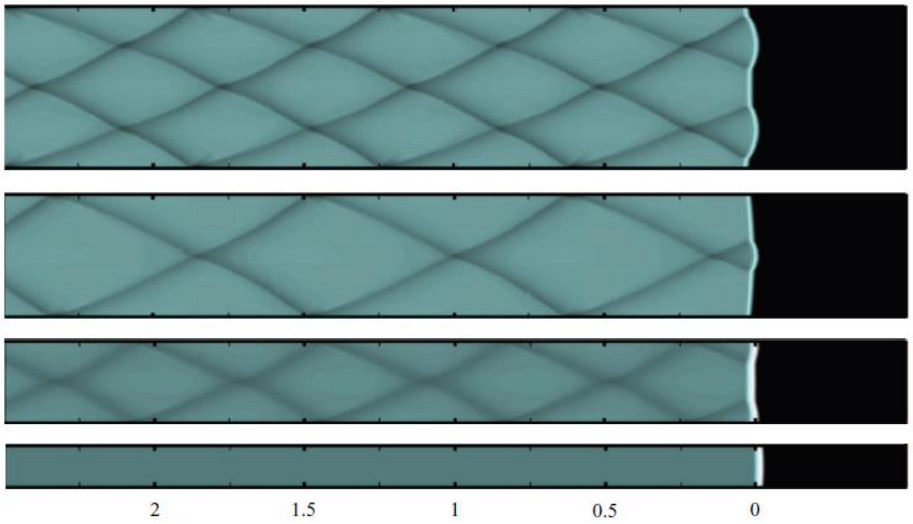

Figure 5.13 Computational study of detonation wave propagation through different channel heights, Top to bottom channel heights: $4H_{ref}, 3H_{ref}, 2H_{ref}, H_{ref}$ (Chinnayya, 2013)

Thus, for the current study, surface flow visualizations of ensemble averaged velocities allow exploration and analysis of the data while depicting the fluid patterns through color or texture. Three–dimensional surface plots of the interaction case studies display the flow velocity in the x and y planes. The Mach number is the z-component depicted by color. Since the axial velocity is much larger than the transverse components, the surface plots of the different velocities are scaled accordingly. In the axial velocity plots, the Mach number is scaled from zero to 5.55; which corresponds to the mean incoming flow speed in the x-direction with the added initial vortical fluctuations. In the transverse velocity plots, however, the velocities are not as high and

vary between positive and negative values. Thus, the Mach number is scaled from -2.22 to 2.22.

The direction of the incoming flow is defined, as is the location of the fixed shock and detonation waves. Emphasis is placed on the post-shock region of the computational domain to capture the far downstream flow behavior. The plots display the turbulent fluctuations, velocity changes, in addition to the shock and detonation wave properties in a series of nine consecutive frames of the flow propagation.

Unforced–Detonation Interaction Surface Plots

The surface plots capture the flow propagation from the computation domain inlet, through the shock/detonation wave front, and in the far downstream region. In the unforced–detonation case study, the incoming flow has no turbulent vortical fluctuations as it travels towards a fixed detonation wave. Massa (2011a) documents numerical schlieren frames of the same unforced–detonation interaction at Mach 5.5. His visualizations depict the instability of the detonation wave and the transverse wave propagation downstream, Figure 5.14.

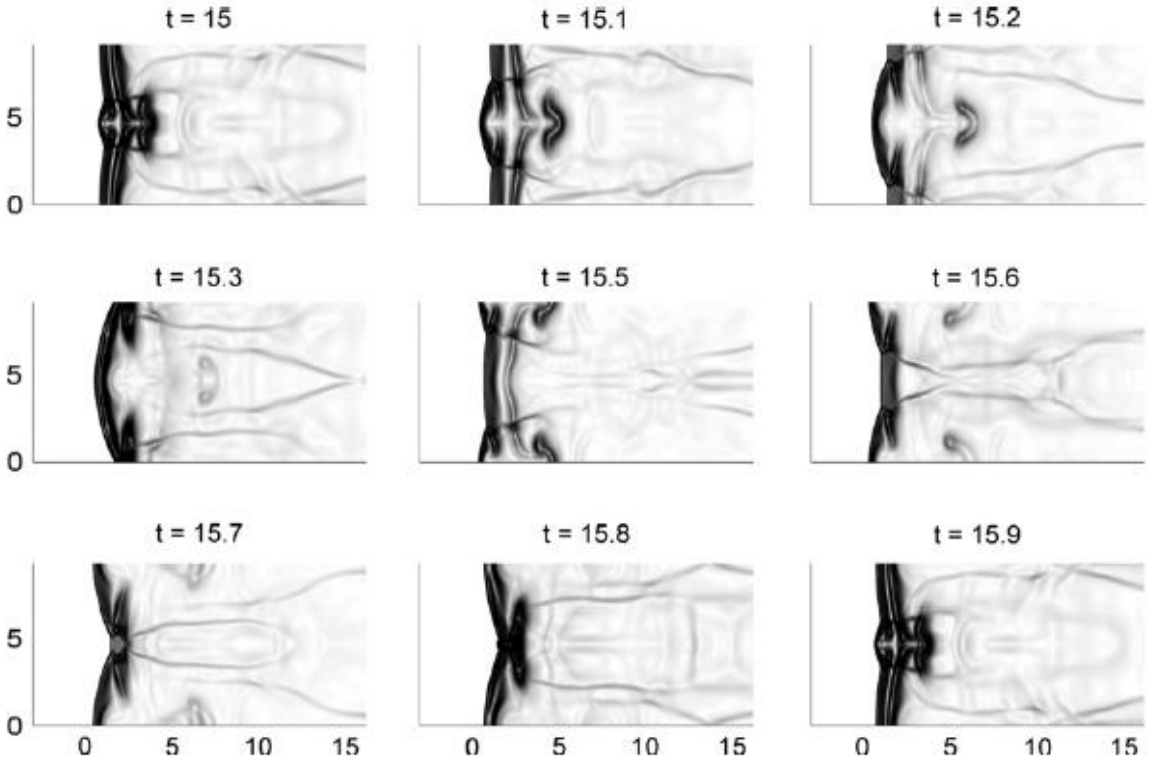

Figure 5.14 Numerical schlieren for unforced–detonation at Mach 5.5, different panels refer to the same slice but at different times (Massa, 2011a)

The surface plots of the axial velocity in the unforced–detonation interaction of this study are shown in Figure 5.15 as nine consecutive frames.

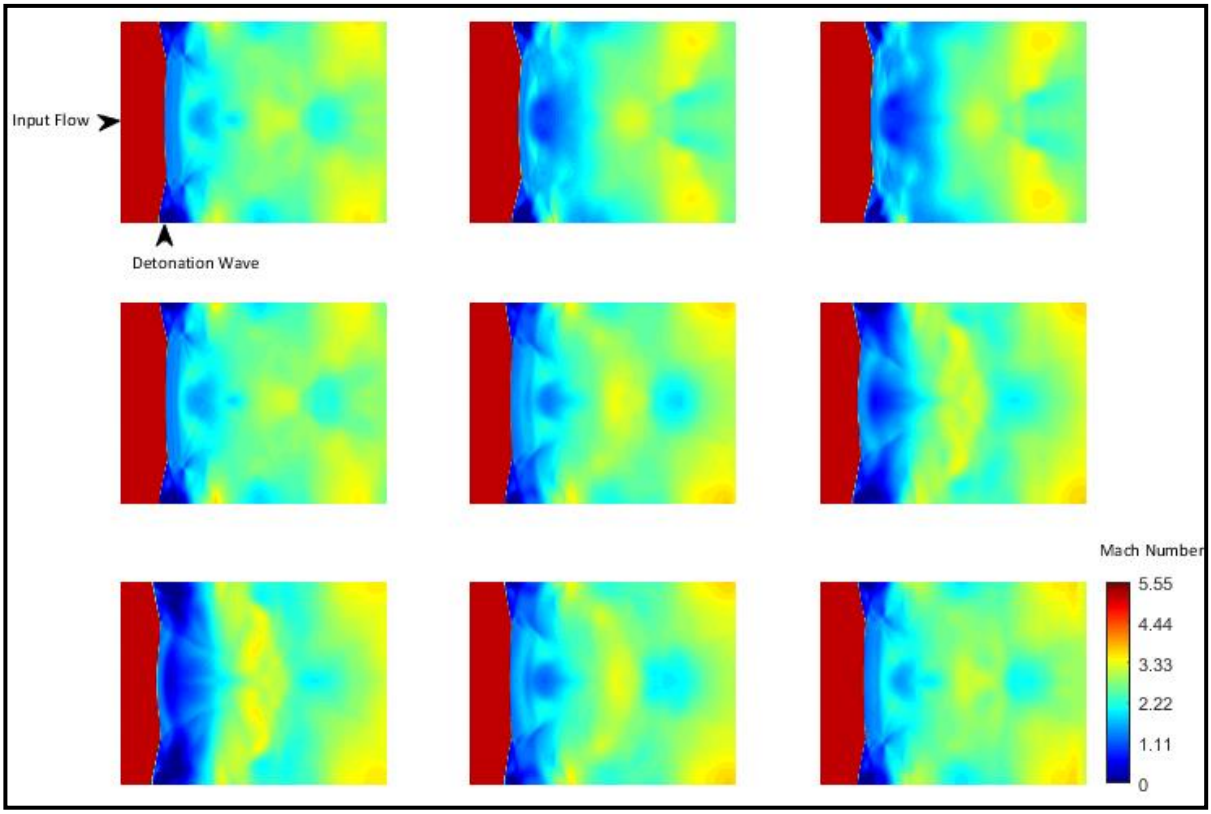

Figure 5.15 Nine consecutive surface plots of the axial velocity in the unforced–detonation interaction case study

The unforced axial velocities depicted in Figure 5.15 show a solid color ahead of the detonation wave front at Mach 5.5 due to the absence of vortical fluctuations. In the absence of incoming turbulence, velocity variations are visible downstream of the wave front as a result of the detonation exothermic heat release. Symmetry is observed in the downstream patterns due to the wave reflection off the imposed computational domain walls, as in Massa's (2011a) numerical schlieren frames. The detonation wave instability is evident as the wave structure is seen to travel ahead of the fixed position in the consecutive frames.

The nine consecutive transverse velocity v surface plots are shown in Figure 5.16.

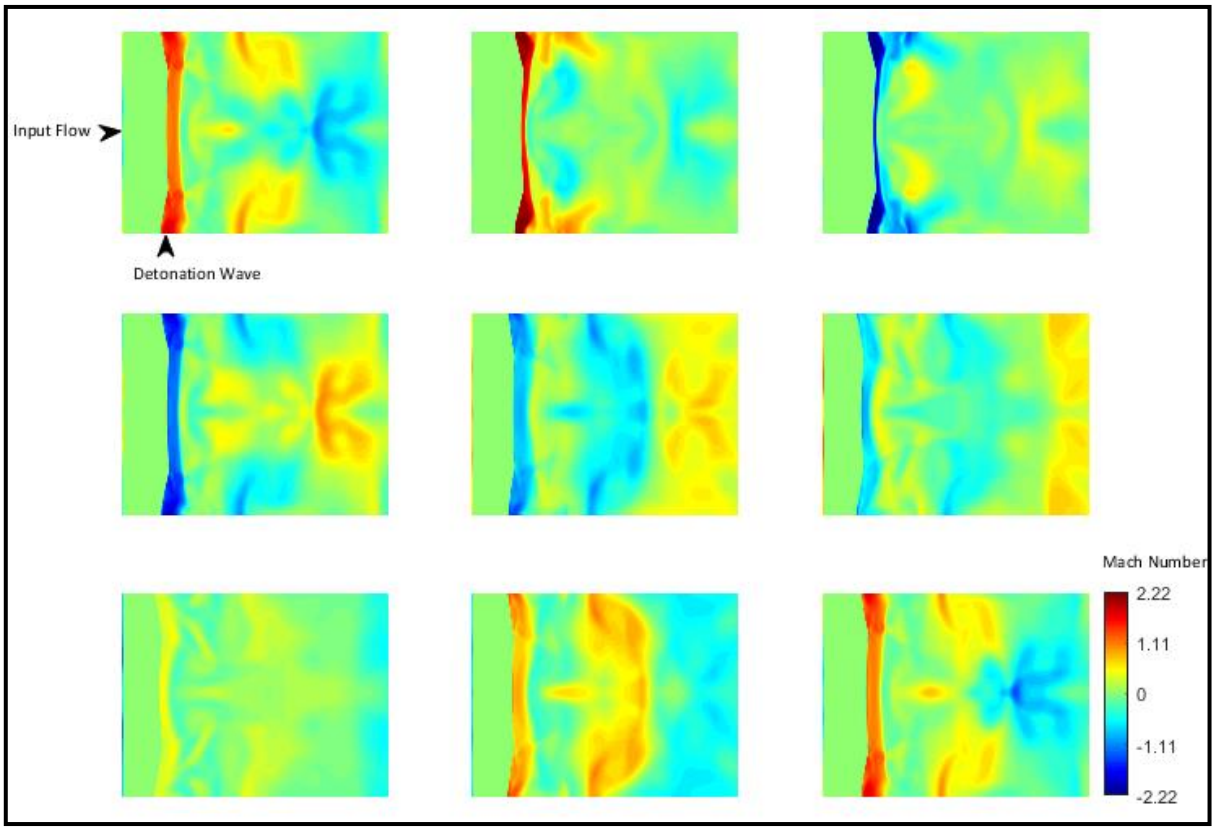

Figure 5.16 Nine consecutive surface plots of the transverse velocity, v, in the unforced–detonation interaction case study

The transverse velocities originate at the computational domain inlet with values close to zero. Upon interacting with the unstable detonation wave, the velocities are driven to increase or derease. The transverse reaction to the detonation wave, thus, is varying. Patterns appear downstream showing symmetry due to the boundary wall restriction and irregularity due to the heat release. A body-shaped structure seems to appear in the far downstream area.

Next, the nine consecutive surface plots of the transverse velocity w are investigated and shown in Figure 5.17.

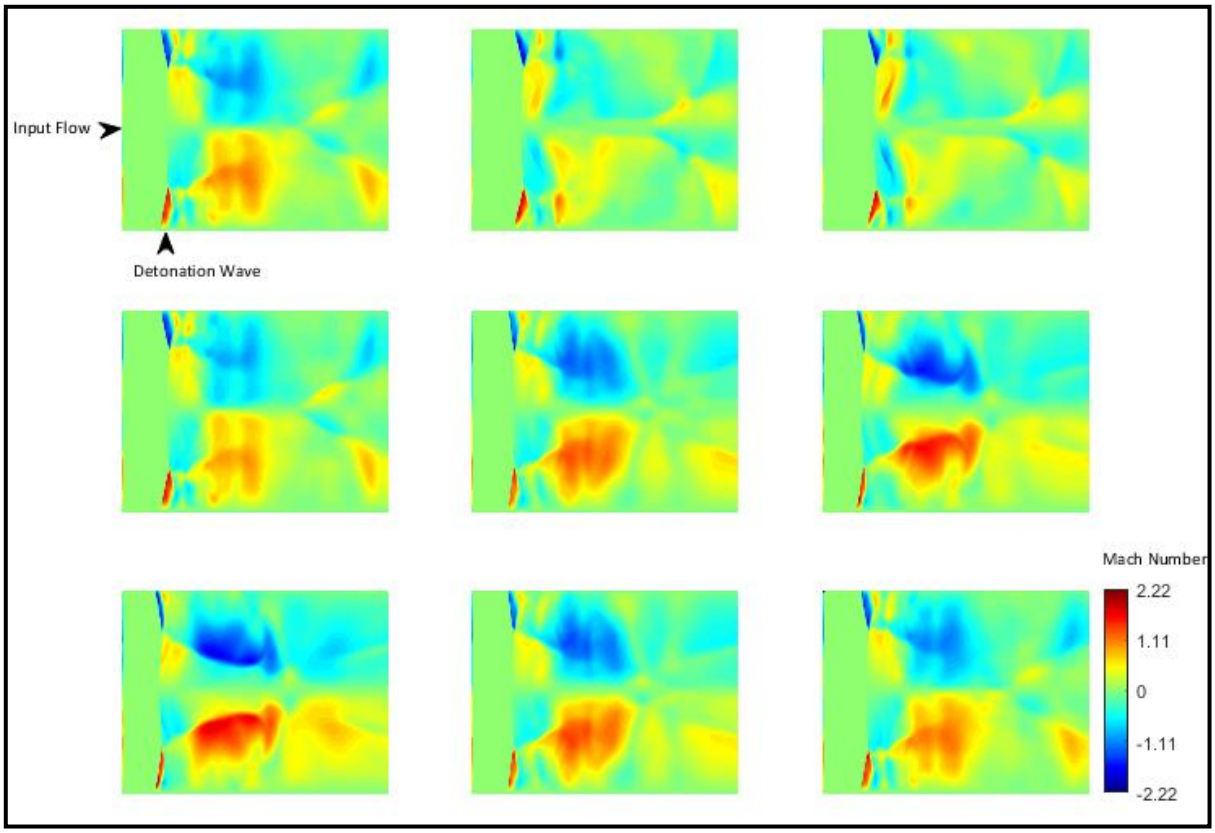

Figure 5.17 Nine consecutive surface plots of the transverse velocity, w, in the unforced–detonation interaction case study

The transverse velocities in these surface plots also start close to zero at the computational domain inlet. However, among the consecutive frames shown in Figure 5.17, symmetry is observed as well as repeated patterns. The blob structures appear downstream of the detonation wave front with co-existing positive and negative speeds within one frame. The heat release and detonation instability cause this irregularity and aggressive tranverse wave reaction.

Shock–Turbulence Interaction Surface Plots

The surface plots of the interaction of an incoming turbulent flow with a fixed shock wave are explored next. The incoming turbulent flow is characterized by vortical fluctuations that drive the mean axial velocity to Mach 5.55. Larsson (2008) reports direct numerical simulation flow visualization of the instantaneous streamwise momentum ρu of shock–turbulence interaction at Mach 1.5, with focus on the immediate post-shock region. The images depict the high velocity fluctuations ahead and behind the shock, as well as the different interaction strengths, Figure 5.18.

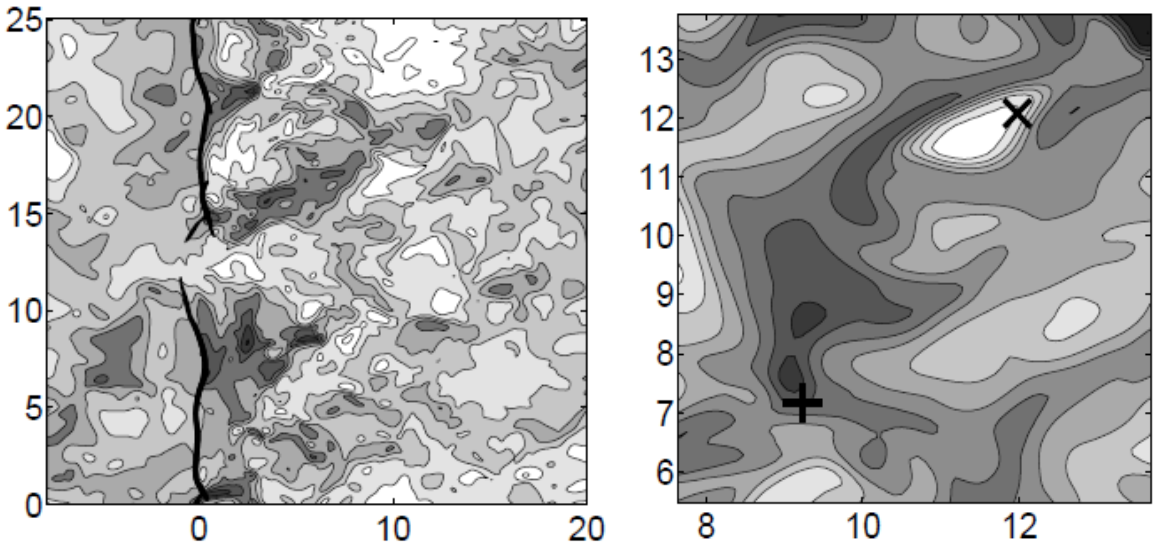

Figure 5.18 Left: Instantaneous shock–turbulence interaction streamwise momentum in gray scale, with dark regions denoting higher momentum at Mach 1.5 - Right: Contours of streamwise velocity immediately behind the shock, with darker regions denoting higher velocities, cross (weak interaction) plus (strong interaction), direct numerical simulation study (Larsson, 2008)

The surface plots of the axial velocity in the shock–turbulence interaction in this study are shown next in Figure 5.19, where the flow characteristics are captured in nine consecutive frames.

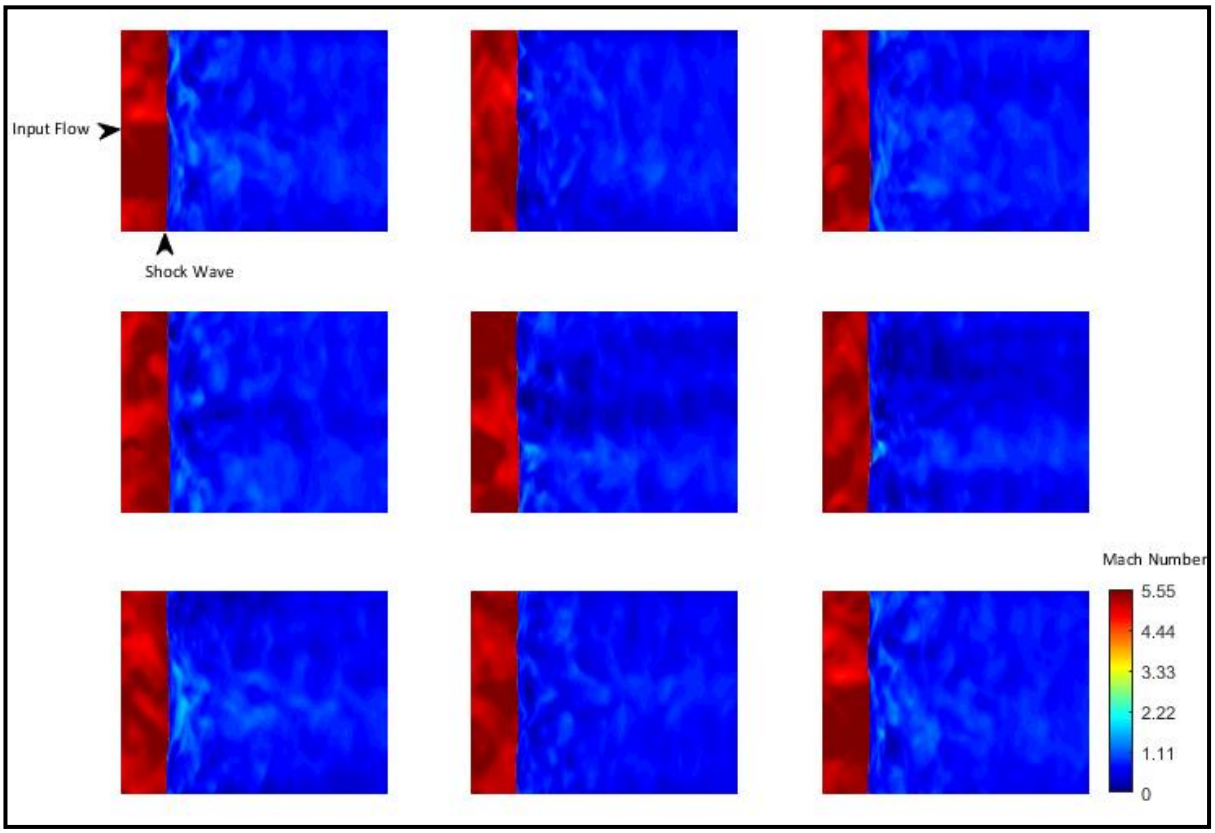

Figure 5.19 Nine consecutive surface plots of the axial velocity in the shock–turbulence interaction case study

The axial velocity surface plots in Figure 5.19 show the incoming flow fluctuations as variations in the red color intensity ahead of the shock wave. The shock is fixed and appears to retain its stability; stands as a still surface almost unaffected by the incoming turbulence. Post-shock, the flow is driven to a minimum velocity with turbulent fluctuations still evident, as in Larsson's (2008) visualization. Neither the shock–turbulence interaction surface plot frames nor Larsson's (2008) visuals show the symmetry that was visible within the unforced–detonation wave interaction.

The transverse velocity v surface plots of the shock–turbulence interaction are shown next in Figure 5.20.

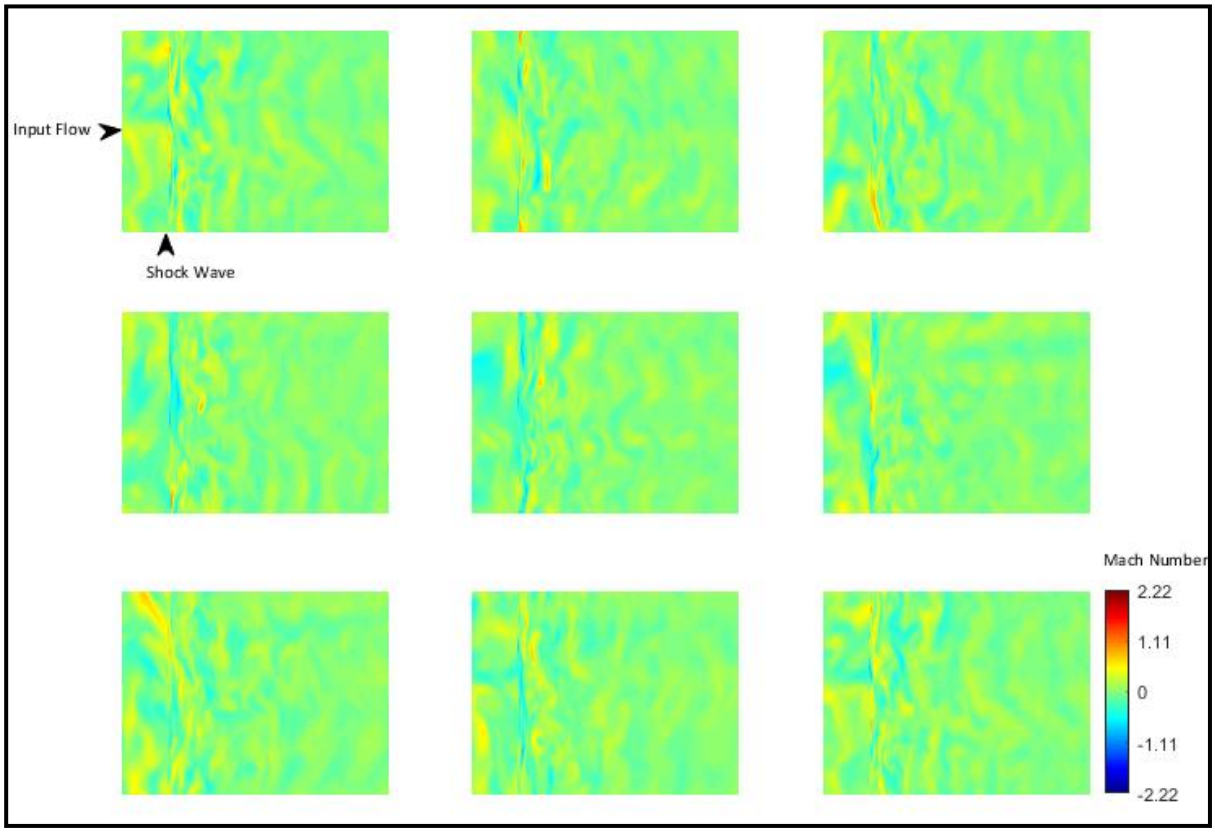

Figure 5.20 Nine consecutive surface plots of the transverse velocity, v, in the shock–turbulence interaction case study

The transverse velocities start around zero, with initial fluctuations and maintain the same variation range around zero across the shock and downstream. The fluctuations are evident downstream and continue to disturb the velocity. The shock wave structure is visible in the sea of velocity variations. Symmetry is not apparent in the consecutive frames, but the disturbances due to incoming turbulent flow are prominent downstream of the shock and in the computational domain far field.

The transverse velocity w surface plots of the shock–turbulence interaction are shown next in Figure 5.21.

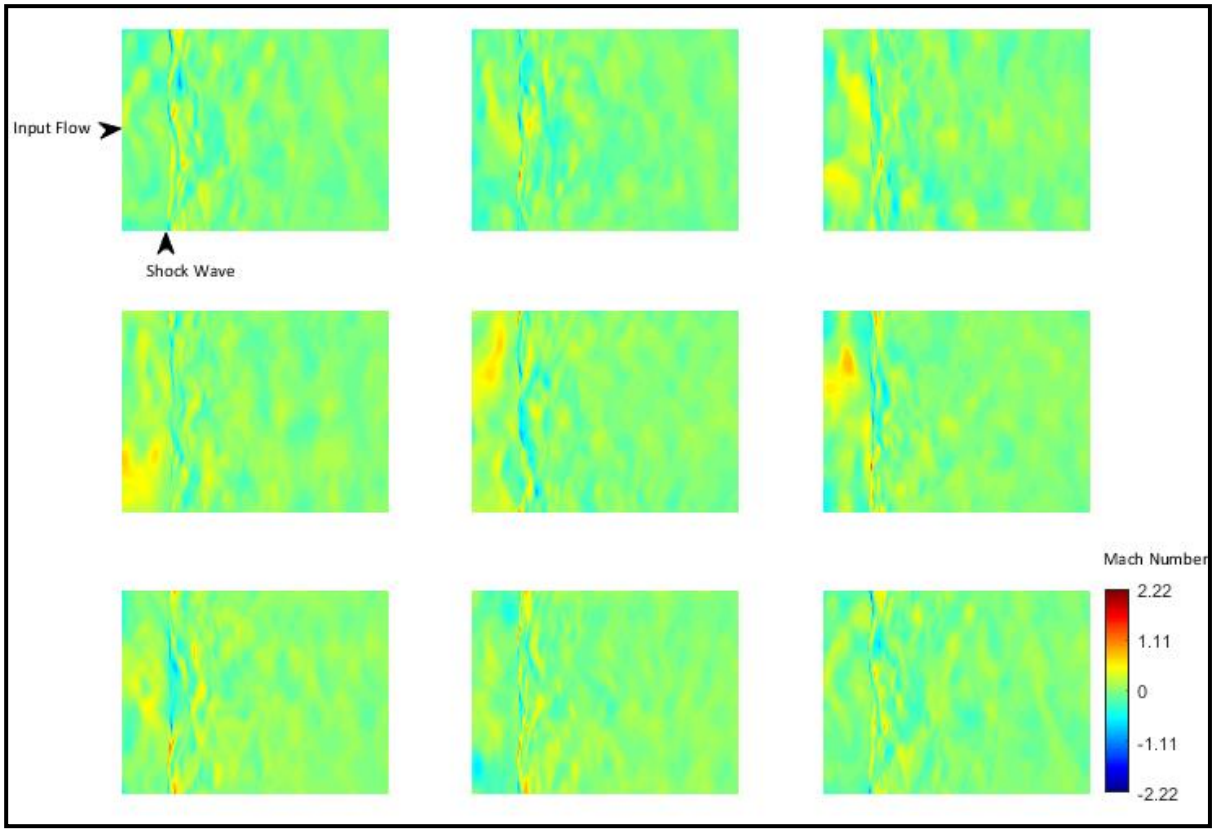

Figure 5.21 Nine consecutive surface plots of the transverse velocity, w, in the shock–turbulence interaction case study

The transverse velocities w follow the patterns of the transverse velocities v in the shock–turbulence interaction case study. The observed fluctuations are primarily driven by the turbulence and the upstream behavior is extended post-shock. Detialed investigation of the fluctuations downstream and the modes of instability can be pursued as follow-up research to trace the turbulence vortical fluctuations' evolution through the shock–turbulence interaction.

Detonation–Turbulence Interaction Surface Plots

In the third and final interaction case study, the incoming turbulent flow interacts with a detonation wave. The detonation wave is fixed in the computational domain but has intrinsic instability. The turbulent vortical fluctuations drive the mean flow in the direction of travel up to Mach 5.55. Massa (2011a) documents numerical schlieren frames of the detonation–turbulence interaction at Mach 5.5. His visualizations depict the instability of the detonation wave with less structured flow downstream due to the detonation and turbulence mutual effects, Figure 5.22. It is evident that the far field symmetry is lost.

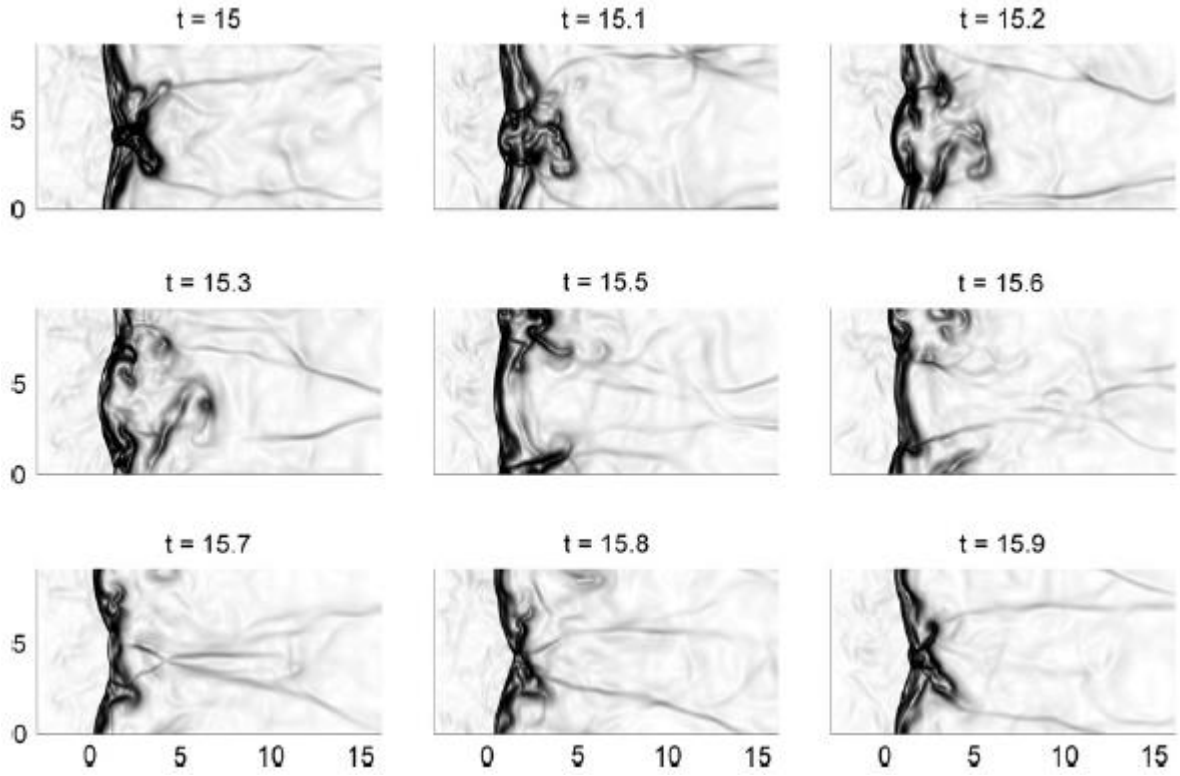

Figure 5.22 Numerical schlieren for vortically forced detonation–turbulence interaction at Mach 5.5, different panels refer to the same slice but at different times (Massa, 2011a)

The surface plots of the axial velocities are shown first in Figure 5.23 where the flow and detonation wave characteristics are captured in nine consecutive frames.

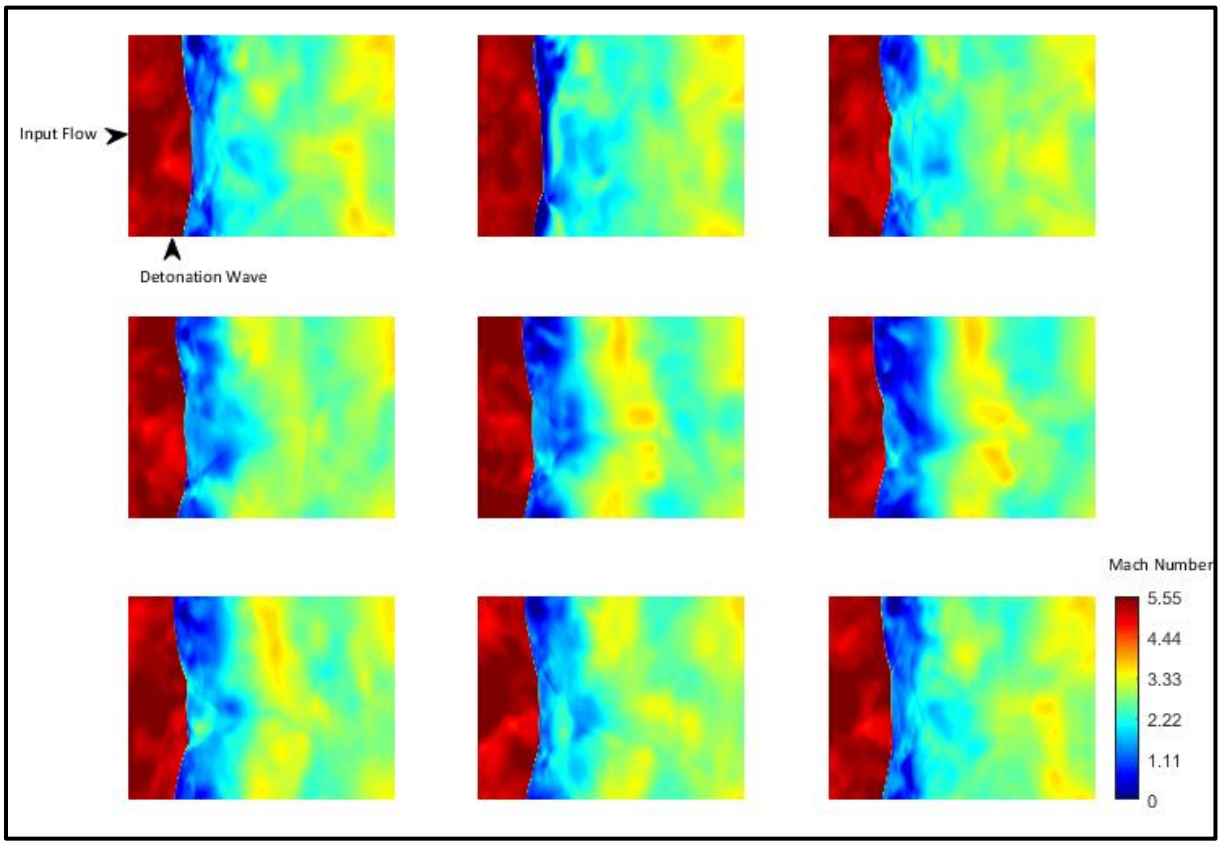

Figure 5.23 Nine consecutive surface plots of the axial velocity in the detonation–turbulence interaction case study

The incoming flow shows fuctuations in the axial velocities as red color variations ahead of the wave front. The detonation wave is unstable. While it is not propagating in the computational domain, it shows violent movement ahead and behind the fixed wave front position. The velocities are strongly affected by the detonation wave. While symmetry is observed in the unforced–detonation case study, it is lost with the introduction of incoming turbulent fluctuations. A mutual interaction is identified between the detonation and the turbulence. While the flow is affected by the detonation wave and heat release, the wave is found to be wrinkled by the incoming turbulence.

The transverse velocity v surface plots of the detonation–turbulence interaction case study are shown next in Figure 5.24.

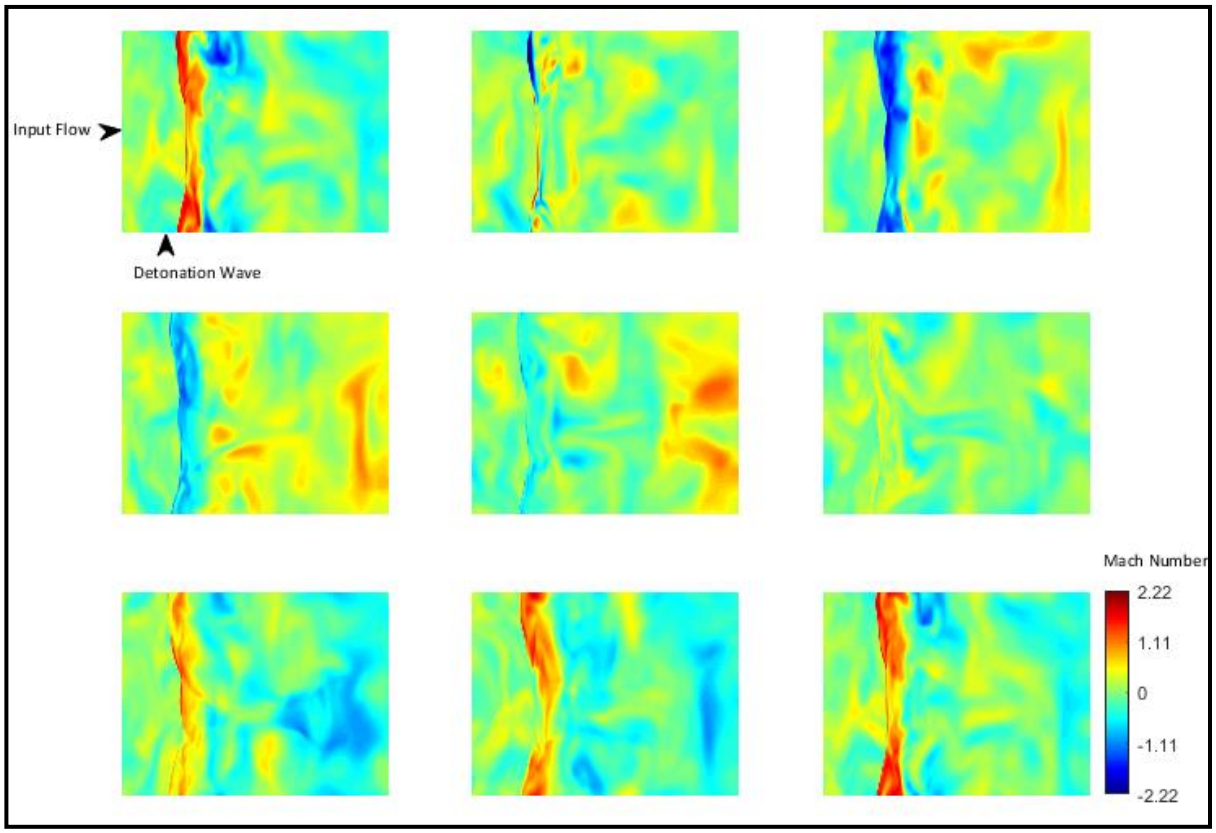

Figure 5.24 Nine consecutive surface plots of the transverse velocity, v, in the detonation–turbulence interaction case study

Transverse velocities show weaker peak values when compared to the axial velocities. The incoming flow is characterized by turbulent fluctuations. The fluctuations persist downstream with unorganized and highly disturbed shapes maintaining velocity values around zero upon interaction with the detonation wave. The post-detonation wave flow symmetry is lost amidst the turbulent fluctuations. The instability and violent detonation movement is evident in the transverse velocity profiles.

The transverse velocity *w* surface plots of the detonation–turbulence interaction case study are shown next in Figure 5.25.

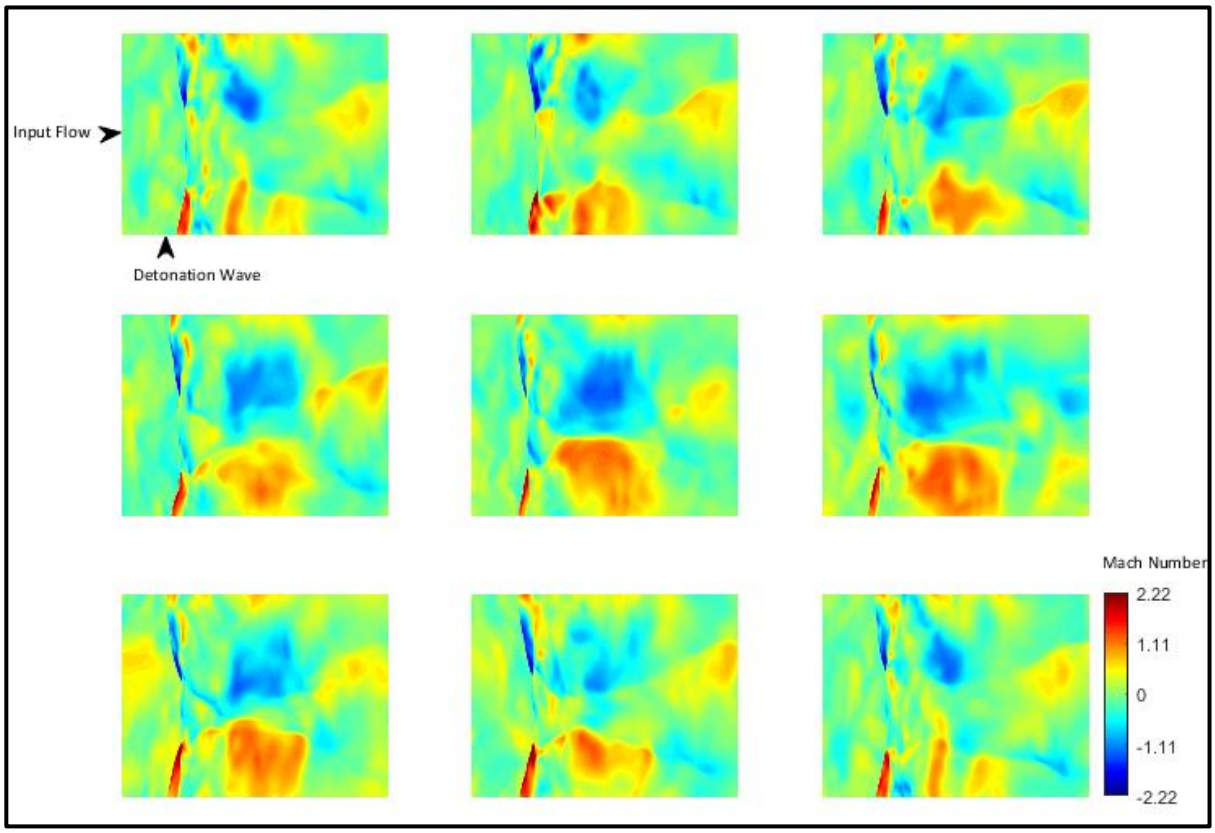

Figure 5.25 Nine consecutive surface plots of the transverse velocity, w, in the detonation–turbulence interaction case study

Lastly, the transverse velocity surface plots maintain similar maximal Mach scale with evident fluctuations both ahead and downstream of the detonation–turbulence interaction. In the consecutive frames shown in Figure 5.25, symmetry is lost and blobs of different velocities appear within a single frame. It is important to note that different flow behavior is depicted in the downstream near zone and far field. Extending the computational domain may reveal more flow behavior that is truncated in these simulation studies.

5.4 Summary of Observations

The direct numerical simulation of the homogeneous isotropic turbulence periodic cube is applied in three case studies: unforced–detonation, shock–turbulence, and detonation–turbulence interactions. The three case studies' velocity profiles are analyzed across the computational domain for averages, root mean square averages, turbulent kinetic energy, and Reynolds stress components. The computational domain size allows assessment of the flow behavior ahead and farther downstream of the wave front. This is important since this study captures crucial far field flow behavior.

It is found that the turbulent flow retains its fluctuating behavior due to vortical forcing throughout the shock and detonation interactions. The turbulent fluctuations cause stretching in the flow response to the wave front. The shock–turbulence interaction, however, shows weaker velocity fluctuations beyond the interaction point. The detonation wave's inherent length scale and heat release parameter yield consistent velocity variation trends downstream and energize the flow strengthening the vortical fluctuations. The highly energized flow shows non-linear and anisotropic behavior downstream of the wave front. The detonation wave's intrinsic instability causes the unforced flow to experience the wave effects ahead of the stationary front position in the absence of turbulent fluctuations. The effects of the detonation instability extend ahead and beyond the wave front over wider regions than the stationary normal shock wave.

In conclusion, frame-by-frame visualizations reveal dynamic detonation wave front movement, even in the unforced case study, as well as a mutual interaction phenomenon between the turbulent flow and the detonation wave. The initially isotropic velocity field of turbulence subjected to the strong detonation wave is altered. The flow

is longitudinally strained. However, the detonation wave appears highly distorted upon interaction with the turbulent instabilities. It is proposed that the turbulence is wrinkling the detonation wave front.

This is a preliminary simple low-order model of the interaction case studies. This work is not representative of naturally occurring turbulence and detonation phenomena, but rather used to establish fundamental physical understanding of the interactions. It is recommended that following research investigates the detonation–turbulence interaction with a traveling detonation wave front and detailed chemistry. While coupling effects will be present, it is crucial to begin to answer the detonation questions posed in the introduction for disaster mitigation applications:

- How does the detonation propagate through the disaster zone?
- Can the detonation, once initiated from the dissociation of the water molecules, be mitigated?
- Does turbulence play a role in destabilizing the detonation wave to make it difficult to control?

This completes the statistical analysis and flow visualization of the homogeneous isotropic turbulence velocity fluctuations in the three interaction case studies. The evolution of the turbulence velocity skewness factor is evaluated next.

6. Turbulence Velocity Skewness Vector

In this study of homogeneous isotropic turbulence, the periodic cube structure and its interaction with a shock and a detonation wave are analyzed statistically. The turbulence is characterized by vortical fluctuations and is assumed to reach fully-developed state when the velocity skewness factor, defined by Tavoularis (1978) and shown in Equation (4.12), approaches $S_{ux} = -0.5$. Following the statistical analysis of the velocity in the turbulence periodic cube, the skewness factor is evaluated and additional skewness components are proposed in Section 4.4. S_{vy} and S_{wz} quantify the variation of the transverse velocity components with respect to their corresponding Cartesian coordinates. It is found that the values of the skewness components are in fact different but vary within a consistent range. The variations show similar trends in the periodic cube. The significance of having multiple components reach the Tavoularis criterion within the same unit of turbulence is evaluated and it is concluded that it may affect turbulence state. Fully-developed turbulence is characterized by both chaotic behavior and instabilities at higher Reynolds numbers (Rose, 1978). It is predicted that these two characteristics become amplified by the additional velocity skewness in the transverse planes. The study is extended to include all three velocity components' variations with respect to the three Cartesian coordinates. A velocity skewness vector is proposed with nine constituent components and assessed in the two turbulence interaction case studies.

Proposing a Velocity Skewness Vector Definition

Experimental, theoretical, and numerical works have used the velocity derivative definition of the skewness factor, in particular utilizing the axial velocity component, for over four decades. This crucial factor is statistically defined as the third moment of the velocity derivative normalized by the second moment of the velocity derivative, which is variance (MIT, 2007). At present, no equation quantifies the turbulence skewness in directions other than the direction of travel and for a component other than the streamwise velocity. This study proposes extending the long-standing Tavoularis velocity skewness criterion to a nine component tensor, shown in Equation (4.15). The nine terms are all the combinations of the skewness variation of the velocity components (u, v, w) over the three Cartesian coordinates (x, y, z) following the original definition.

$$S_{uy} \equiv -\frac{\overline{\left(\frac{\partial u}{\partial y}\right)^3}}{\left[\overline{\left(\frac{\partial u}{\partial y}\right)^2}\right]^{3/2}} \quad , \quad S_{uz} \equiv -\frac{\overline{\left(\frac{\partial u}{\partial z}\right)^3}}{\left[\overline{\left(\frac{\partial u}{\partial z}\right)^2}\right]^{3/2}} \tag{6.1}$$

$$S_{vx} \equiv -\frac{\overline{\left(\frac{\partial v}{\partial x}\right)^3}}{\left[\overline{\left(\frac{\partial v}{\partial x}\right)^2}\right]^{3/2}} \quad , \quad S_{vz} \equiv -\frac{\overline{\left(\frac{\partial v}{\partial z}\right)^3}}{\left[\overline{\left(\frac{\partial v}{\partial z}\right)^2}\right]^{3/2}} \tag{6.2}$$

$$S_{wx} \equiv -\frac{\overline{\left(\frac{\partial w}{\partial x}\right)^3}}{\left[\overline{\left(\frac{\partial w}{\partial x}\right)^2}\right]^{3/2}} \quad , \quad S_{wy} \equiv -\frac{\overline{\left(\frac{\partial w}{\partial y}\right)^3}}{\left[\overline{\left(\frac{\partial w}{\partial y}\right)^2}\right]^{3/2}} \tag{6.3}$$

While experimentally challenging, with the advancements in computational power and resources, calculating all nine skewness components of a turbulent flow is feasible. The nine components are evaluated for the shock–turbulence and detonation–turbulence interaction case studies to assess the velocity skewness vector constituents: their similarities, differences, and significance. Within this framework it is possible to address the question posed in Section (4.4): **Is the Tavoularis criterion for streamwise velocity variation sufficient to characterize the turbulence state?**

The goals of this turbulence velocity skewness vector study are:

- To calculate the original velocity skewness factor S_{ux} and track its evolution throughout the computational domain in the shock–turbulence and detonation–turbulence interactions
- To find the additional eight skewness components for the shock–turbulence and detonation–turbulence interactions
- To evaluate if the proposed velocity skewness tensor is symmetrical across its diagonal components
- To show if the eight proposed additional components carry physical information about the turbulence state

The calculation methodology of the velocity skewness vector components is outlined and the results for the two turbulence interaction case studies are documented next.

6.1 Calculation Methodology

The turbulence skewness expression consists of a velocity derivative and an average quantity. The methodology used to acquire both these terms is discussed. The computational domain of the interaction case studies is a $815 \times 163 \times 163$ units cuboid. Therefore, unlike the turbulence periodic cube, the differential distances (dx, dy, dz) are not equivalent even though the grid resolution is fixed. The velocity derivatives in the x-direction are calculated across the computational domain, as shown in Figure 6.1, and averaged over rectangular planes of the cuboid.

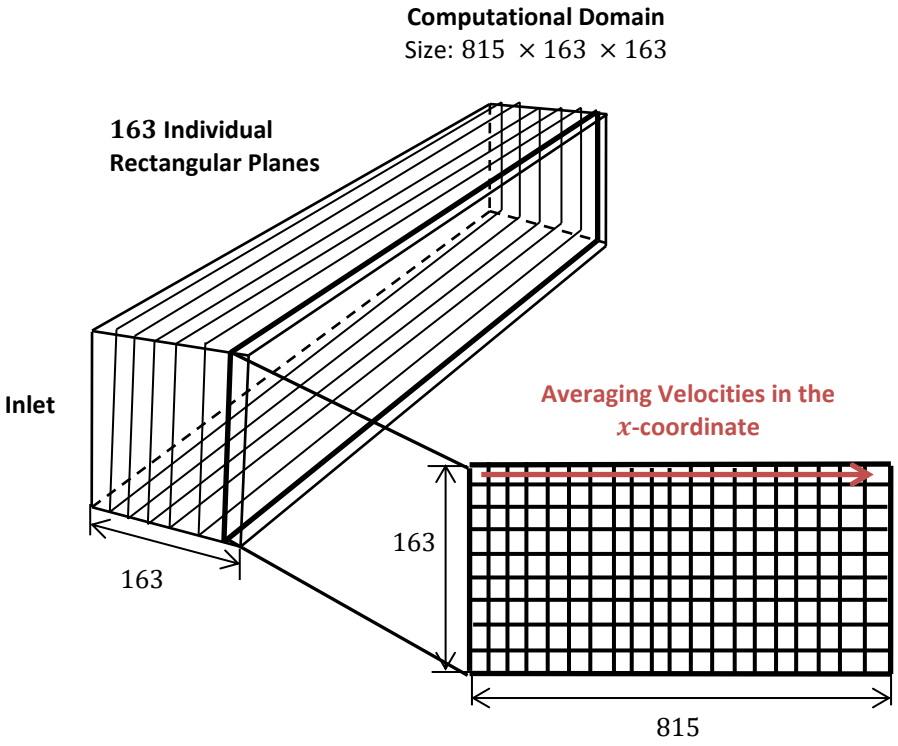

Figure 6.1 Averaging velocities in the x-coordinates in individual rectangular planes

The cuboid computational domain is divided into 163 parallel rectangular planes, as shown in Figure 6.1. The velocity derivative is calculated by applying the central differencing method, shown in Figure 3.3 and Equation (3.4), over unit cubes in the x-

direction progressively. It must be noted that the rectangular planes are not homogenous due to the presence of the wave front. Thus, the averaging cannot be taken over the entire row. A short interval averaging technique is employed instead; where the average of each ten points is considered separately within the rectangular plane. Ten point intervals are selected as they are large enough for the average not to be erratic but small enough not to lose the flow physics. These independent values are averaged across the other parallel rectangular planes. The averages are then connected to show a trend line of the evolution of the velocity skewness term in the x-direction throughout the computational domain. The velocity derivatives in the y and z-directions are calculated in the transverse planes, as shown in Figure 6.2, and averaged over the square planes across the length of the computational domain.

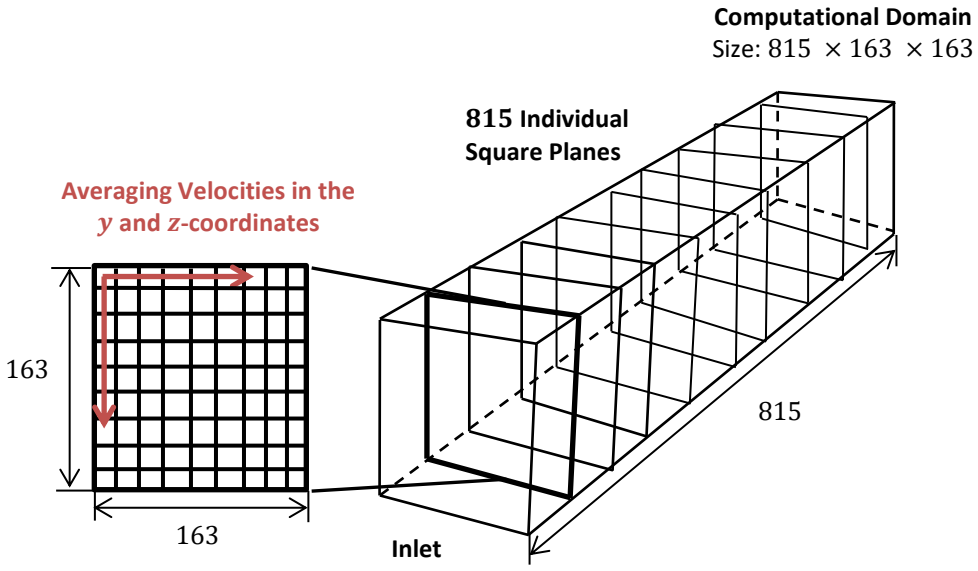

Figure 6.2 Averaging velocities in the y and z-coordinates in individual square planes

The computational domain is divided into 815 parallel square planes for the skewness calculations in the transverse coordinates, as shown in Figure 6.2. The velocity derivative is calculated by applying the central differencing method in the specified directions of y and z. The average is then found for the entire homogeneous square plane following each direction. This leads to a single skewness point value per square plane. The average skewness points of the square planes from the inlet to the end of the cuboid are plotted to find the distribution over the computational domain.

6.2 Application in the Turbulence Interaction Case Studies

The skewness is a statistical measure of the velocity fluctuations, thus it is only applicable to flow with initial fluctuations. The vortical fluctuations of the flow in the shock–turbulence and detonation–turbulence interaction case studies vary in the Cartesian coordinates. The fluctuations' variations are quantified in nine velocity skewness vector components, calculated and plotted. First, the standard velocity skewness factor S_{ux} is evaluated for the case studies in Figure 6.3.

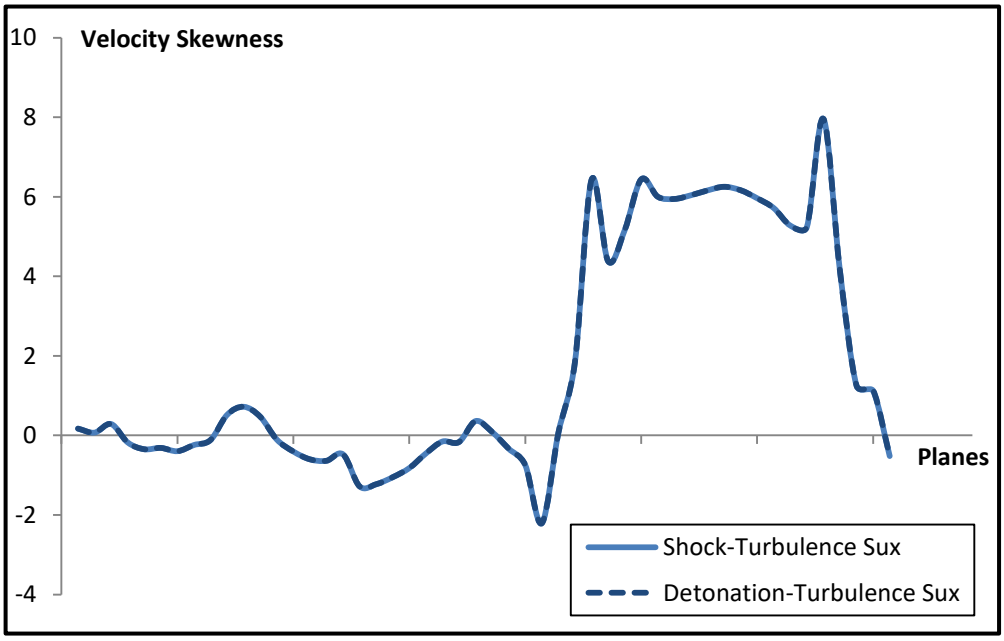

Figure 6.3 Evolution of the velocity skewness factor S_{ux} across the computational domain in the two turbulence interaction case studies

The variation of the streamwise velocity in the axial direction begins around zero at the computational domain inlet. This average quantity is expected from the definition of the vortical fluctuations and observed in the skewness analysis of the turbulence periodic cube, Figure 4.14 and Table 4.6. The turbulence periodic cube acquires mean travel velocity and propagates down the cuboid towards the wave front at Mach 5.5. The

velocity skewness values continue to vary around zero within the -1 to 1 range. They reach a low close to -2 followed by a drastic rise to a maximum above 8. This rise is consistent with the axial straining of the turbulence due to the fluctuations' interaction with the wave front, also observed in the statistical analysis of the three case studies in Section 0. Downstream, the velocity variation drops to values close to zero returning to the original flow state. The two case studies show very similar trend lines. Thus, the detonation heat release, inherent length scale, and intrinsic instability do not play a significant role in the velocity skewness alteration across the wave front. Next, the variation of the two transverse velocity components v and w in the flow direction of travel is evaluated and displayed in Figure 6.4.

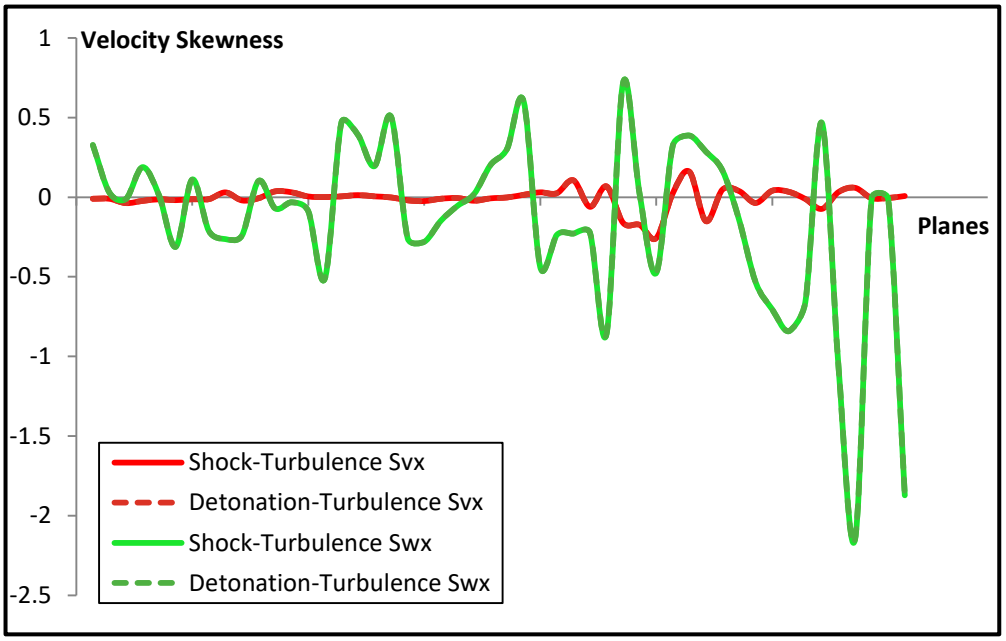

Figure 6.4 Evolution of the velocity skewness vector components S_{vx} and S_{wx} across the computational domain in the two turbulence interaction case studies

While the turbulent flow gains mean velocity in the streamwise direction, the transverse velocities are still solely composed of the vortical fluctuations. The transverse velocity skewness components vary around zero ahead of the wave front

and continue in a similar manner downstream past the interaction. The skewness values show a slight reaction to the interaction with the wave front, where the fluctuations become more prominent and occupy wider interval values. However, overall, the velocity variations continue to maintain values close to zero. The maximum and minimum values are still within the turbulence fluctuations' defined distribution interval of -2 to 2, shown in Figure 4.15. As in the plot of the evolution of S_{ux}, Figure 6.3, the two case studies continue to show very closely related trend lines with no indications of the effects of the detonation heat release or instability on the skewness terms. This concludes the evolution of the three velocity components in the axial direction. Now, the diagonal velocity skewness components are quantified. Previously evaluated for the turbulence periodic cube, the diagonal velocity skewness components show the variation of each velocity component in its respective direction. The streamwise component evaluation S_{ux} is complete, S_{vy} and S_{wz} calculations are displayed in Figure 6.5.

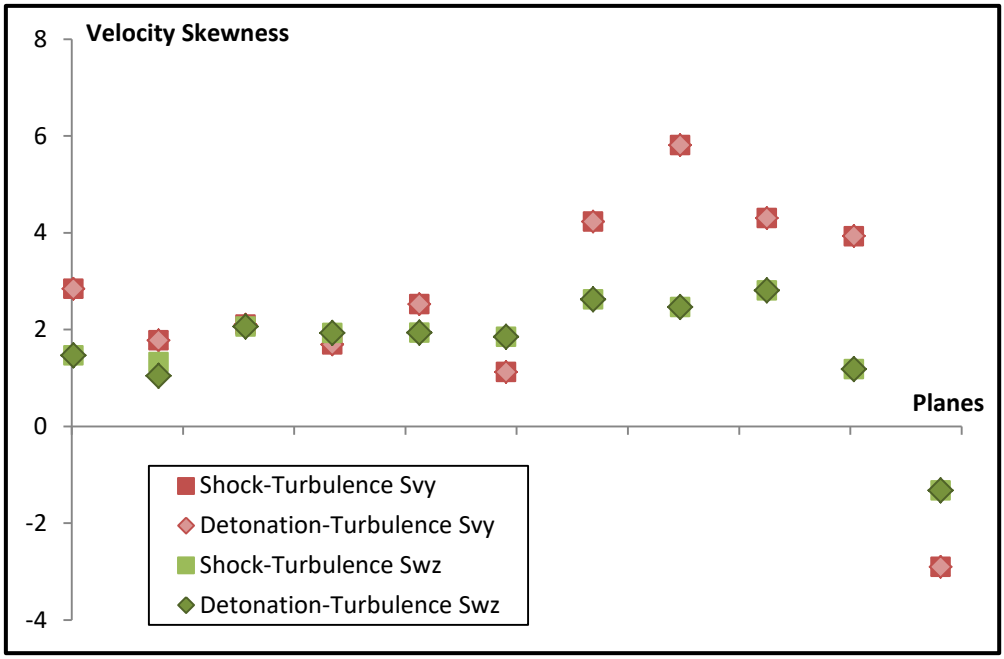

Figure 6.5 Velocity skewness vector components S_{vy} and S_{wz} in the two turbulence interaction case studies

The two diagonal skewness terms S_{vy} and S_{wz}, which vary around zero in the turbulence periodic cube, Figure 4.14, do not start around zero in the interaction case studies. In Figure 6.5, the two terms show positive skewness ahead of the wave front. The skewness is increased under the flow's own fluctuation instability once the flow attains mean travel velocity in the axial direction. The flow is furthermore strained by the interaction with the wave front, leading to higher skewness measures reaching a value of 6 post-shock. Farther downstream of the wave front interaction, the velocity variations return to negative skewness values.

Thus, the flow shows instability straining effects in the three diagonal skewness vector components. On a smaller velocity scale, the differences between the shock–turbulence and the detonation–turbulence case studies begin to appear showing that the two case studies' velocity skewness values are closely related but not identical.

Finally, the remaining four off-diagonal velocity skewness components are evaluated in Figure 6.6.

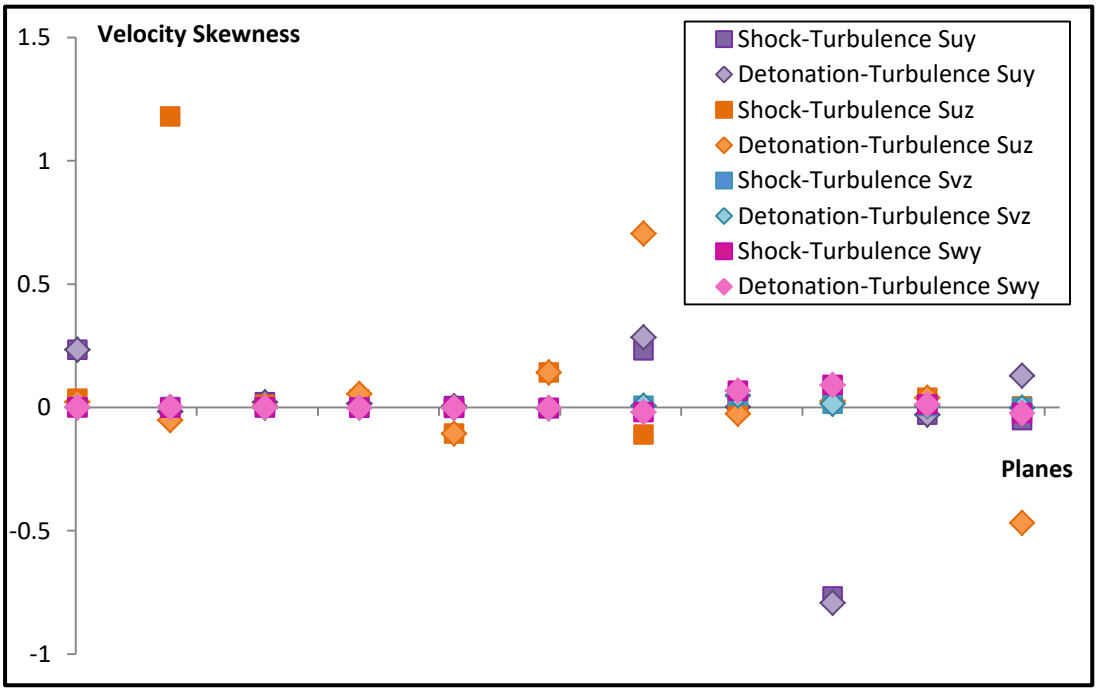

Figure 6.6 Velocity skewness vector components S_{uy}, S_{uz}, S_{vz}, and S_{wy} in the two turbulence interaction case studies

After evaluating the skewness vector constituents in the axial direction and the diagonal terms, four components remain: S_{uy}, S_{uz}, S_{vz}, and S_{wy}. The off-diagonal components vary close to zero ahead of the wave interaction and farther downstream. The skewness values occupy a range between -1 and 1, with the most dense concentration between -0.5 and 0.5. These trends closely follow the velocity fluctuations' distribution in Figure 4.15 and occurrence frequency within the periodic cube in Figure 4.16. The reaction to the wave front interaction is still present, but very weak. Once again, on the smaller velocity scale, the differences between the two interaction case study velocities are showing, but still following the same behavioral trends.

6.3 Summary of Observations

In this study, an extension of the long-standing velocity skewness factor definition is proposed. The velocity skewness vector consists of nine components quantifying the variation of the three velocity terms in all three Cartesian coordinates. It is a comprehensive approach to evaluating the effects of the vortical forcing on the state of the turbulence field. The nine skewness vector constituents are calculated and graphed for the shock–turbulence and detonation–turbulence interaction case studies.

It is found that the diagonal components (S_{ux}, S_{vy}, S_{wz}) show the effects of the vortical fluctuations on the evolution of the flow through the computational domain. The inherent fluctuation instability causes straining of the flow past the wave front to skewness values as high as 8. The fluctuations also cause higher positive skewness values in the transverse velocity components ahead of the wave front. The flow instability increases in the transverse directions once the flow acquires mean travel velocity in the axial direction. The flow returns to the initial conditions farther downstream with the velocity variations decreasing to values near zero and showing negative skewness.

The six off-diagonal components ($S_{uy}, S_{uz}, S_{vx}, S_{vz}, S_{wx}, S_{wy}$) show trends of variation around zero within the set velocity fluctuation interval. Weak reaction to the wave front interaction is observed. Thus, the velocity skewness vector can be considered symmetrical for homogeneous isotropic turbulence. It is recommended that following research investigates the possible differences within these six off-diagonal terms in non-homogenous turbulence.

The shock–turbulence and detonation–turbulence interaction case studies show similar trends in all nine velocity skewness vector components. Thus, the effects of the detonation heat release, inherent length scale, or intrinsic instability on the velocity fluctuations are not evident in the skewness calculations.

In conclusion, the axial velocity skewness factor, defined by Tavoularis (1978), carries important physical description of the flow behavior. The two additional diagonal components of the velocity skewness vector depict important turbulent flow evolution properties as well in the interaction of turbulence with a shock and a detonation wave. These components should not be overlooked in turbulence interaction case studies.

The velocity skewness factor, thus, is assessed for the vortically forced turbulence. The question that arises is: **What skewness expression can be used for the entropic and acoustic fluctuations of turbulence?** Entropic and acoustic fluctuations are related through thermodynamics and through the Strong Reynolds analogy. The fully-developed state of turbulence is reached beyond the transition to turbulence region. Thus, the temperature and pressure fluctuations in a turbulent flow are coupled with the velocity and can affect the state of the turbulence. A skewness expression should take the coupling effects into consideration.

7. Conclusions

Turbulence is a term used to describe a fluid field characterized by chaotic unorganized properties. It has challenged scientific minds for years and its applications cover a wide spectrum of topics. In this study, an attempt is made to bring order to the chaos while searching turbulent fluctuations for patterns, trends, and physical insight.

A study of homogeneous isotropic turbulence with vortical fluctuations begins with the development of a direct numerical simulation code to generate a turbulent field and turbulence interaction applications. The turbulence periodic cube is found to be a facilitated and efficient geometry to investigate fundamental turbulence physics through direct numerical simulation. The turbulence periodic cube is used as incoming flow to a shock and detonation wave in a cuboid computational domain. The interaction case studies yield important conclusions about the role of the turbulence fluctuations in straining the flow past the wave front. In addition, the heat release, detonation inherent length scale, and intrinsic instability are found to cause velocity variations in the flow far field and highly energize the flow. A mutual interaction is observed in the detonation–turbulence case study; while the flow is affected by the strong detonation wave, the wave is wrinkled by the turbulent fluctuations.

The statistical property of turbulence velocity skewness factor is assessed in this study to evaluate the turbulence's fully-developed state. The long-standing definition in terms of the streamwise velocity in the axial domain is extended to a nine component vector and applied in the two turbulence case studies. It is found that the additional diagonal components carry physical insight regarding the turbulent flow evolution throughout the interaction case studies' computational domain. The proposed tensor is

found to be symmetrical for homogeneous isotropic turbulence and a valuable measure to consider in fully-developed turbulence studies.

7.1 Summary of Scientific Contributions

The original scientific contributions of this doctoral research work are summarized in the following list.

1. The conduction of a literature review of turbulence research, homogeneous isotropic turbulence, turbulence interaction case studies of interest, as well as turbulence modelling and simulation techniques.
2. The documentation of the turbulence Navier–Stokes governing equations, normal shock relations, detonation heat release parameters, and velocity fluctuation generation technique.
3. The development of a direct numerical simulation tool that produces simple low-order models of a turbulence periodic cube with vortical fluctuations as well as the three case studies of unforced–detonation, shock–turbulence, and detonation–turbulence interactions. The direct numerical simulation tool lays the groundwork for upcoming research in direct numerical and large eddy simulations of homogeneous isotropic turbulence.
4. The assessment of the periodic cube geometry in the direct numerical simulation of homogeneous isotropic turbulence. The assumptions associated with this simplified structure are evaluated. Its constituent velocity fluctuations are statistically analyzed for averages, root mean square averages, turbulent kinetic energy, and Reynolds stress components.
5. The analysis of the three interaction case studies and comparison against the normal shock solution as well as against the ideal Zel’dovich, von Neumann, Döring detonation model to evaluate the effects of the turbulence, the shock

wave, and the detonation heat release on the flow evolution. The statistical analysis covers velocity averages, root mean square averages, turbulent kinetic energy, and Reynolds stress relations. The computational domain is extended to investigate the far downstream flow behavior and the flow is visualized in the form of surface plots.

6. The investigation of the velocity skewness factor defined by Tavoularis (1978). The skewness factor is evaluated for the turbulence periodic cube and the turbulence interaction case studies. A velocity skewness vector is proposed to provide a more comprehensive evaluation of the velocity variation in the three Cartesian coordinates.
7. The showcasing of the work in numerous research symposiums through oral presentations and posters. Parts of the work have been published as a senior honors thesis and conference papers:

   Hussein, S.M., Lu, F.K. “Statistical Analysis of Velocity Fluctuations in a Strong Detonation-Turbulence Interaction”, UT Arlington Honors College Senior Thesis, April 2012.

   Hussein, S.M., Blaiszik, E.M., and Lu, F.K., “Velocity fluctuations in the interaction of homogeneous, isotropic turbulence and a detonation wave” No. 0246-000173, 29th International Symposium on Shock Waves, Madison, Wisconsin, 2013.

Hussein, S.M., and Lu, F.K., “Single and two–point analysis of velocity fluctuations in a detonation–turbulence interaction” 45th AIAA Fluid Dynamics Conference, AIAA Aviation, Dallas, Texas, 2015.

7.2 Direct Numerical Simulation Tool Usage

The direct numerical simulation tool developed in this study is an original MATLAB code that is organized and well–documented for use by future researchers. The driver file and subroutines can be accessed to build upon the work of this project or to investigate other branches of turbulence interaction studies through direct numerical simulation. In particular,

- The initial and boundary conditions can be adjusted for different problem setups.
- The vortical fluctuations can be replaced by entropic, acoustic, or a combination of fluctuation types.
- The random number generator algorithm can be switched off to eliminate turbulent fluctuations and analyze laminar flow.
- The geometry of the periodic cube can be replaced by a more realistic turbulence field.
- The computational domain size can be increased to depict more shock and detonation phenomena, such as shocklets and detonation cells.
- The shock and detonation waves can be eliminated or replaced by other interferences to the turbulent flow.
- Detailed chemistry can replace the single-step Arrhenius law to investigate detonation, combustion, and explosion phenomena.

The direct numerical simulation code can be used to validate other direct numerical simulation codes, large eddy simulation codes, as well as experimental studies. With the coding advancements today, legacy code written in different programming languages can be reused within MATLAB in conjunction with this direct numerical

simulation tool. Moreover, this MATLAB code can be called as an executable file in other programming languages, packaged as a software component and integrated into other language-specific applications, or converted to other programming languages that are faster and more efficient. MATLAB provides flexible, two-way integration with other programming languages (Mathworks, 2018b) as shown in Figure 7.1.

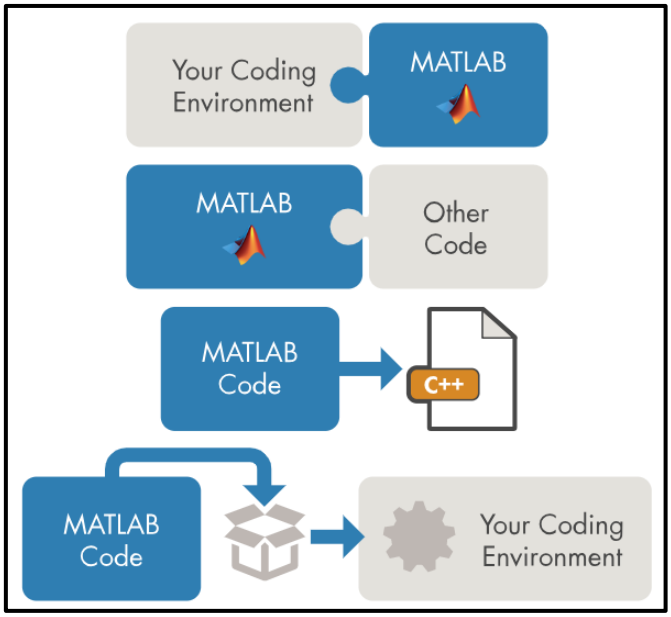

Figure 7.1 MATLAB code usage with other programming languages (MATHWORKS, 2018b)

7.3 Recommendations

The work completed in this project opens the doors to further research in the subject matter.

In this research study, the next step is to investigate the energy cascade throughout the computational domain in the three interaction case studies of unforced–detonation, shock–turbulence, and detonation–turbulence. The statistical analysis of single-point velocity correlations evaluated in the polar coordinates can give real insight into the flow behavior depicting wave structure, elongation parameters, and cellular detonation shapes. Two-point velocity correlation analysis would follow. The properties of vorticity and enstrophy should be evaluated. Vorticity is a vector that describes the curl of the flow velocity expressed as the cross product of the del operator and the velocity vector.

$$\omega = \nabla \times u \tag{7.1}$$

The vorticity describes the spinning motion of a fluid particle near a particular point of interest. Enstrophy is the integral of vorticity over a surface representing the dissipation effects in a fluid with relation to its kinetic energy.

$$\Omega = |\omega^2| \tag{7.2}$$

The time evolution of the velocity properties should be analyzed. It is recommended to run different flow Mach numbers and heat release parameters to compare outputs. The computational domain size ought to be increased to acquire larger data sets for numerical analysis and potentially capture more detailed shock and detonation properties. The single-step Arrhenius law must be replaced by detailed chemistry where different gaseous combinations are tested and analyzed. Employing advanced flow visualization tools in three dimensions can depict interesting flow behavior and

interaction properties not traceable through quantitative numerical analysis and surface plot visuals. In addition, the modes of the turbulence instabilities can be studied in detail to understand the flow evolution in the far field past the shock wave front.

It is recommended that follow-up research look into eliminating the cube periodicity and the fluid field homogeneity and isotropy conditions. For the non-homogeneous turbulence, the proposed velocity skewness vector should be evaluated to assess its symmetry. Entropic and acoustic fluctuations in turbulence can be studied next, in combination with vortical fluctuations. The skewness of the entropic and acoustic fluctuations ought to be questioned. The detonation wave must be allowed to propagate through the computational domain for more realistic representation. Finally, the employment of large eddy simulation will allow the study of more realistic turbulence and interaction case studies with industrial applications.

Appendix

A. Turbulence Research Timeline from 1600 to 2017

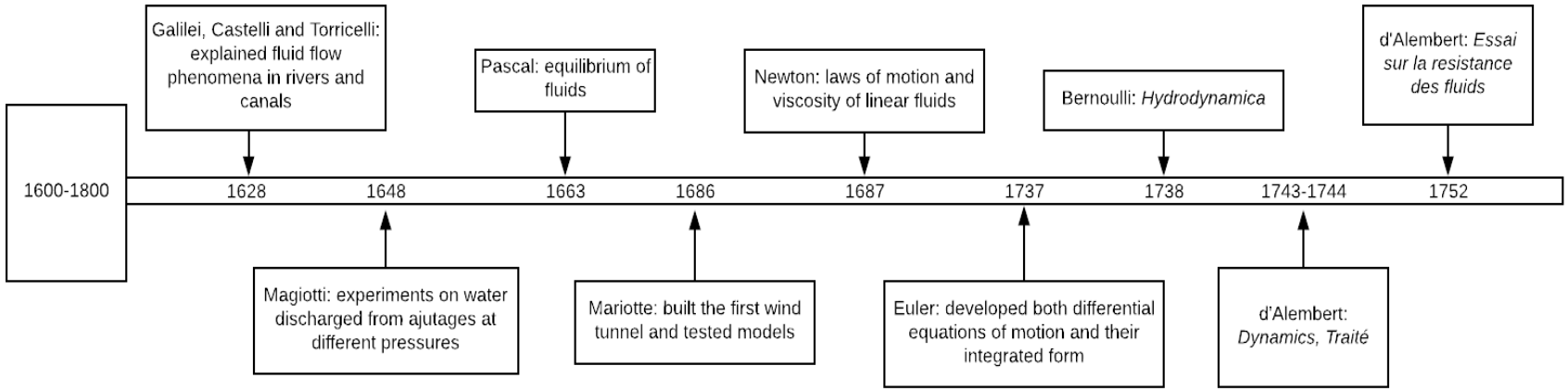
1600-1800
1628
1648
1663
1686
1687
1737
1738
1743-1744
1752
Galilei, Castelli and Torricelli: explained fluid flow phenomena in rivers and canals
Pascal: equilibrium of fluids
Newton: laws of motion and viscosity of linear fluids
Bernoulli: Hydrodynamica
d'Alembert: Essai sur la resistance des fluids
Magiotti: experiments on water discharged from ajutages at different pressures
Mariotte: built the first wind tunnel and tested models
Euler: developed both differential equations of motion and their integrated form
d'Alembert: Dynamics, Traité

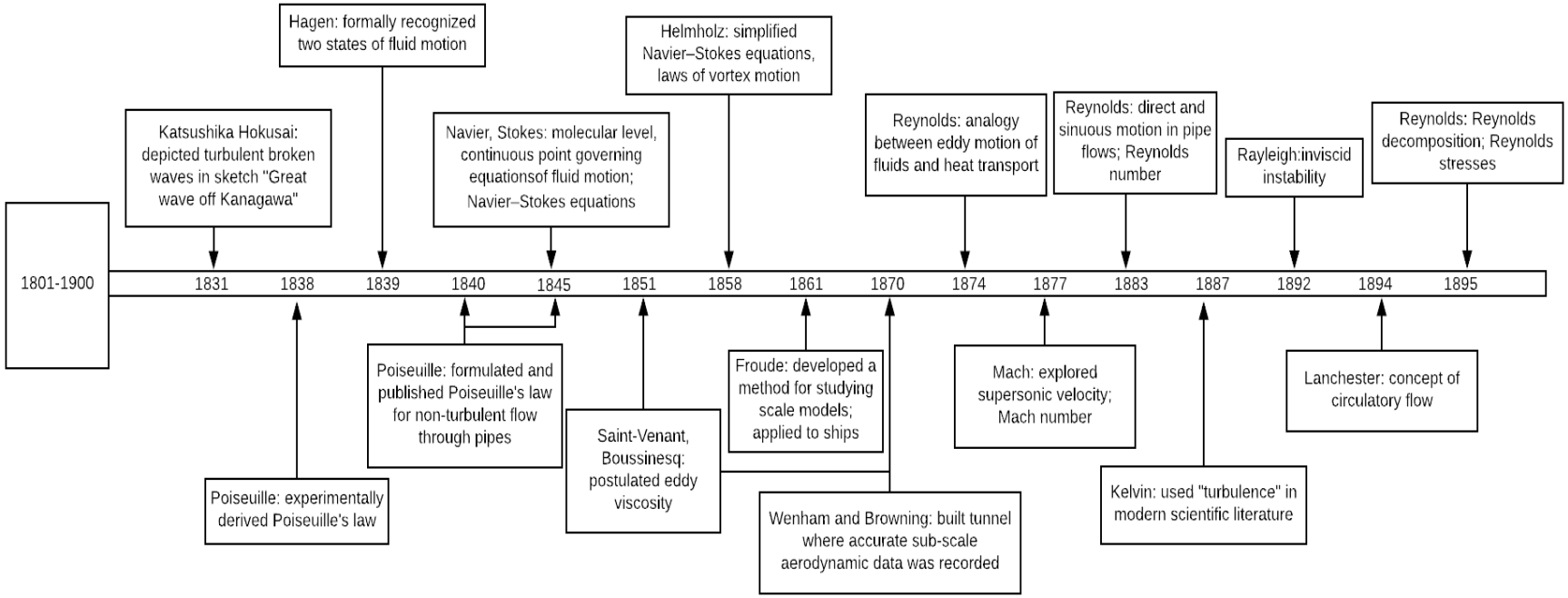
1801-1900
1831
1838
1839
1840
1845
1851
1858
1861
1870
1874
1877
1883
1887
1892
1894
1895
Katsushika Hokusai: depicted turbulent broken waves in sketch "Great wave off Kanagawa"
Hagen: formally recognized two states of fluid motion
Navier, Stokes: molecular level, continuous point governing equationsof fluid motion; Navier–Stokes equations
Helmholz: simplified Navier–Stokes equations, laws of vortex motion
Reynolds: analogy between eddy motion of fluids and heat transport
Reynolds: direct and sinuous motion in pipe flows; Reynolds number
Rayleigh:inviscid instability
Reynolds: Reynolds decomposition; Reynolds stresses
Poiseuille: experimentally derived Poiseuille's law
Poiseuille: formulated and published Poiseuille's law for non-turbulent flow through pipes
Saint-Venant, Boussinesq: postulated eddy viscosity
Froude: developed a method for studying scale models; applied to ships
Wenham and Browning: built tunnel where accurate sub-scale aerodynamic data was recorded
Mach: explored supersonic velocity; Mach number
Kelvin: used "turbulence" in modern scientific literature
Lanchester: concept of circulatory flow

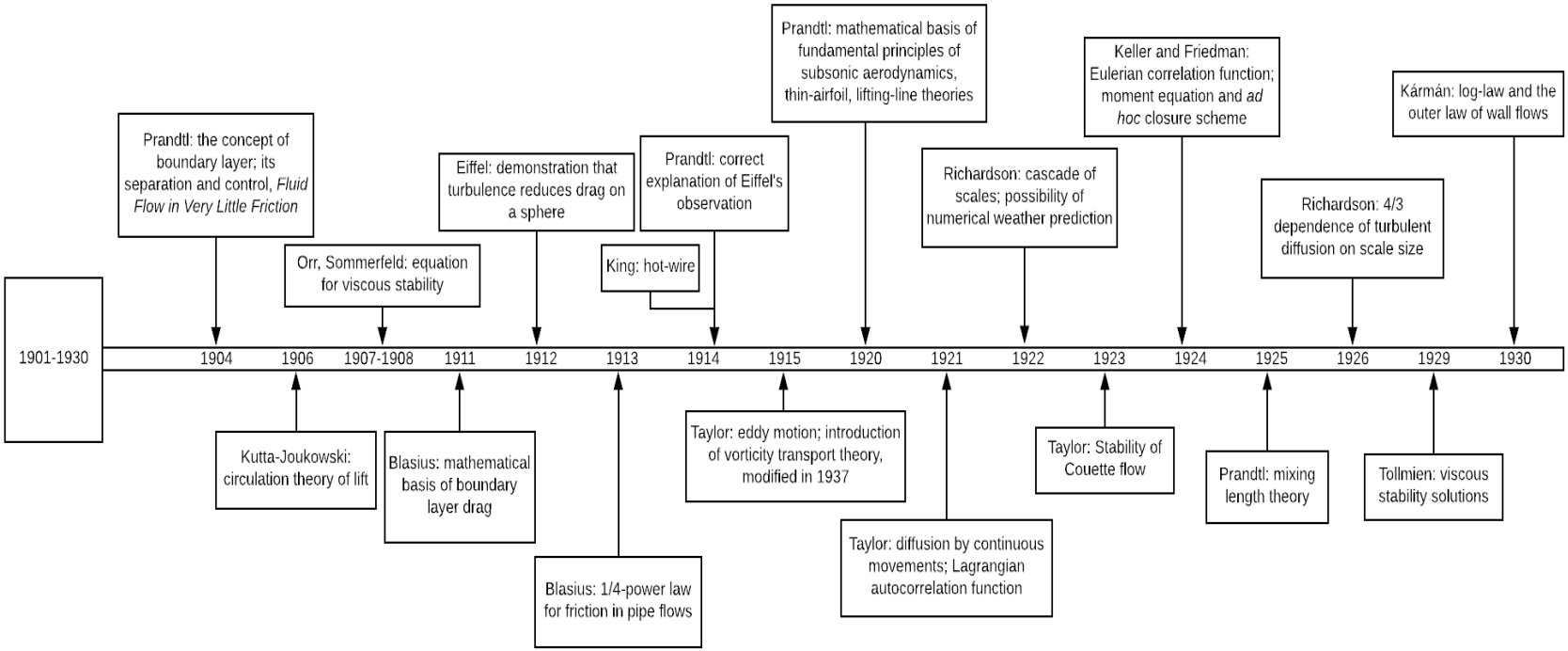
1901-1930
1904
1906
1907-1908
1911
1912
1913
1914
1915
1920
1921
1922
1923
1924
1925
1926
1929
1930
Prandtl: the concept of boundary layer; its separation and control, *Fluid Flow in Very Little Friction*
Orr, Sommerfeld: equation for viscous stability
Eiffel: demonstration that turbulence reduces drag on a sphere
King: hot-wire
Prandtl: correct explanation of Eiffel's observation
Prandtl: mathematical basis of fundamental principles of subsonic aerodynamics, thin-airfoil, lifting-line theories
Richardson: cascade of scales; possibility of numerical weather prediction
Keller and Friedman: Eulerian correlation function; moment equation and *ad hoc* closure scheme
Richardson: 4/3 dependence of turbulent diffusion on scale size
Kármán: log-law and the outer law of wall flows
Kutta-Joukowski: circulation theory of lift
Blasius: mathematical basis of boundary layer drag
Blasius: 1/4-power law for friction in pipe flows
Taylor: eddy motion; introduction of vorticity transport theory, modified in 1937
Taylor: diffusion by continuous movements; Lagrangian autocorrelation function
Taylor: Stability of Couette flow
Prandtl: mixing length theory
Tollmien: viscous stability solutions

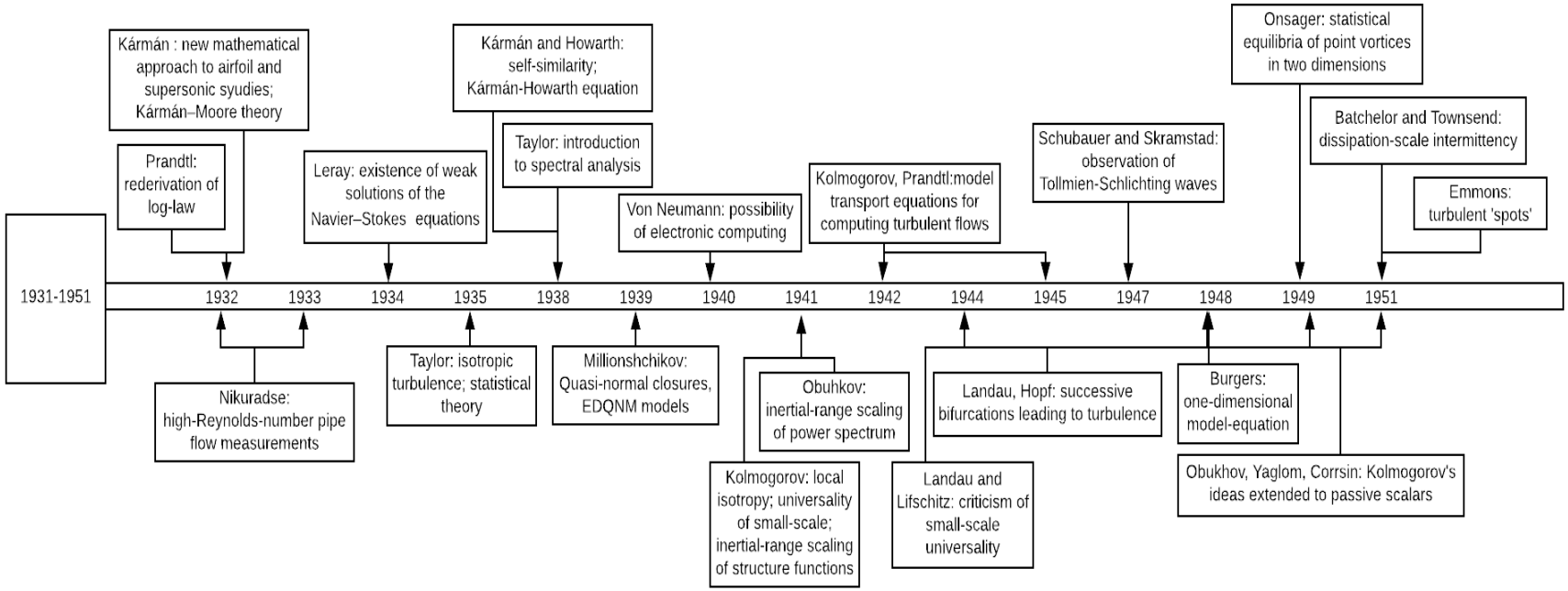
1931-1951
1932
1933
1934
1935
1938
1939
1940
1941
1942
1944
1945
1947
1948
1949
1951
Kármán : new mathematical approach to airfoil and supersonic syudies; Kármán–Moore theory
Prandtl: rederivation of log-law
Leray: existence of weak solutions of the Navier–Stokes equations
Kármán and Howarth: self-similarity; Kármán-Howarth equation
Taylor: introduction to spectral analysis
Von Neumann: possibility of electronic computing
Kolmogorov, Prandtl:model transport equations for computing turbulent flows
Schubauer and Skramstad: observation of Tollmien-Schlichting waves
Onsager: statistical equilibria of point vortices in two dimensions
Batchelor and Townsend: dissipation-scale intermittency
Emmons: turbulent 'spots'
Nikuradse: high-Reynolds-number pipe flow measurements
Taylor: isotropic turbulence; statistical theory
Millionshchikov: Quasi-normal closures, EDQNM models
Kolmogorov: local isotropy; universality of small-scale; inertial-range scaling of structure functions
Obuhkov: inertial-range scaling of power spectrum
Landau and Lifschitz: criticism of small-scale universality
Landau, Hopf: successive bifurcations leading to turbulence
Burgers: one-dimensional model-equation
Obukhov, Yaglom, Corrsin: Kolmogorov's ideas extended to passive scalars

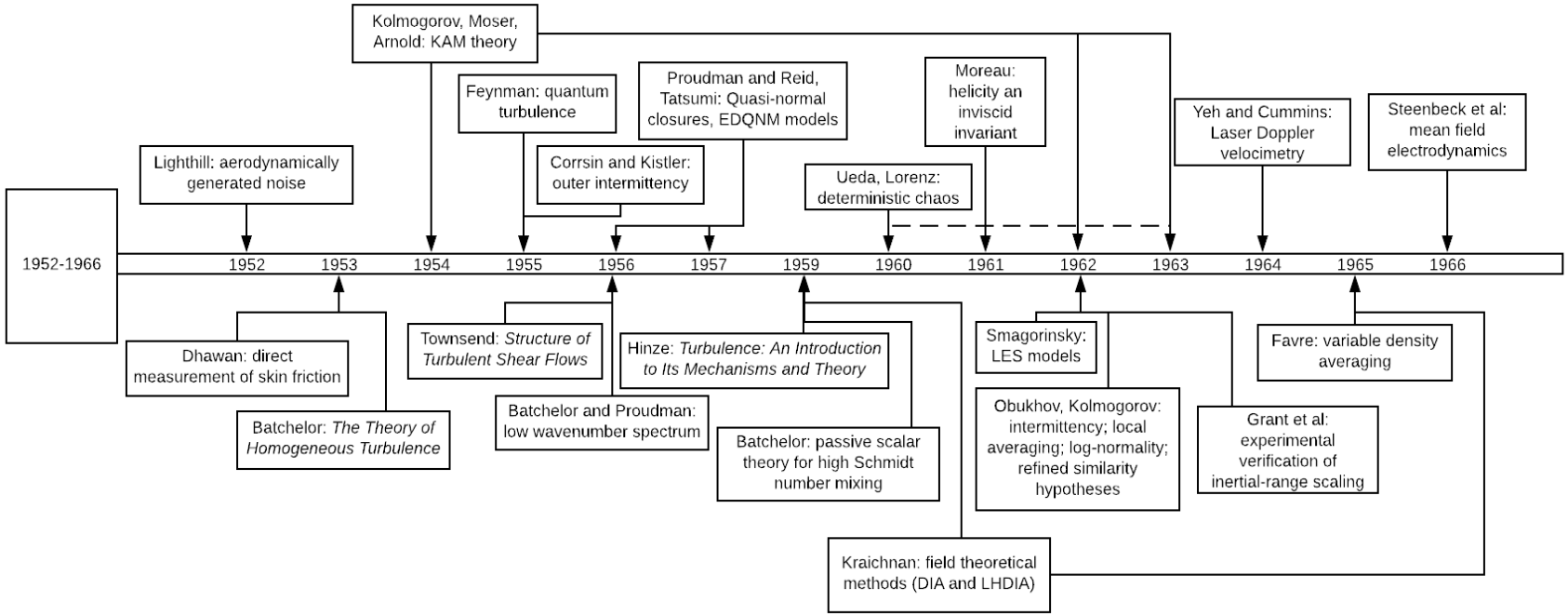
1952-1966
1952
1953
1954
1955
1956
1957
1959
1960
1961
1962
1963
1964
1965
1966
Kolmogorov, Moser, Arnold: KAM theory
Feynman: quantum turbulence
Proudman and Reid, Tatsumi: Quasi-normal closures, EDQNM models
Moreau: helicity an inviscid invariant
Yeh and Cummins: Laser Doppler velocimetry
Steenbeck et al: mean field electrodynamics
Lighthill: aerodynamically generated noise
Corrsin and Kistler: outer intermittency
Ueda, Lorenz: deterministic chaos
Dhawan: direct measurement of skin friction
Batchelor: The Theory of Homogeneous Turbulence
Townsend: Structure of Turbulent Shear Flows
Batchelor and Proudman: low wavenumber spectrum
Hinze: Turbulence: An Introduction to Its Mechanisms and Theory
Batchelor: passive scalar theory for high Schmidt number mixing
Smagorinsky: LES models
Obukhov, Kolmogorov: intermittency; local averaging; log-normality; refined similarity hypotheses
Favre: variable density averaging
Grant et al: experimental verification of inertial-range scaling
Kraichnan: field theoretical methods (DIA and LHDIA)

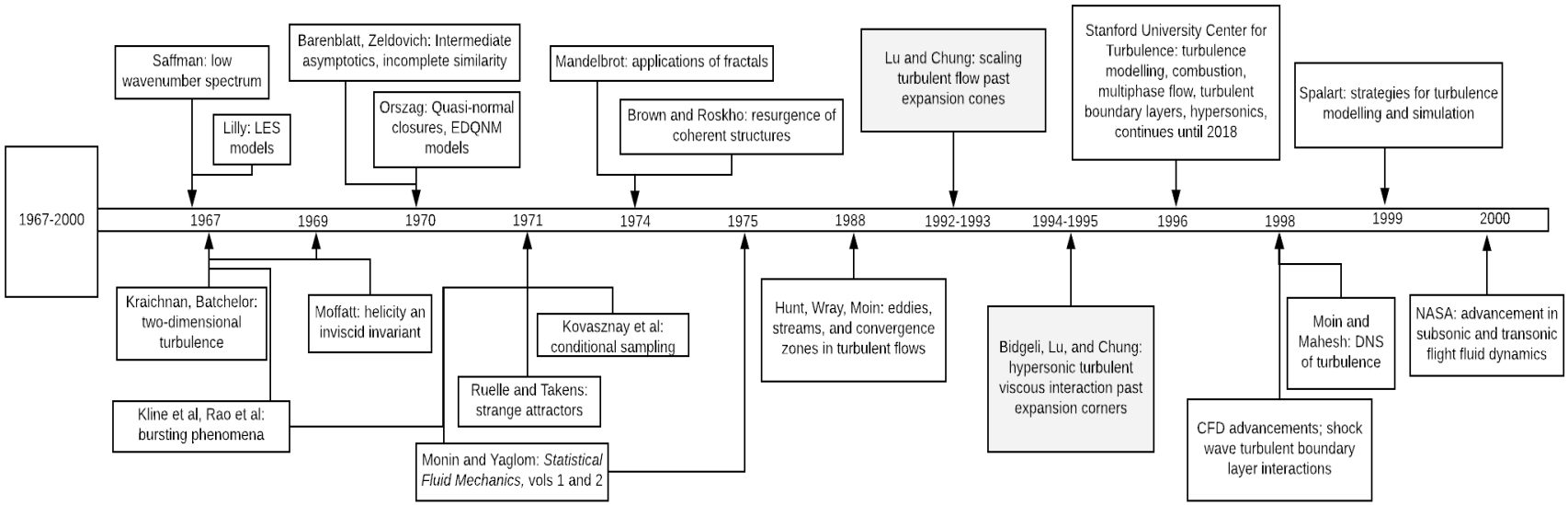
1967-2000
1967
1969
1970
1971
1974
1975
1988
1992-1993
1994-1995
1996
1998
1999
2000
Saffman: low wavenumber spectrum
Lilly: LES models
Barenblatt, Zeldovich: Intermediate asymptotics, incomplete similarity
Orszag: Quasi-normal closures, EDQNM models
Mandelbrot: applications of fractals
Brown and Roskho: resurgence of coherent structures
Lu and Chung: scaling turbulent flow past expansion cones
Stanford University Center for Turbulence: turbulence modelling, combustion, multiphase flow, turbulent boundary layers, hypersonics, continues until 2018
Spalart: strategies for turbulence modelling and simulation
Kraichnan, Batchelor: two-dimensional turbulence
Moffatt: helicity an inviscid invariant
Kline et al, Rao et al: bursting phenomena
Ruelle and Takens: strange attractors
Kovasznay et al: conditional sampling
Monin and Yaglom: *Statistical Fluid Mechanics,* vols 1 and 2
Hunt, Wray, Moin: eddies, streams, and convergence zones in turbulent flows
Bidgeli, Lu, and Chung: hypersonic turbulent viscous interaction past expansion corners
CFD advancements; shock wave turbulent boundary layer interactions
Moin and Mahesh: DNS of turbulence
NASA: advancement in subsonic and transonic flight fluid dynamics

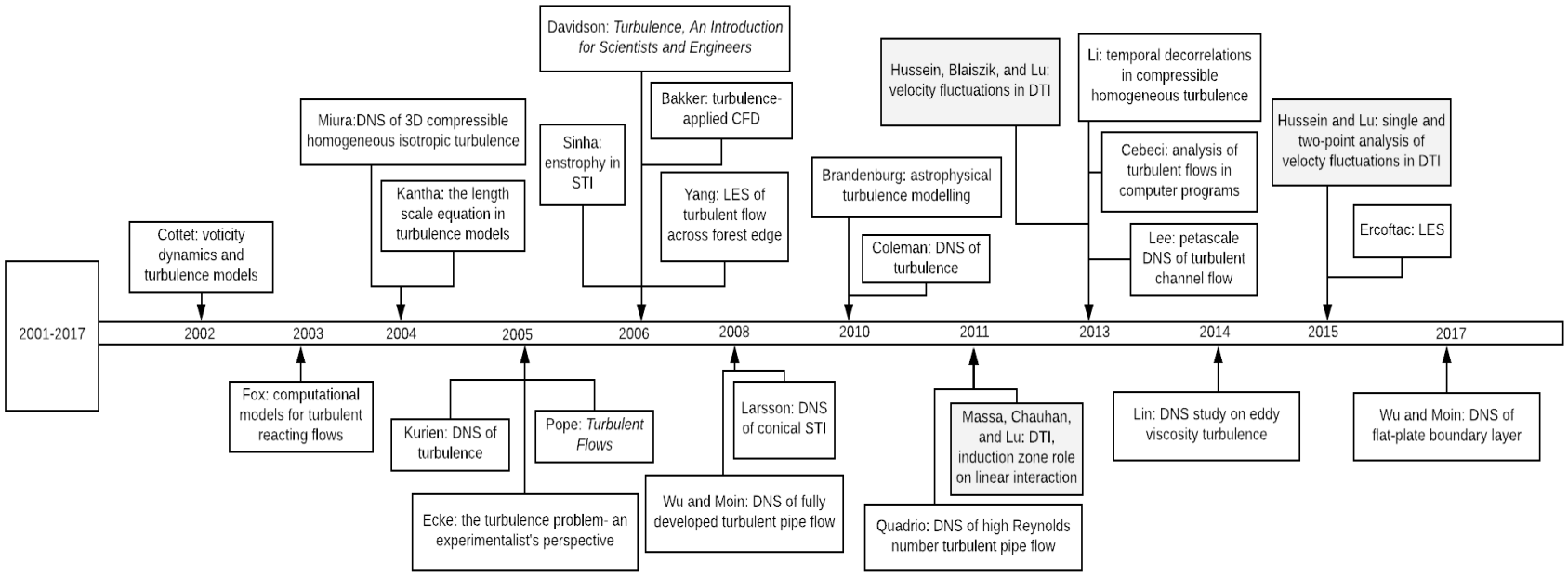
2001-2017
2002
2003
2004
2005
2006
2008
2010
2011
2013
2014
2015
2017
Cottet: voticity dynamics and turbulence models
Fox: computational models for turbulent reacting flows
Miura:DNS of 3D compressible homogeneous isotropic turbulence
Kantha: the length scale equation in turbulence models
Kurien: DNS of turbulence
Ecke: the turbulence problem- an experimentalist's perspective
Davidson: Turbulence, An Introduction for Scientists and Engineers
Sinha: enstrophy in STI
Pope: Turbulent Flows
Bakker: turbulence-applied CFD
Yang: LES of turbulent flow across forest edge
Wu and Moin: DNS of fully developed turbulent pipe flow
Larsson: DNS of conical STI
Brandenburg: astrophysical turbulence modelling
Coleman: DNS of turbulence
Hussein, Blaiszik, and Lu: velocity fluctuations in DTI
Massa, Chauhan, and Lu: DTI, induction zone role on linear interaction
Quadrio: DNS of high Reynolds number turbulent pipe flow
Li: temporal decorrelations in compressible homogeneous turbulence
Cebeci: analysis of turbulent flows in computer programs
Lee: petascale DNS of turbulent channel flow
Lin: DNS study on eddy viscosity turbulence
Hussein and Lu: single and two-point analysis of velocty fluctuations in DTI
Ercoftac: LES
Wu and Moin: DNS of flat-plate boundary layer

B. Notation Description

Three Term Product Rule

$$\frac{d}{dx}(f(x)g(x)h(x)) = g(x)[(h(x)f'(x)) + (f(x)h'(x))] + f(x)[h(x)g'(x)]$$

Index Notation

$\sigma_{ij} = \sigma_{33}$ for *i* = 1, 2, 3 and *j* = 1, 2, 3

$$\sigma_{ij} = \begin{bmatrix} \sigma_{i1j1} & \sigma_{i1j2} & \sigma_{i1j3} \\ \sigma_{i2j1} & \sigma_{i2j2} & \sigma_{i2j3} \\ \sigma_{i3j1} & \sigma_{i3j2} & \sigma_{i3j3} \end{bmatrix}$$

$$\nabla = \left(\frac{\partial}{\partial x}\right) i + \left(\frac{\partial}{\partial y}\right) j + \left(\frac{\partial}{\partial z}\right) k$$

for f, a scalar function

$$\nabla \mathrm{f} = \left(\frac{\partial f}{\partial x}\right) i + \left(\frac{\partial f}{\partial y}\right) j + \left(\frac{\partial f}{\partial z}\right) k$$

for $\vec{u}$, a vector quantity

$$\nabla \vec{u} = \left(\frac{\partial}{\partial x} u\right) i + \left(\frac{\partial}{\partial y} v\right) j + \left(\frac{\partial}{\partial z} w\right) k$$

the transpose function is then defined and results in a scalar quantity

$$\nabla \vec{u}^T = u\frac{\partial}{\partial x} + v\frac{\partial}{\partial y} + w\frac{\partial}{\partial z}$$

the divergence of $\vec{u}$, a vector quantity, results in a scalar quantity

$$\mathrm{div}(\vec{u}) = \nabla . \vec{u} = \frac{\partial u}{\partial x} + \frac{\partial v}{\partial y} + \frac{\partial w}{\partial z}$$

C. MATLAB Code Flowchart Shapes

The following are the shapes and their corresponding coding reference that are used in the direct numerical simulation MATLAB code flowcharts, as documented by Lucidchart, the online visual communication tool.

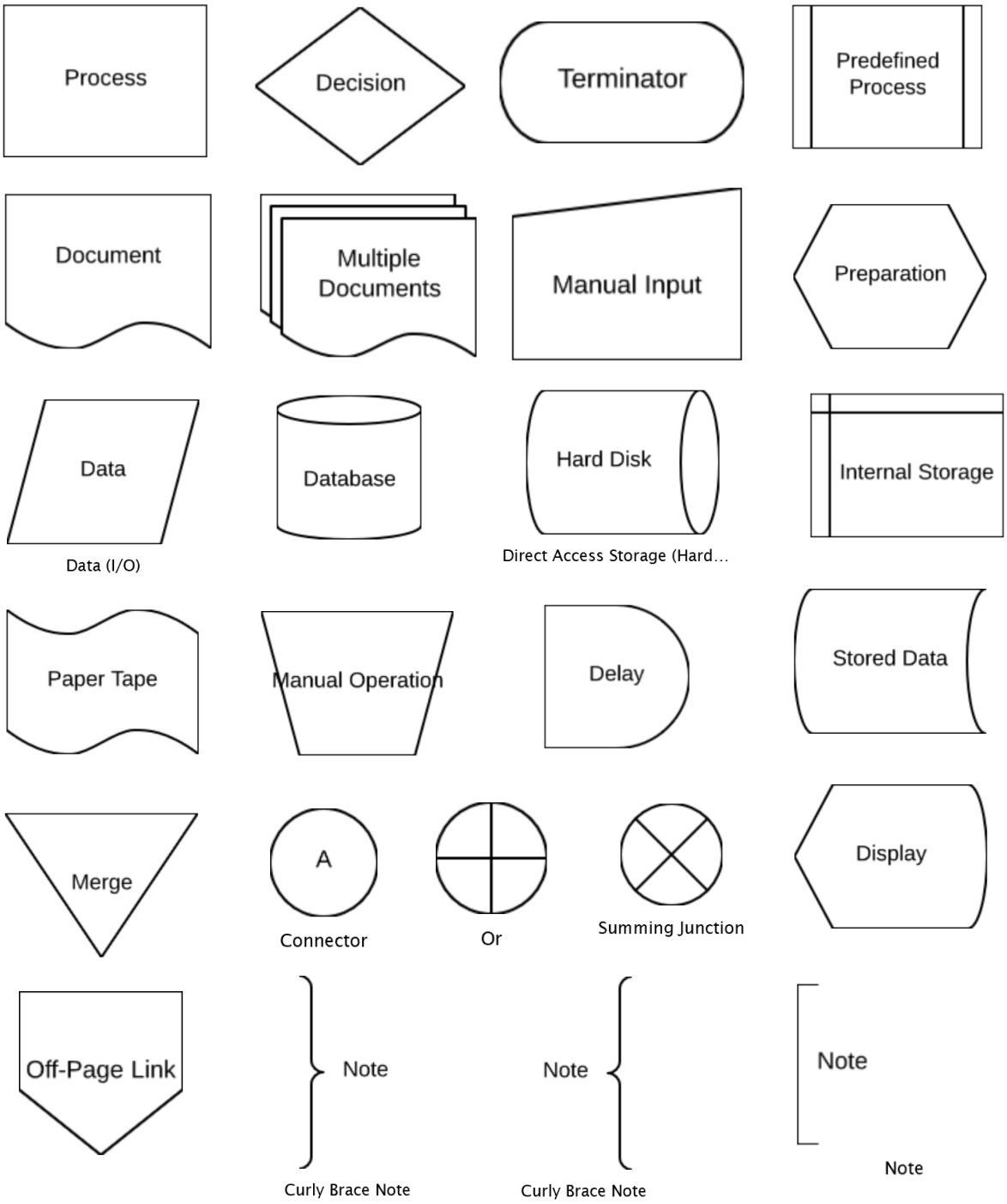

References

1. Absi, R., "A roughness and time dependent mixing length equation", Journal of Hydraulic, Coastal and Environmental Engineering, Japan Society of Civil Engineers, Vol. 62 -No. 4, pp: 437-446, 2006.
2. Agui, J. H., Briassulis, G., and Andreopoulos, Y.," Studies of interactions of a propagating shock wave with decaying grid turbulence: velocity and vorticity fields" J. Fluid Mech. 524, pp: 143-195, 2005.
3. Anderson, J.J., "Fundamentals of Aerodynamics", Vol. 5th Edition, New York: McGraw Hills, pp. 540-553, 2011.
4. Andreopoulos, Y., Agui, J.H., and Briassulis, G., "Shock wave–turbulence interactions" Ann Rev Fluid Mech 32, pp: 309-345, 2000.
5. Austin, J., "The Role of Instability in Gaseous Detonation," Doctoral thesis, California Institute of Technology, 2003.
6. Baldwin, B. S., and Lomax, H., "Thin layer approximation and algebraic model for separated turbulent flows", AIAA, pp: 78-257, 1978.
7. Baldwin, B.S., and Barth, T.J.," A one-equation turbulence transport model for high Reynolds number wall-bounded flows" NASA TM 102847, 1990.
8. Bardina, J.E., Huang, P.G., and Coakley, T.J., "Turbulence modeling validation, testing, and development", NASA Technical Memorandum 110446, 1997.
9. Barre, S., Alem, D., and Bonnet, J. P., "Experimental study of a normal shock/homogeneous turbulence interaction" AIAA J. 34 (5), pp: 968–974, 1996.
10. Bašić, J., "Turbulent History of Fluid Mechanics" A brief essay, Research Gate, 2016. (accessed online)

11. Bataille, F., and Zhou, Y., “Nature of the energy transfer process in compressible turbulence” The American Physical Society, Vol. 59, pp: 5417-5426, 1999.
12. Batchelor, G.K., and Townsend, A.A., Proc. Roy. Soc. A, p: 527, 1948.
13. Batchelor, G.K., “The theory of homogeneous turbulence” Cambridge University Press, Cambridge, 1953.
14. Bendat, J.S., and Piersol, A.G. “Random Data: Analysis and Measurement Procedures”, Fourth Edition, Wiley and Sons Inc. Publication, Hoboken, New Jersey, 2010.
15. Bennett, J.C., and Corrsin, S., “Small Reynolds number nearly isotropic turbulence in a straight duct and a contraction” Physics of Fluids 21, p: 2129, 1978.
16. Bermejo-Moreno, I., Larsson, J., and Lele, S.K., “LES of canonical shock–turbulence interaction” Center of Turbulence Research Annual Research Briefs, pp: 210-222, 2010.
17. Betchov, R., and Lorenzen, C., Physics of Fluids 17, p: 1503, 1974.
18. Biferale, L., and Toschi, F., “Anisotropic Homogeneous Turbulence: Hierarchy and Intermittency of Scaling Exponents in the Anisotropic Sectors” Physical Review Letters, Volume 86, number 21, 2001.
19. Bouteloup, P., “Thermal Conductivity of Air vs. Temperature Plot” (accessed online, 2018).
http://bouteloup.pierre.free.fr/lica/phythe/don/air/air_k_plot.pdf
20. Brewer, and Jess H., “Divergence of a vector field” Vector Calculus, Retrieved 09, 28, 2007, 1994.

21. Canuto, V.M., “Compressible turbulence” The Astrophysical Journal, 482, pp: 827-851, 1997.
22. Cebeci, T., “Turbulence models and their applications” Springer, 2004.
23. Chauhan, M., “Numerical analysis of the interaction between a detonation wave and compressible homogeneous isotropic turbulence” Master’s thesis, University of Texas at Arlington, 2011.
24. Chen, C.J., and Jaw, S.Y., “Fundamentals of turbulence modeling” Taylor and Francis, 1998.
25. CFD Online, “Turbulence modeling”, GNU Free Documentation, 2009.
26. CDFSupport, “Laminar vs. Turbulence Flow” OpenFOAM Training, Czech Republic, 2013. (accessed online)
27. Chinnayya, A., Hadjadj, A., and Ngomo, D., “Computational study of detonation wave propagation in narrow channels” Physics of Fluids, 25, 036101, 2013.
28. Coleman, G.N., and Sandberg, R.D., “Direct numerical simulation of turbulent fluid flow” Encyclopedia of Aerospace Engineering, 2010.
29. Craft, T.J., “Near-wall modelling” MSc Fluid Mechanics, 2010.
30. Currie, I.G., “Fundamental mechanics of fluids” CRC Press, Taylor & Francis Group, Florida, 2013.
31. Davidson, P.A., “Turbulence an introduction for scientists and engineers” Oxford University Press, New York, 2004.
32. Davidson, P.A., Kaneda, Y., Moffatt, K., and Sreenivasan, K.R., “A voyage through turbulence” Cambridge University Press, 2011.

33. Deledicque, V., and Papalexandris, M.V., “Computational study of three–dimensional gaseous detonation structures” Combust Flame 144 (4), pp: 821-837, 2006.
34. Deledicque, V., “Modeling and simulation of multidimensional compressible flows of gaseous and heterogeneous reactive mixtures” Doctoral thesis, Universite Catholique de Louvain, 2007.
35. Doering, C.R. and Gibbon, J.D., “Applied Analysis of the Navier-Stokes Equations”, Cambridge University Press, Cambridge, 1995.
36. Donati, F., “Student Visualizations” Philofluid, Politecnico di Torino, 2011. *https://areeweb.polito.it/ricerca/philofluid/gallery/213-students-visualization.html*
37. Donzis, D.A., “Shock structure in shock–turbulence interactions” Phys Fluids 24 (12), 126101, 2012.
38. Dou, H.S., Tsai, H.M., Khoo, B.C., and Qiu, J., “Simulations of detonation wave propagation in rectangular ducts using a three–dimensional WENO scheme” Combust Flame 154 (4), pp: 644-659, 2008.
39. Fickett, W., Davis, “Detonation” Mineola, NY, 11501, 1979.
40. Frenkiel, F., and Klebanoff, P.S., J. Fluid Mechanics, pp: 1948-183, 1971.
41. Frisch, U., “Turbulence: The Legacy of A.N. Kolmogorov” Cambridge University Press, Cambridge, 1995.
42. Gad-el-Hak, M., “Flow Control: Passive, Active, and Reactive Flow Management” Cambridge University Press, 2000.
43. Gavrilyuk, S.L., and Saurel, R., “Estimation of the turbulence energy production across a shock wave“ J. Fluid Mechanics, 549, p:131, 2006.

44. Gelfand, B., Frolov, S., and Nettleton, M., "Gaseous detonations. A selective review," Prog. Energy Combustion, Sci. 17, pp. 327-371, 1991.
45. George, W.K., and Arndt, R., “Advances in Turbulence” Hemisphere Publishing Corporations, 1989.
46. Gholamrezaei, M., “Turbulence”, Sharif Univ. of Tech, PhD Student website, 2018.
http://ae.sharif.ir/~gholamrezaei/Turbulence.htm
47. Glassman, I., and Yetter, R.A., “Combustion” Chapter 5: Detonation, 4th Edition, pp: 261-309, 2008.
48. Goodman, L., Levine, E.R., and Lueck, R.G., “On measuring the terms of the turbulent kinetic energy budget form AUV” Goodman et al, p. 977, 2006.
49. Goto, S., “A physical mechanism of the energy cascade in homogeneous isotropic turbulence” Jou Fluid Mechanics, Vol.605, pp: 355-366, 2008.
50. Gotoh, T., and Kaneda, Y., “Lagrangian velocity autocorrelation and eddy viscosity in two–dimensional turbulence” Phys. Fluids A3, pp: 24-26, 1991.
51. Gotoh, T., “Lagrangian velocity correlations in homogeneous isotropic turbulence” Physics of Fluids 5- pp: 28-46, 1993.
52. Gotoh, T., “Energy spectrum in the inertial and dissipation ranges of two–dimensional steady turbulence” Phys. Rev. E- 57, pp: 29-84, 1998.
53. Gravanis, E., and Akylas, E., “Stationarity of linearly forced turbulence in finite domains” PhysRevE.84.046312, 2011.
54. Gregg, M.C., “Diapycnal mixing in the thermocline: A review” J. Geophysics, Res. 92, pp: 5249-5284, 1987.

55. Grube, N.E., Taylor, E.M., Pino Martin, M., “Numerical Investigation of shock–wave/isotropic turbulence interaction” AIAA 2011-480, 2011.
56. Hanana, M., Lefebvre, M.H., Van Tiggelen, P.J., “Pressure profiles in detonation cells with rectangular or diagonal structure” ICDERS, 160, 1999.
57. Hinze, J.O., “Turbulence” Mc-Graw-Hill, New York, 1975.
58. **Hussein**, S.M., Lu, F.K. “Statistical Analysis of Velocity Fluctuations in a Strong Detonation-Turbulence Interaction”, UT Arlington Honors College Senior Thesis, April 2012.
59. **Hussein**, S.M., Blaiszik, E.M., and Lu, F.K., “Velocity fluctuations in the interaction of homogeneous, isotropic turbulence and a detonation wave” No. 0246-000173, 29th International Symposium on Shock Waves, Madison, Wisconsin, 2013.
60. **Hussein**, S.M., and Lu, F.K., “Single and two–point analysis of velocity fluctuations in a detonation–turbulence interaction” 45th AIAA Fluid Dynamics Conference, AIAA Aviation, Dallas, Texas, 2015.
61. Jaberi, F.A., Livescu, D., and Madnia, C.K., “Characteristics of chemically reacting compressible homogeneous turbulence” Physics of Fluids, Vol. 12, pp: 1189-1209, 2000.
62. Jackson, T.L., Hussaini, M.Y., and Ribner, H.S., “Interaction of turbulence with a detonation wave” Phys Fluids A-5 (3), pp: 745-749, 1993.
63. Johns Hopkins University, “Forced Isotopic Turbulence Dataset”, Johns Hopkins Turbulence Databases (JHTDB), 2018.
http://turbulence.pha.jhu.edu/

64. Johnson, D.A., and KING, L.S., "A mathematically simple turbulence closure model for attached and separated turbulent boundary layers", AIAA Journal, Vol. 23- No. 11, pp: 1684-1692, 1985.
65. Jones, H., “Dynamics of spinning detonation–waves” Proc Roy Soc Lond, A 348, 1654, pp: 299-316, 1976.
66. Kaneda, Y., and Gotoh, T., “Lagrangian velocity autocorrelation in isotropic turbulence” Physics of Fluids A: Fluid Dynamics, 1991.
67. Khalaf, S. G., “History of the Phoenician Canaanites”, Phoenician Encyclopedia, 2018.
https://phoenicia.org/history.html
68. Khasainov, B., Virot, F., Presles, H.-N., Desbordes, D., “Parametric study of double cellular detonation structure” Shock Waves, 23- pp: 213-220, 2013.
69. Kida, S., and Orszag, S. A., “Energy and Spectral Dynamics in Decaying Compressible Turbulence” Journal of Scientific Computing, Vol. 7, No. 1, 1992.
70. Kolmogorov, A.N., “The local structure of turbulence in incompressible viscous fluid for very large Reynolds numbers” Dokl. Akad. Nauk SSSR 30, pp: 299-303, 1941. (in Russian)
71. Kuo, A.Y., Corrsin, S., J. Fluid Mechanics, 50, p: 285, 1971.
72. Lane, D.M., “Introduction to Statistics” Chapter 7, Online Statistics Education: A Multimedia Course of Study, Rice University, 2013.
http://onlinestatbook.com/
73. Larsson, J. “Direct numerical simulation of canonical shock/turbulence interaction” Annual Research Briefs, Center of Turbulence Research, 2008.

74. Larsson, J., Bermejo-Moreno, I., and Lele, S.K., “Reynolds- and Mach- number effects in canonical shock–turbulence interaction” J Fluid Mech 717, pp: 293-321, 2013.
75. Lee, S., Lele, S.K., and Moin, P., “Eddy shocklets in decaying compressible turbulence” Phys of Fluids, Vol. 3, pp:657-664, 1991.
76. Lee, S., “Interaction of isotropic turbulence with a shockwave” Doctoral thesis, Stanford University, 1992. (a)
77. Lee, S., Lele, S.K., and Moin, P., “Simulation of spatially evolving turbulence and applicability of Taylor’s hypothesis in compressible flow” Phys of Fluids A, Vol. 4, pp: 1521-1530, 1992. (b)
78. Lee, S., Lele, S.K., and Moin, P., “Interaction of isotropic turbulence with shock waves: effect of shock strength” Journal of Fluid Mechanics, Vol. 340, pp: 225-247, 1997.
79. Lele, S.K., “Compressibility effects on turbulence” Annu Rev Fluid Mech, Vol. 26, pp: 211-254, 1994.
80. Lele, S., and Larsson, J., "Shock-turbulence interaction: what we know and what we can learn from peta scale simulations" J. Phys. Conference Series, p: 180, 2009.
81. Lesieur, M., “Turbulence in fluids” Mechanics of Fluids and Transport Processes, Martinus Nijhoff Publishers, 1987.
82. Liepmann, H.W., “The rise and fall of ideas in turbulence” American Scientist, Vol 67, No. 2, pp: 221-228, 1979.

83. Lu, F., Chauhan, M., and Massa, L., "Evolution of autocorrelation in detonation interaction with homogeneous, isotropic turbulnce," ISSW28, Manchester, UK, 2011.
84. Mahesh, K., Lele, S.K., and Moin, P., “The influence of entropy fluctuations on the interaction of turbulence with a shock wave” J. Fluid Mechanics, volume 334, pp: 353-379, 1997.
85. Mansour, N.N., Kim, J., and Moin, P., “Reynolds stress and dissipation rate budgets in turbulent channel flow” NASA Ames Research Center, Moffett Field, California, 94035, 1987. (web access)
86. Mansour, N.N., and Wray, A.A., “Decay of isotropic turbulence at low Reynolds number” Physics of Fluids, Vol. 6, pp: 808-814, 1994.
87. Mark, J.J., “Phoenicia” Ancient History Encyclopedia, 2009. *http://www.ancient.eu/phoenicia/*
88. Massa, L., and Lu, F., “Turbulence–detonation linear interaction analysis” AIAA 2009-3949, 2009.
89. Massa, L., Chauhan, M., and Lu, F., “Detonation–turbulence interaction” Combustion and Flame 158 (9), pp: 1788-1806, 2011. (a)
90. Massa, L., Chauhan, M., and Lu, F., “Effects of vortical and entropic forcing on detonation dynamics” Paper 2512, ISSW28, Manchester, UK, 2011. (b)
91. Massa, L., and Lu, F., “The role of the induction zone on the detonation–turbulence linear interaction” Combust Theory Model 15 (3), pp: 347-371, 2011. (c)
92. Mathworks, “MATLAB”, Product description page, 2018. (a)

https://www.mathworks.com/products/matlab.html

93. Mathworks, “Using MATLAB with Other Programming Languages”, Product description page, 2018. (b) *https://www.mathworks.com/products/matlab/matlab-and-other-programming-languages.html*
94. Mills, R.R., Kistler, A.L., O’Brien, V., and Corrsin, S., N.A.C.A. Tech. Note no 4288, 1958.
95. MIT, “A Statistical Description of Turbulence”, Turbulence in the ocean and Atmosphere, Earth Atmospheric and Planetary Sciences, Spring 2007, Course notes, Chapter 3, 2007. *https://ocw.mit.edu/courses/earth-atmospheric-and-planetary-sciences/12-820-turbulence-in-the-ocean-and-atmosphere-spring-2007/lecture-notes/ch3.pdf*.
96. Moin, P., and Mahesh, K., “ Direct numerical simulation: a tool in turbulence research” Ann. Rev. Fluid Mech, 30, pp: 539-578, 1998.
97. Monaghan, J.J., and Kajtar, J.B., “Leonardo da Vinci’s turbulent tank in two dimensions” European Journal of Mechanics- B/Fluids, Vol. 44, pp:1-9, 2014.
98. Moriconi, L., and Rosa, R., “Theoretical aspects of homogeneous isotropic turbulence” J. of Braz Soc of Mech Sci and Eng, Vol. 26, pp: 391-399, 1993.
99. Muller, C., “Turbulence, energy cascade and self–similarity” Turbulence Laurent, LadyHx, 2014.
100. Nagarajan, H.N., “Direct numerical simulation of interaction of detonation wave with homogeneous isotropic turbulence” Master’s thesis, University of Texas at Arlington, 2009. (a)

101. Nagarajan, H., Massa, L., and Lu, F.K., “DNS of detonation wave and isotropic turbulence interaction,” 19th AIAA Computational Fluid Dynamics Conference, AIAA Paper 2009-3800, San Antonio, Texas, 2009. (b)

102. Nguyen, C., “Turbulence modeling” www.mit.edu, 2005.

103. Oran, E. S., Weber, J. W. JR., Stefaniw, E. I., Lefebvre, M. H., and Anderson, J.D. JR. “A Numerical Study of a Two-Dimensional H2-O2-Ar Detonation Using a Detailed Chemical Reaction Model” Combustion and Flame, 113- pp: 147-163, 1998.

104. Pan, S., and Johnsen, E., “The role of bulk viscosity on the decay of compressible, homogeneous, isotropic turbulence” Journal of Fluid Mechanics. 833- pp: 717-744, 2017.

105. Pirozzoli, S., “Conservative Hybrid Compact-WENO Schemes for Shock-Turbulence Interaction” Journal of Computational Physics, Vol. 178, Issue 1, pp: 81-117 2002.

106. Pirozzoli, S., and Grasso, F., “Direct numerical simulations of isotropic compressible turbulence, influence of compressibility on dynamics and structures” Phys of Fluids Vol.16, pp: 4386-4407, 2004.

107. Pope, S.B., “Turbulent flows” 2nd ed., Cambridge, New York, 2000.

108. Powers, J.M., “Review of multiscale modeling of detonation” Journal of Propulsion and Power, Vol. 22, pp: 1217-1229, 2006.

109. Qin, Z.C., Fang, L., and Fang, J., “How isotropic are turbulent flows generated by using periodic conditions in a cube?” Physics Letters A, Elsevier, 2016.

110. Rawat, P., and Zhong, X., "Numerical Simulation of Shock-Turbulence Interactions using High-Order Shock-Fitting Algorithms," AIAA 2010-114, Orlando, FL., 2010.

111. Richardson, L.F., “Weather prediction by numerical process” Cambridge: Cambridge University Press, 1922.

112. Ribner, H.S., “Spectra of noise and amplified turbulence emanating from shock–turbulence interaction” AIAA, Vol. 25, pp: 436-442, 1987.

113. Rogallo, R.S., “Numerical experiments in homogeneous turbulence” NASA TM-81315, pp: 1-91, 1981.

114. Rose, H.A., Sulem, P.L., “Fully developed turbulence and statistical mechanics” Journal de Physique, 39 (5), pp: 441-484, 1978.

115. Rybanin, S.S., “Turbulence in detonation, combustion explosion shock waves” 2 (1), pp: 15-18, 1966.

116. Sagaut, P., “Large eddy simulation for incompressible flows” 3rd Edition, Springer, ISBN 3-540-26344-6, 2006.

117. Sagaut, P., Claude, C., “Homogeneous Turbulence Dynamics” Cambridge University Press, 2008.

118. Šavli, M., “Turbulent kinetic energy – TKE” University of Ljubljana, Faculty of Mathematics and Physics, Department of Meteorology, Seminar: 4th class, 2012.

119. Shepherd, J.E., “Chemical Kinetics of Hydrogen-Air-Diluent Detonation” Progress in Astronautics and Aeronautics, Vol. 106, pp: 263-293, AIAA, New York, 1986.

120. Short, M., Stewart, S.D., “Cellular detonation stability” Journal of Fluid Mechanics, Vol. 368, pp: 229-262, 1998.

121. Sinha, K., “Evolution of enstrophy in shock/homogeneous turbulence interaction” J Fluid Mech, 707, pp: 74-110, 2012.

122. Smith, A.M.O., and Cebeci, T., "Numerical solution of the turbulent boundary layer equations" Douglas Aircraft Division Report DAC 33735, 1967.

123. Spalart, P. R., and Allmaras, S. R., "A one-equation turbulence model for aerodynamic flows" AIAA 92-0439, 1992.

124. Spalart, P. R., and Allmaras, S. R., "A one-equation turbulence model for aerodynamic flows" La Recherche Aerospatiale n 1, pp: 5-21, 1994.

125. Spalart, P.R., Jou, W.H., Stretlets, M., and Allmaras, S.R., “Comments on the feasibility of LES for wings and on the hybrid RANS/LES approach” Advances in DNS/LES, Proceedings of the First AFOSR International Conference on DNS/ LES, 1997.

126. Squires, K.D., and Eaton, J.K., “Lagrangian and eulerian statistics obtained from direct numerical simulations of homogeneous turbulence” Phys. Fluids A-3, p: 130, 1991.

127. Sreenivasan, K.R., “On the universality of the Kolmogorov constant” Phys. Fluids 7, pp: 2778-2784, 1995.

128. Stewart, R.W., and Townsend, A.A., Phil. Trans. Roy. Soc. A 243, 359, 1951.

129. Sutherland, W., “The viscosity of gases and molecular force" Philosophical Magazine, S-5, 36, pp: 507-531, 1893.

130. Tavoularis, S., Bennett, J.C., and Corrsin, S., “Velocity–derivative skewness in small Reynolds number, nearly isotropic turbulence” J. Fluid Mech, 88, pp:63-69,1978.

131. Taylor, G.T. Proc. Roy. Soc. A 164, 15, 1938.

132. Tennekes, H. and Lumley, J.L., “A First Course in Turbulence” the MIT press, Seventeenth Print, 1999.

133. Velikovich, A.L., Huete, C., Wouchuk, J.G., “Effect of shock–generated turbulence on the Hugoniot jump conditions” Phys Rev E 85, 016301, 2012.

134. Wang, C., Shu, C.-W., Han, W., and Ning, J., “High resolution WENO simulation of 3D detonation waves” Combust Flame 160 (2), pp: 447-462, 2013.

135. White, D.R., “Turbulent structure of gaseous detonation” Phys Fluids 4 (4), pp: 465-480, 1961.

136. White, F.T., Fluid Mechanics, Seventh Edition, McGraw-Hill, New York, 2011.

137. Wilcox, D.C., “Turbulence modeling for CFD” ISBN 1-928729-10-X, 2nd Edition, DCW Industries, Inc., 2004.

138. Wu, X., and Moin, P., Journal of Fluid Mechanics, Vol. 608, pp: 81-112, 2008.

139. Wu, X., Moin, P., Wallace, J.M., Skarda, J., Lozano-Duran, A., and Hickey, J-P, “Transitional– turbulent spots and turbulent–turbulent spots in boundary layers” Proceedings of National Academy of Sciences, USA, PNAS.1704671114, 2017.

140. Yee, H.C., Sandham, N.D., Djomehri, M.J., “Low-Dissipative High-Order Shock-Capturing Methods Using Characteristic-Based Filters” Journal of Computational Physics, Vol. 150, Issue 1, pp: 199-238, 1999.

141. Yeung, P.K., and Pope, S.B., “An algorithm for tracking fluid particles in numerical simulation of homogeneous turbulence” J. Comput. Phys.79, p: 373, 1988.

142. Yeung P.K., and Pope, S.B., “Lagrangian statistics from direct numerical simulations of isotropic turbulence” J. Fluid Mech. 207, p: 531, 1989.

143. Zang, T.A., Hussaini, M.Y., and Bushnell, D.M., “Numerical computations of turbulence amplification in shock–wave interactions” AIAA, Vol.22, pp: 13-21, 1984.

144. Zbrozek, J.K. “Some effects of atmospheric turbulence on aircraft”, Royal Aircraft Establishment, Weather, 13, pp: 215-227, 1958.

Biological Information

Sarah Moussa Hussein was born in Beirut, Lebanon. She first attended the University of Texas at Arlington in Fall 2009. During her undergraduate studies, she joined the Aerodynamics Research Center in Spring 2011 and started working on turbulence studies under the supervision of Dr. Frank Lu. She received the National Science Foundation funded Louis Stokes Alliances for Minority Participation (LSAMP) Summer Research Academy fellowship over two summer semesters, participated in numerous conferences and research symposiums, and was selected to partake in the LSAMP International Research Experience in Athens, Greece in December 2012. Her research work was also supported by the Department of Mechanical and Aerospace Engineering Undergraduate Research Opportunity fund in 2012.

After graduating with an Honors Bachelor of Science degree in Aerospace Engineering in May 2013, she joined the B.S. to Ph.D. program and continued working on the same research topic at the Aerodynamics Research Center. She received the Honors Bridge to Graduate School Fellowship upon joining the Ph.D. program. In 2014, she received the prestigious National Science Foundation Graduate Research Fellowship Program fellowship. She continued to attend research conferences and present at different symposiums. Moreover, she extended her outreach to different summer camps, school visits, and mentoring opportunities.